3D-FE MODEL FIELD-CALIBRATION AND RATING STUDIES ON EXISTING R/C BUILDINGS

A THESIS SUBMITTED TO
THE GRADUATE SCHOOL OF NATURAL AND APPLIED SCIENCES
OF
MIDDLE EAST TECHNICAL UNIVERSITY

BY

EMEL DEMİROK

IN PARTIAL FULFILLMENT OF THE REQUIREMENTS
FOR
THE DEGREE OF MASTER OF SCIENCE
IN
CIVIL ENGINEERING

APRIL 2006

Approval of the Graduate School of Natural and Applied Sciences

_____

Prof. Dr. Canan Özgen
Director

I certify that this thesis satisfies all the requirements as a thesis for the degree of Master of Science.

_____

Prof. Dr. Erdal Çokca

Head of Department

This is to certify that we have read this thesis and that in our opinion it is fully adequate, in scope and quality, as a thesis for the degree of Master of Science.

_____

Assist. Prof. Dr. Ahmet Türer
Supervisor

Examining Committee Members

Prof. Dr. Polat Gülkan	(METU, CE)	_____
Assist. Prof Dr. Ahmet Türer	(METU, CE)	_____
Assoc. Prof Dr. Ahmet Yakut	(METU, CE)	_____
Assist. Prof Dr. Erdem Canbay	(METU, CE)	_____
M.S. Sinan ÖZER	(Aysa Engineering)	_____

I hereby declare that all information in this document has been obtained and presented in accordance with academic rules and ethical conduct. I also declare that, as required by these rules and conduct, I have fully cited and referenced all material and results that are not original to this work.

Name, Last name: Emel Demirok

Signature

ABSTRACT

3D-FE MODEL FIELD-CALIBRATION AND RATING STUDIES ON EXISTING R/C BUILDINGS

Demirok, Emel

M.Sc., Department of Civil Engineering

Supervisor: Assist. Prof. Dr. Ahmet Türer

April 2006, 147 pages

Dynamic instrumentation and a series of ambient vibration tests were performed on a four storey strengthened R/C building within the scope of this study. Traffic load and wind load were accepted as natural dynamic loads and the vibrations were recorded by sensitive accelerometers. For that study, 12 uniaxial, 1 triaxial accelerometers and a 15 channel data logger system were used.

Four sets of dynamic measurements were recorded over a period of 6 months. Recorded readings were analyzed using UPC, PC, and CVA algorithms and Artemis software. The natural frequencies, mode shapes of the tested building were determined. The experimental results were compared against each other. A 3D-FE model of the building was prepared and analytical results were also compared against the experimental results. The calibration (updating) of the analytical model was carried out using the experimentally obtained mode shapes and frequencies.

The results of the study indicate that first few mode shapes and frequencies of the building can be obtained successfully within zero to 10 Hz range using ambient monitoring. Field calibrated FE models can effectively simulate the first translational and torsional modes of the building. Calibration studies indicate that the upper floor

is more flexible than the nominal model and there are weaknesses between the shear wall and roof slab connections.

Keywords: ambient vibration measurement, calibration, natural frequencies, mode shape

ÖZ

BETONARME BİNALARIN ÜÇ BOYUTLU MODELLERİNİN DENEYSEL KALİBRASYONU VE DEĞERLENDİRİLMESİ

Demirok, Emel
Yüksek Lisans, İnşaat Mühendisliği Bölümü
Tez Yöneticisi: Y. Doç. Dr. Ahmet Türer

Nisan 2006, 147 sayfa

Bu çalışma kapsamında dört katlı betonarme bir bina üzerinde dinamik yerleştirme ve bir dizi doğal titreşim testi yapılmıştır. Trafik yükü ve rüzgar yükü doğal dinamik yükler olarak kabul edilmiş ve çok hassas aletler tarafından yapının yaptığı salınımlar kaydedilmiştir. Bu çalışma için 12 adet akselerometre, 1 adet üç eksenli akselerometre ve 15 kanallı veri toplama sistemi kullanılmıştır.

Dört adet dinamik ölçüm altı aylık zaman diliminde kaydedilmiştir. Kaydedilen okumalar üç farklı algoritma kullanılarak analiz edilmiştir. Test edilen binanın doğal frekansları, mod şekilleri tespit edilmiştir. Deneysel sonuçlar birbirleriyle karşılaştırılmıştır. Binanın üç boyutlu sonlu eleman modeli yaratılmış ve analiz sonuçları deneysel sonuçlarla karşılaştırılmıştır. Analitik modelin kalibrasyonu, deneysel olarak elde edilen mod şekilleri ve frekanslar kullanılarak yapılmıştır.

Bu çalışmanın sonuçları, binanın ilk bir kaç mod şeklinin ve frekansının 0 ile 10 Hz'lük frekans aralığı için doğal titreşim izlemesi kullanılarak başarılı bir şeklide saptanacağını göstermektedir. Deneysel olarak kalibre edilmiş olan sonlu eleman modeli etkili bir şekilde binanın ilk eğilme ve burulma modlarını taklit edebilmektedir. Kalibrasyon çalışması üst katın nominal modeldekinden daha sünek

olduğunu ve perde duvarlar ile çatı döşemesi arasındaki bağlantılarda zayıflıklar olduğunu göstermiştir.

Anahtar Kelimeler: Doğal titreşim testi, kalibrasyon, doğal frekanslar, mod şekli

Dedicated to the memories of my grandmothers

ACKNOWLEDGEMENTS

I would like to express my grateful thanks to my supervisor Asst. Prof. Dr. Ahmet Türer for his guidance, support and patience during this study.

I would like to thank Mr. Karluk Çetinkaya from Is Bank for helping with arrangements on instrumentation and Asst. Prof. Dr. Erdem Canbay for their kind support with the instrumentation. I also would like to thank to Assoc. Prof Dr. Ahmet Yakut for his helpful ideas and support in Pushover Analysis.

Finally, I wish to present my deepest thanks to my father and mother for their invaluable support. Their understanding and love prettifies my life.

TABLE OF CONTENTS

LIST OF TABLES

LIST OF FIGURES

CHAPTER 1

INTRODUCTION

1.1. Vibration Testing

In structural engineering, vibration testing is used to understand the behavior of the structures, damage detections and modal updating of the structures. Several options as vibration tests exist. Forced vibration, free vibration and ambient vibration measurement tests are the common types.

In the forced vibration testing, periodic or random signals are created by mechanical excitations. A forced excitation is applied to the test object/structure by means of a shaker, and the response is continuously monitored. The shaker test method has the advantage of being able to control the nature of the test excitation input like frequency content, intensity, and sweep rate. The results from shaker tests are relatively more accurate and more complete but also tests might be more complex and costly.

In the free vibration testing, response measurements are made on free decay of the test object following an initial excitation. That excitation can be created by using either initial velocity or initial displacement. The required testing time for the initial velocity (impulsive excitation) and initial-displacement tests methods is relatively small in comparison to forced vibration test results. Therefore, free vibration tests are often preferred in preliminary testing before conducting the main tests.

The vibration tests which use random signals are called ambient vibration measurement tests. Ambient vibration testing is generally preferred to non-destructive forced vibration measurement techniques for obtaining the modal

parameters of structures. The advantage of this method is that, generally no artificial excitation needs to be applied to the structure. Furthermore if artificial loading is required, the forces do not need to be measured. In ambient vibration measurements, all parameter estimation are based on response signals therefore it is also called Output Only Modal Analysis.

In ambient vibration measurements, a structure can be adequately excited by wind, traffic and human activities. These vibrations are hardly felt by human senses and highly sensitive instruments are required to read these measurements since its amplitudes are very small.

Ambient vibration measurements have several other advantages. First one is that testing the structure is cheap because equipment for excitation is not needed. The other important point is that the measured response is representative of the real operating conditions of the structure. Also testing does not interfere with the operation of the structure. However, as mentioned above the response of the structure is small and often partly covered noise in ambient vibration measurements. Further, the excitation is unknown, and thus, the identification becomes more difficult than in input-output modal identification (Artemis Manual). The main difficulties are:

- Sensitive equipment is needed.
- Careful data analysis is needed.

But today equipment of necessary quality is now available and needed analysis is provided by software programs of output only modal identification analysis.

1.2. Steps of Vibration Testing

When applying a vibration measurement test, engineer has to deal with several subjects and decisions like the vibration testing method, data acquisition system, software for the analysis of dynamic response measurements, finite element model of the models, environmental conditions, etc (Ewins,1995). General procedure of the vibration measurement testing may be summarized as below:

- Pre-investigation of the structure (plans, site visit)
- Data acquisition system and selection criteria
- Testing, measurement and post processing of measured data
- Comparison against FEM, validation, calibration and evaluation

1.2.1. Pre-Investigation of the Structure

Pre-investigation stage mainly consists of examination of available plans and photographs of the structure and visually examining the structure by site visit. During the pre-investigation stage, apparent problems (e.g., visible cracks, excessive deformation, soft-storey, unfavorable site conditions) are recorded. History and plans of the structure are studied. Possible monitoring strategies and locations are roughly planned. Monitoring system requirements, such as number of transducers, data acquisition system type, cabling requirements, mounting locations, are determined. The importance of the structure is evaluated; monitoring duration and testing intervals are roughly decided.

1.2.2. Data Acquisition System and Selection Criteria

The data acquisition part involves selecting the types of sensors to be used, selecting the location where the sensors should be placed, determining the number of sensors to be used, and defining the data acquisition hardware and installation process. Pre-investigation of the structure and economic constraints play a major role in these decisions.

Firstly, accelerometers, cables, and data acquisition system must be chosen according to their quality and prices. The accelerometer locations should be decided based on the mode shapes expected to obtain from the structure. The number of accelerometer locations is a function of the structure size and complexity. For small and simple structures it might be just 6-12 points; however, a larger number of accelerometers might be needed for large structures. After the installation of the transducers on chosen locations, and completing all the connections, set-ups of the data acquisition system must be done. By using these set-ups, required measurements can be taken from the data acquisition system.

1.2.3. Testing, Measurement, and Post Processing of Measured Data

The dynamic response measurements, which are received from the data acquisition system, are recorded by using a simplistic data acquisition software. Stored measurement files are translated into suitable file formats for the subsequent processing steps.

The recorded and translated data records are analyzed in another commercially available software to obtain the experimental modal parameters. These experimental modal parameters can be verified by using different sets of measurements which are taken in different times of a year. Furthermore, the quality of the measurements can also be investigated by using different experimental testing techniques together such as forced vibration testing and ambient vibration testing. This study provides the engineer a chance to control the reliability of experiments. Another option is that different estimation techniques of one vibration measurement type can be used to analyze post-processing reliability of the recorded data for the same time interval. Using different estimation techniques can be repeated several times for different time intervals.

1.2.4. Comparison against FEM and Evaluation

The behavior of a structure under various types of loadings is simulated by Finite Element Analysis (FEA). FEA is a predictive approach that relies on the quality of simulation model, software to analyze it, and engineering judgment of the analyst interpreting the results. Several assumptions are made by engineers when the finite element model of the structure is created in any computer software. These assumptions and the reliability of the finite element model can be controlled in light of the results of vibration measurement testing. Simply, that experimental study provides a comparison between the real structure and computer model of the structure. In light of that comparison, if necessary, calibration of the finite element model can be done. Calibration or Model Updating is carried out by modifying the mass, stiffness, support conditions, and damping parameters of the FE model until an improved agreement between finite element analysis data and test data is achieved. For that comparison, required true modal parameters are natural frequency (resonance frequency), mode shapes (the way that structure moves at certain resonance frequency), static loading test results, and damping ratio. Static loading tests may not be available for buildings and are mostly common to bridges. Modal parameters are important because they describe the dynamic properties of a structure. They constitute unique information that can be used for model validation and model updating.

The conclusion part of the experimental study (vibration testing) provides information about the reliability of the structure's finite element model. A comparison between the true modal parameters which are received from the experimental study and the modal parameters of the structure's finite element model is made. If the analysis shows any divergence between the true model and finite element model of the structure, then there exist two options: First one states that the finite element model of the structure is not dependable and calibration works are required. The divergence can also occur due to wrong assumptions which were made by the engineer, wrong information about material property, about structural system, support conditions, geometric dimensions, and/or mass of the structure. Second option is that structure may be damaged because of any environmental

affects. Both results require to start a new study on the structure. Following steps include either calibration of the analytical model or the strengthening of the structure.

1.3. Previous Studies of Ambient Vibration Measurements:

In the early 1930's ambient vibration measurements had been used to measure the fundamental periods of buildings and in 1960's it had been developed to determine the lowest frequencies and mode shapes of the structures. Today ambient vibration analyses involves identification of natural frequencies, mode-shapes of vibration and equivalent viscous damping parameters of buildings, stadiums, ancient structures, statues, dams, bridges and nuclear power plants (Ivanović, et al., 2000).

One good example of the ambient vibration measurement tests was applied by The University of Sheffield, UK (Reynolds, et al., 2003). They tested a stadium structure (Midland Road Stand) which was built in 1996 at Valley Parade, Bradford, UK. The stand consists of a series of steel frames at 7.19 m centers. The seating deck is constructed from L-shaped precast concrete units, which are simply-supported between the steel frames. The structure is a single tiered stand, with a concourse area located beneath the tier. The stand cantilevers back about 4 m towards the Midland Road behind it. The roof cantilevers over the entire tier, and has additional support at the ends of the stand. Main goal of that study was to understand the changes of modal properties of stadium structures when occupied by crowds. In September 2001, three tests were carried out. One of them was model testing using chirp excitation applied by an electro dynamic shaker, one was heel drop testing at various locations and the last one was ambient vibration measurements (using natural excitation by wind, traffic, etc.) For the above tests, transducers was positioned in vertical and horizontal (front to back) directions. In May 2003, one more test was carried out on the empty stadium to identify the longitudinal modes also by using ambient vibration measurements. The same test points as used previously utilized with the longitudinal points together in this test. During the ambient vibration tests they took dynamic measurement readings for seven crowd configurations: empty structure, stadium filling up with people before a

sport event, stadium emptying after a sport event, half time (mainly seated with some people milling around), people seated during a sport event, people standing up following a goal event (when peak response is less than 0.3m/s²) and people standing up following a goal event (when peak response is equal or greater than 0.3m/s²). These crowd configurations were identified from the match reports and the vibration data using the video data which were taken from the two videos located at each end of the stadium. Eigensystem Realization Algorithm (ERA), Frequency Domain Decomposition (FDD), Enhanced Frequency Domain Decomposition (EFDD) and Stochastic Subspace Identification (SSI) were used for ambient vibration analysis. FDD, EFDD and SSI analysis was performed by Artemis Software. After the analysis, the results showed that a crowd has significant effect on the natural frequencies and damping ratios of the stadium compared when it is empty. All stages of crowd occupation tend to reduce the natural frequencies and increase the damping ratios compared with the empty stand. These results proved an idea that the crowd should be modeled as a SDOF damped spring mass system (rather than a simple added mass) attached to a SDOF system representing a mode of the empty structure. Furthermore they got the same modal parameters from the shaker modal testing and ambient modal testing of the empty structure. Thus that study again proved the reliability of the ambient vibration measurement tests.

A series of ambient vibration tests was applied to the 48-storey One Wall Centre, Vancouver, B.C., Canada on April10, 2001 by a group of researchers from the University of British Columbia (Ventura, et al., 2001). One Wall Centre is 137 m tall and is 23.4 m by 48.8 m and is oval shaped with pointed ends. The building is made up of a central reinforced concrete core whose walls are up to 900 mm thick at the base. The core contains six elevator shafts and two stairways. The floor slabs are typically 175 mm thick. At level 5, a 6.4 m deep outrigger beam transfers the loads to the outrigger columns. More outrigger beams are found at levels 21 and 31 and are 2.1 m deep. The concrete water tanks on the roof of the building act as outriggers. Two 183 m³ tuned liquid column dampers are located on the roof of the structure. Each damper contains two water columns connected by a sluice gate to regulate the water flow. Because of its oval-shaped floor plan, tuned liquid column dampers and its height, this reinforced concrete shear core structure is chosen as the

model building. For the output-only modal analysis, a 16-channel data acquisition system, signal conditioner, A/D converter, force balanced accelerometers and a laptop computer for data acquisition and data storage were used. The data was recorded for a period of 12 minutes per set-up at 2000 samples per second (sps) and decimated to 250 sps. Because of the story number of the building, they created 7 set-up configurations and measured 3 floors for each set-up. Also two reference sensors were placed on the 45th floor. Frequency Domain Decomposition (FDD) and the Stochastic Subspace Identification (SSI) techniques of the computer program Artemis was used to perform the modal identification of the structure. After the analytical study, they captured eight modes from the ambient vibration measurements but the fundamental frequencies estimated by finite element model are about 15% lower than these modes. Furthermore computer model (finite element model) predicts the 2nd torsional mode to have a lower order than the 2nd EW mode. Since these results showed that Model #1 needed to be stiffened, calibration study is done and gravity load columns, the exterior cladding were added to Model #1. After that calibration, the order of 2nd torsional and 2nd EW modes reversed and the fundamental frequencies were within a more reasonable 10% difference.

1.4. Objectives and Scope:

This thesis study was a part of NATO-SfP 977231 (Typical Applications and Monitoring of Rehabilitated Structures) and TUBITAK ICTAG-I576 (Typical Applications and Instrumentation) projects. In that study, first phase of structural monitoring project was conducted on a ground + four story RC building using ambient vibration measurements. The objectives and scope of the study are given below in bullet list format:

Objectives:

- Gain ability to instrument a building using dynamic measurement systems,
- Gain ability to obtain structural dynamic properties using ambient monitoring,

- Investigate the differences between nominal and calibrated FEM predictions,

Scope:

- Construct a nominal FE Model of the building,
- Select a suitable data acquisition system and instruments to monitor the building,
- Instrument a RC building which has been strengthened in the past,
- Conduct ambient monitoring tests and download data by remote connection,
- Post-process data and extract dynamic properties of the building
- Compare experimental results that were obtained at different times of a year,
- Calibrate FEM to match field measured dynamic data,
- Draw conclusions from results.

CHAPTER 2

EXPERIMENTAL STUDY

2.1. Pre-Investigation of the Building:

The ambient vibration method was applied to a four-story strengthened reinforced concrete bank building (Figure 2.1) in Kabataş, İstanbul. Kabataş is located in the second earthquake region. Soil type of the building was taken as Z4 according to the information on the key plan.

Figure 2.1 Four-story strengthened RC bank building

Total height of the bank building is 14.80 m and it has an almost square plan of 16.70 m by 16.0 m. During the construction of the building, used concrete is BS16, and the used reinforcement is St I (S220). Except the ground and the roof floors, all stories have the same plan except column sizes, but unfortunately they have an unsymmetrical plan (Figure 2.2).

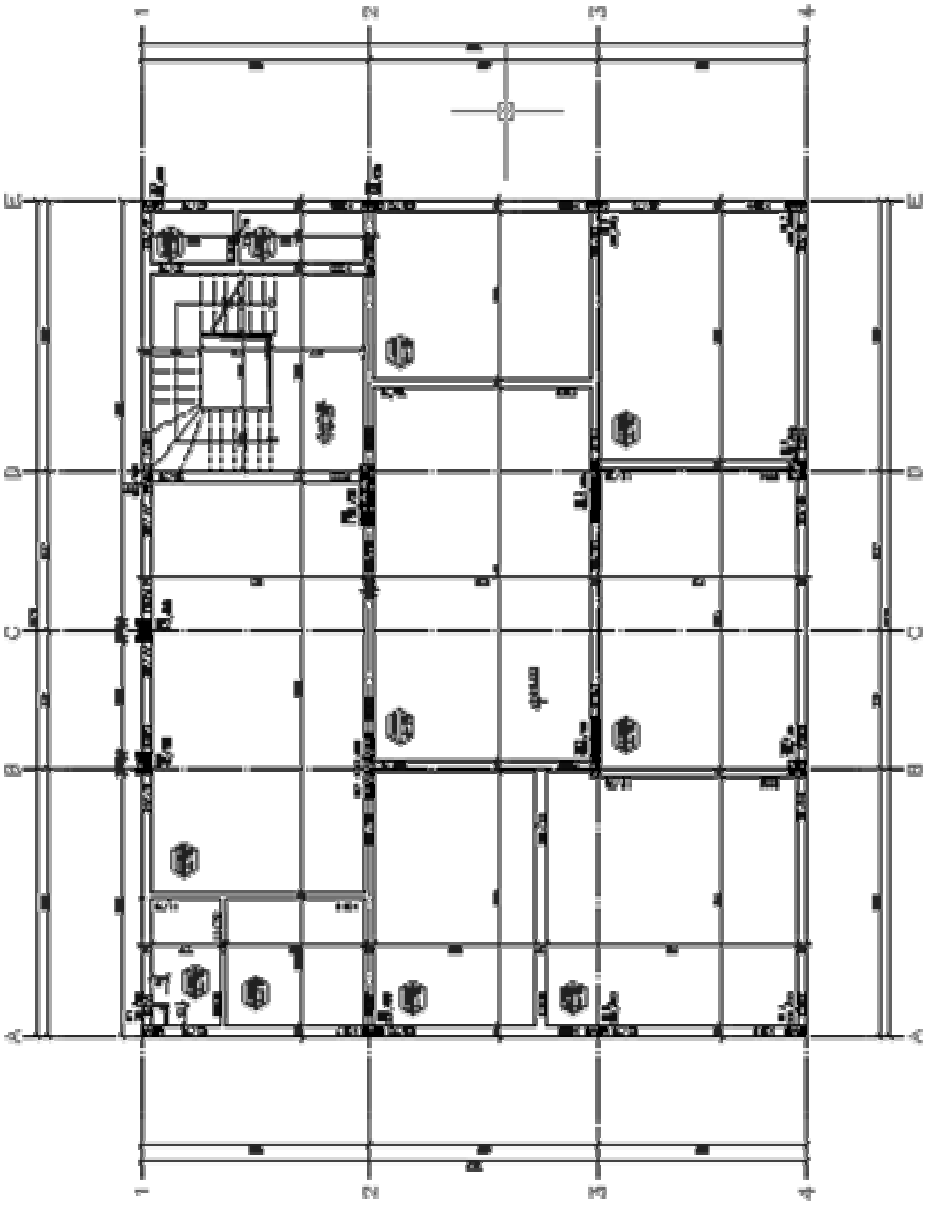

Figure 2.2 Plan view of second story of the building before strengthening

Turkish Code's limitations like the minimum sizes of the column and beam, continuity of the frames, minimum concrete and reinforcement quality and continuity of the column sizes through all stories are not satisfied by most of the structural elements of the building. Many unnecessary cantilever beams had been

used in that design because of ignoring the continuity of the frames. Furthermore column capacities had been reduced by changing their sizes in each story. For example some column sizes get bigger and inversely some of them get smaller in higher stories (Figure 2.3).

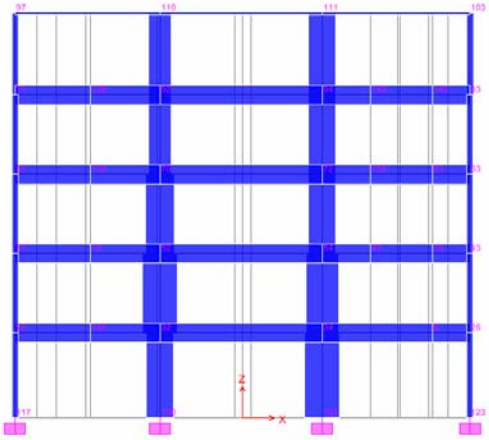

Figure 2.3 Irregular column sizes of the experimented building

During the strengthening project, outside corners of the building are covered by eight shear walls which are constructed by using epoxy. Used concrete is BS20 and the used reinforcement is St III (S420) for the shear walls. Plan view of second story of the building after strengthening project is shown in Figure 2.4.

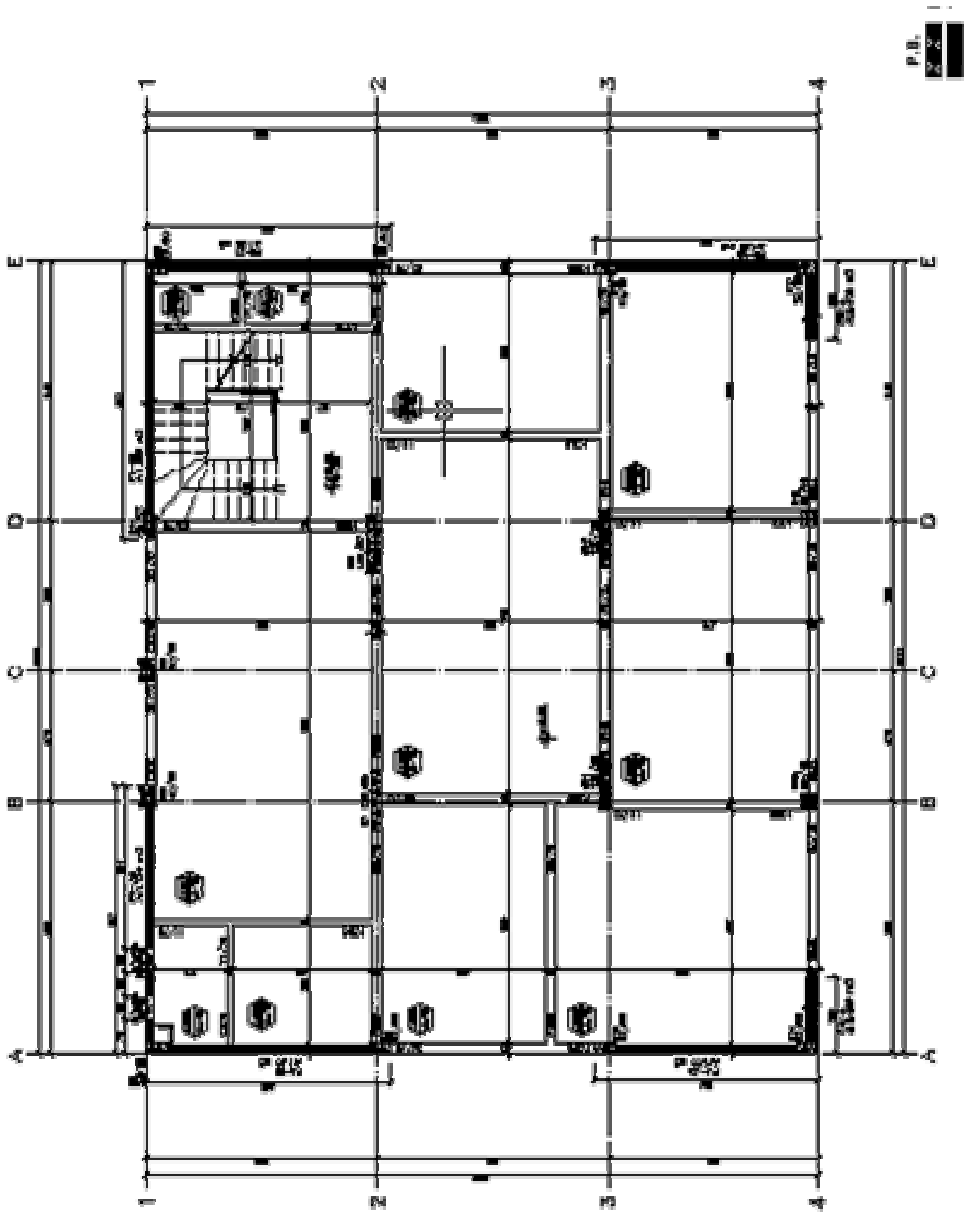

Figure 2.4 Plan view of second story of the building after strengthening

Furthermore, detailed information about the roof plan, foundation type and design, and the reinforcement details of the beams and columns do not exist.

Earthquake effects are seen as possible damages for that building, thus transducers were chosen as accelerometers and located in horizontal directions.

Building selection depends on some cases. Most important case is that the director or the owner of the structure should be guaranteeing the safety of the instruments. Since any location changes of the instruments or any break down of the data acquisition system vitiate the vibration testing. The other important factor is related with the philosophy of the ambient vibration measurement technique. Since that technique needs natural loads, mostly structures in use are chosen for these studies. There is a four lane (two-way) busy street just in front of the building which provides adequate ambient vibration especially during rush hours. Bank building provides a human crowd and movement in the building. Also that building is located at the sea side therefore it takes the winds coming from the Bosphorus and this is another natural load.

2.2. Data Acquisition System and Selection Criteria:

2.2.1. Data Acquisition System

The data acquisition system used in that project is CMG-DM24S12AMS (Figure 2.5) which is purchased from Guralp Systems Company.

Figure 2.5 Front view of the data logger system

It is a self-contained seismic data collection station configured to operate 12 single-component strong motion accelerometers (CMG-DM24S12AMS manual). The sockets of these twelve accelerometers are placed at the back side of the data logger. Other six sockets are placed at the front side of the data logger for digital output seismometers. In addition to these six digital seismometers, auxiliary inputs are placed on the front side of the data logger system. Power can be supplied to the sensors by these sockets. At the right part of the front side, there are also other six sockets: one for telephone cable, one for network cable, one for GPS cable, one for USB connection and the others are for power sources. A typical setup for DM24S12AMS acquisition and monitoring system is shown in Figure 2.6.

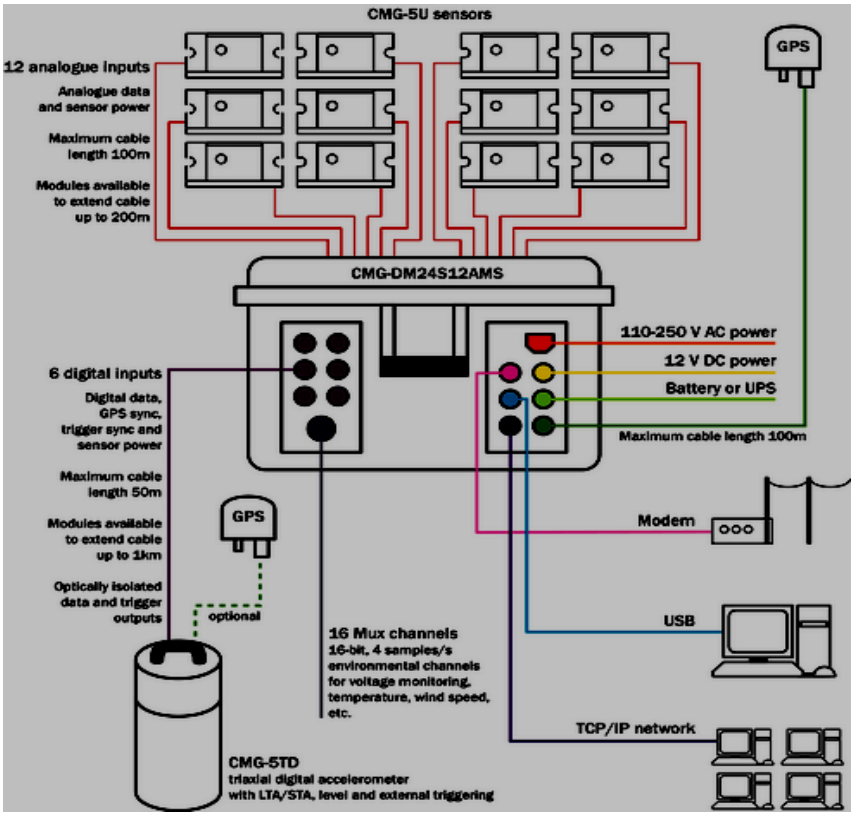

Figure 2.6 A typical setup for DM24S12AMS acquisition and monitoring system (DM24S12AMS manual)

Furthermore, an integrated laptop PC is combined by the data logger system for viewing and transmitting the recorded data. Loaded software in the laptop PC is Scream. All setups and controls are provided by Scream.

Twelve strong motion accelerometers (uniaxials) and a digital output sensor (triaxial) were connected to the data logger which was placed in Kabataş İşbank building. The data taken from all thirteen instruments is fed into the data logger (DM24S12AMS), where it can be stored and processed on-site or alternatively sent across a local network or the Internet. In that project, a remote connection is created between the laptop PC of the data logger and our computers.

There are three options for the power supply. The DM24S12AMS can be powered either from 110-250V AC mains power, or from a 12 V DC power source. But if any power cut occurs when one of these two options is chosen, all setups of the data logger are lost. To prevent that situation, there is also a rechargeable BATTERY/UPS connection option. In that project, BATTERY connection and 110-250V AC mains power options were used together.

The CMG-GPS2 (Figure 2.7) is used as GPS in that project. It is a stand-alone unit requiring only one cable connection to the DM24S12AMS, which carries both signals and power. GPS provides time synchronization according to the Greenwich Mean Time. Maintaining a good fix from the available satellites is the most important point about the GPS. If that situation is provided exactly, the system will then switch on the control process and set the internal clock. Otherwise, a discontinuity occurs in the recorded data.

Figure 2.7 CMG-GPS2

Units based on the CMG-DM24 digitizer provide a range of 16-bit, 4 Hz auxiliary channels, known as multiplexed ("Mux") channels. They can be used for reporting the sensor mass position, receiving calibration signals and measuring the internal temperature of the digitizer (CMG-DM24 manual). In that project, Auxiliary Input socket was not used.

2.2.2. Strong Motion Accelerometer

The CMG-5U accelerometer (Figure 2.8) was used as a strong motion accelerometer. It is a single-axis strong-motion force feedback accelerometer in a sealed case, which can be used either in vertical or horizontal orientations (CMG-5U manual).

Figure 2.8 CMG-5U Strong Motion Accelerometer

When the motion reaches the level where humans can feel it, typically 1-2%g, it is often called strong motion. Strong motion accelerometers are designed to record the strongest events and weak motion accelerometers are designed to record very weak events (Silva,1999). Using weak motion accelerometers may result in clipped records of the strongest and most important events. In that study ambient vibration measurement testing is applied to the model building therefore highly sensitive accelerometers are required. CMG-5U is a strong motion accelerometer and also it is enough sensitive to capture the natural events.

Acceleration is measured in "g", where 1g corresponds to the vertical acceleration force due to gravity. During an earthquake, the forces vary a lot and keep changing, back and forth and side to side. The largest earthquake forces that have been measured are about 1 to 2g; most earthquakes have much lower forces (Silva,1999). Full - scale low - gain sensitivity of 5U sensor is available from 4.0g down to 0.1g and the high gain sensitivity of 5U sensor is available from 0.4g-0.01g (CMG-5U manual). g level range determines the maximum g load a device can measure accurately. It also indicates the maximum acceleration that a device can withstand without damage or permanent scale shift. It should be noted that the

maximum acceleration encountered can be substantially higher than expected, because of incorrect mounting or loose parts (CMG-5U manual).

The standard frequency pass band is flat to acceleration from DC to 100 Hz. A high frequency option provides flat acceleration from DC to 200 Hz. An internal DC-DC converter exists on that sensor (CMG-5U manual). A DC to DC converter is a device that accepts a DC input voltage and produces a DC output voltage. Typically the output produced is at a different voltage level than the input. In addition, DC to DC converters are used to provide noise isolation. An internal DC-DC converter of the CMG-5U ensures an isolated sensor system and allows the system to operate from 10 to 12 volts.

Twelve CMG-5U accelerometers were used for that study. Except the roof and ground floors, three accelerometers were located on each story. The dynamic response measurements of the experimental building are firstly recorded by accelerometers and these readings are send to the data logger system for storing by the help of the cables.

2.2.3. Digital Output Seismometers (Triaxial)

The digital output seismometer used in that experiment is CMG-5TD (Figure 2.9). The CMG-5TD transducers use low noise components, high feedback loop gain, and computer-aided design to produce linear, wide dynamic range, precision transducer. An internal DC-DC converter ensures an isolated system and allows the system to operate 10 to 36 Volts. Full-scale low-gain sensitivity can be specified as ±0.1, 0.2, 0.4, 0.5, 1.0, 2.0 or 4.0 g. The standard frequency pass band is flat to acceleration from dc to 200 Hz (CMG-5TD manual).

Figure 2.9 Front view of the CMG-5TD

Also it has a simple installation procedure. The CMG-5TD output offsets can be reduced down to the sub mill volt range; they are adjusted electronically without exposing the inside of the accelerometer. The access to the offset adjustment is as simple as removing an "O" ring sealed cap next to the sensor connector.

In that project one CMG-5TD is located on the ground floor. Continues and trigger readings are recorded on the ground floor by triaxial accelerometer.

2.2.4. Scream Software

Simply, Scream is the brain of the data acquisition system. All the configurations, controls of the sensors, recording and trigger options are supported by Scream software. By using Scream software the options given below can be controlled.

- The type of sensors
- GPS power cycling options
- The short-term and long-term average values for triggering
- The length of pre-trigger and post-trigger periods

- Calibration signal inputs
- Length of the record data
- Frequency of the continuous and trigger readings
- Transmitting data

In the Configuration Setup Window, Scream provides a GPS option. GPS unit receive time signals constantly. And that gives the most accurate results with ample power. But if a power problem occurs in the system, there is another option about GPS. In that option, the GPS time is only checked at intervals of a specified number of hours. Any whole number of hours can be chosen for the interval. Since enough power is provided to our data acquisition system by re-chargeable battery and AC main power option, GPS receive time signals constantly in that project.

In the scream software, incoming data is internally sampled at 2000Hz. After filtering and reducing that data to a lower rate, DM24S12AMS record data continuously at a relatively sample rate and record at a much higher sample rate during short periods when the trigger is active (DM24S12AMS manual). In that project, continuous readings were recorded at 100Hz and trigger readings were recorded at 200Hz. Output control window of Scream for trigger and continuous readings is seen in Figure 2.10.

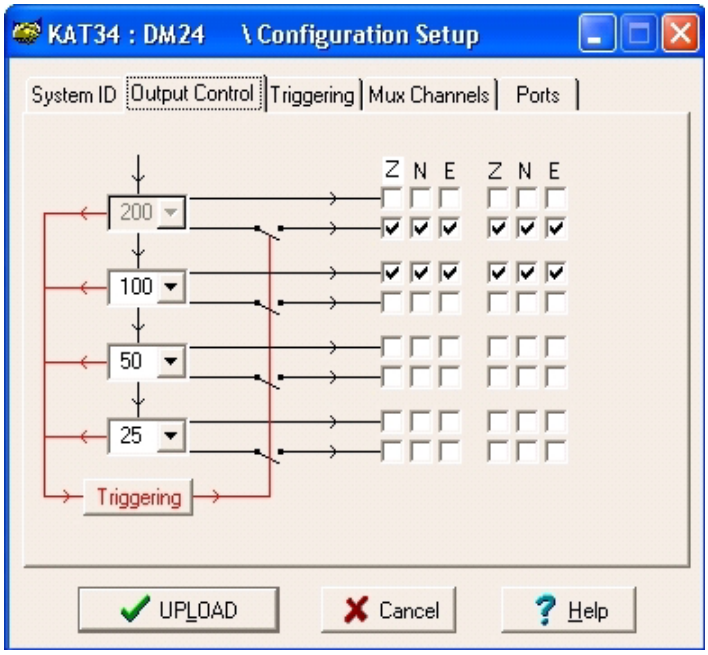

Figure 2.10 View from Scream's configuration setup window of the recording data

In the Scream software two trigger options exist. One of them is STA/LTA Triggering and the other is Level Triggering. The STA/LTA algorithm applies a simple short term average long term average calculation to the triggering stream. That calculation is based on the ratio of the STA/LTA algorithm. When the ratio of the averages exceeds the chosen ratio value an event is usually present and data starts being recorded in a file. In this way record of the noise data will be prevented. These ratios can be given to the Scream for each channel to determine a trigger. But the important point is that STA/LTA ratios of the all chosen channels must be same. If any of the chosen channels passes the trigger condition, the trigger will activate and will not detrigger until all of the chosen channels have fallen below their respective ratio values (DM24S12AMS manual). In that project STA/LTA ratios are chosen for all analog channels.

Short term averages and long term averages are calculated in time intervals. Typically, the time interval of the short term average should be about as long as the signals wanted to be trigger on and the time interval of the long term average should be taken over a much longer interval. These time intervals were chosen as 1 second for STA and as 10 second for LTA. It means that scream

determines the maximum recorded value as STA for every 1 second and the maximum recorded value as LTA for every 10 second. If the ratio between these maximum values of STA and LTA exceeds the given ratio which was 4 in that project, system process the trigger condition. Both the STA and LTA values are recalculated continually, even during a trigger. In the trigger condition, scream starts to record trigger readings during pre-trigger and post-trigger time intervals for every channel. Trigger options for the STA and LTA are seen in the Figure 2.11.

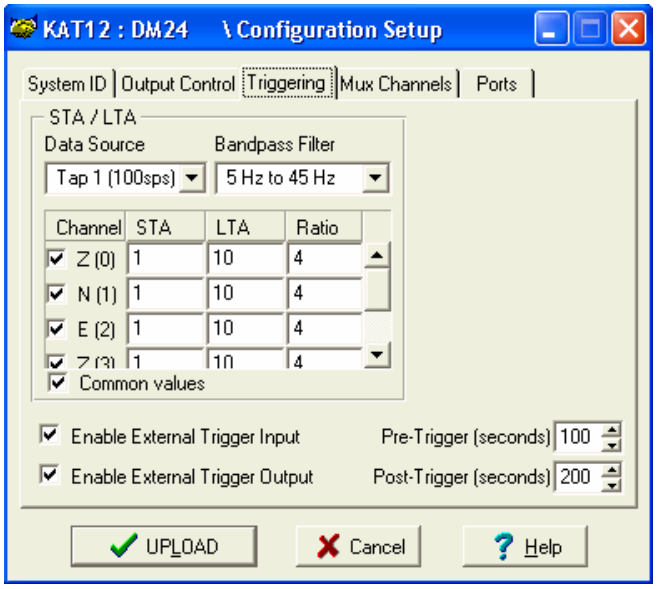

Figure 2.11 View from Scream's configuration setup window of the triggering options

In Figure 2.12, a view of the recording channels of the data logger are seen. SPS 200 represents the trigger records and SPS 100 represents the continuous records in the figure. Furthermore, a graphical view of the continuous recording of the channels were shown in Figure 2.13.

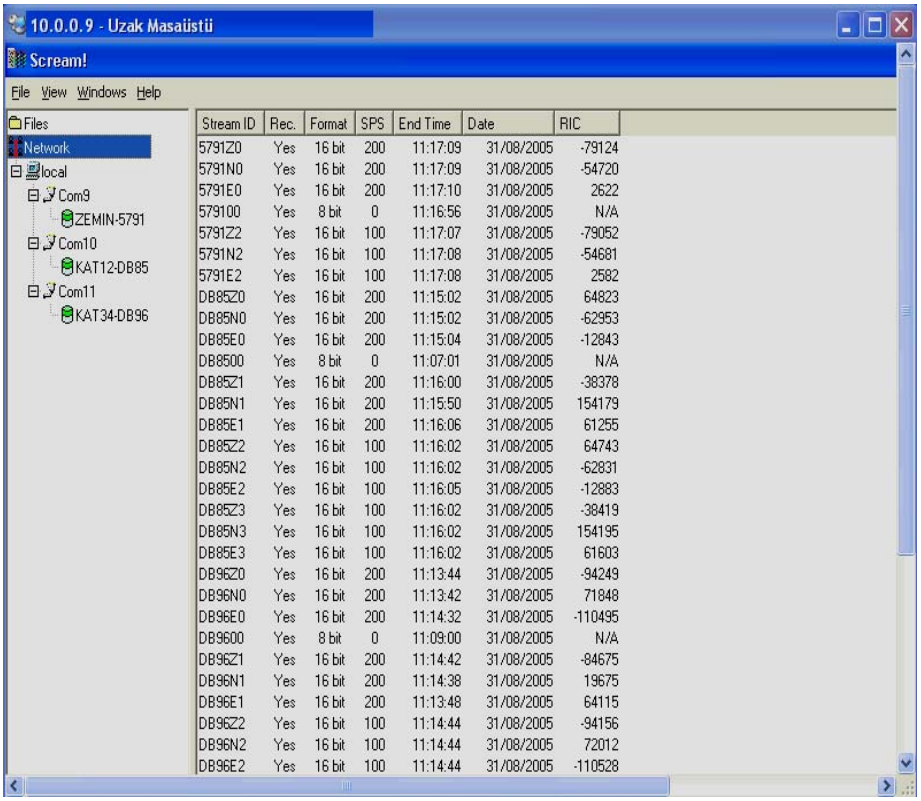

Stream ID	Rec.	Format	SPS	End Time	Date	RIC
5791Z0	Yes	16 bit	200	11:17:09	31/08/2005	-79124
5791N0	Yes	16 bit	200	11:17:09	31/08/2005	-54720
5791E0	Yes	16 bit	200	11:17:10	31/08/2005	2622
579100	Yes	8 bit	0	11:16:56	31/08/2005	N/A
5791Z2	Yes	16 bit	100	11:17:07	31/08/2005	-79052
5791N2	Yes	16 bit	100	11:17:08	31/08/2005	-54681
5791E2	Yes	16 bit	100	11:17:08	31/08/2005	2582
DB85Z0	Yes	16 bit	200	11:15:02	31/08/2005	64823
DB85N0	Yes	16 bit	200	11:15:02	31/08/2005	-62953
DB85E0	Yes	16 bit	200	11:15:04	31/08/2005	-12843
DB8500	Yes	8 bit	0	11:07:01	31/08/2005	N/A
DB85Z1	Yes	16 bit	200	11:16:00	31/08/2005	-38378
DB85N1	Yes	16 bit	200	11:15:50	31/08/2005	154179
DB85E1	Yes	16 bit	200	11:16:06	31/08/2005	61255
DB85Z2	Yes	16 bit	100	11:16:02	31/08/2005	64743
DB85N2	Yes	16 bit	100	11:16:02	31/08/2005	-62831
DB85E2	Yes	16 bit	100	11:16:05	31/08/2005	-12883
DB85Z3	Yes	16 bit	100	11:16:02	31/08/2005	-38419
DB85N3	Yes	16 bit	100	11:16:02	31/08/2005	154195
DB85E3	Yes	16 bit	100	11:16:02	31/08/2005	61603
DB96Z0	Yes	16 bit	200	11:13:44	31/08/2005	-94249
DB96N0	Yes	16 bit	200	11:13:42	31/08/2005	71848
DB96E0	Yes	16 bit	200	11:14:32	31/08/2005	-110495
DB9600	Yes	8 bit	0	11:09:00	31/08/2005	N/A
DB96Z1	Yes	16 bit	200	11:14:42	31/08/2005	-84675
DB96N1	Yes	16 bit	200	11:14:38	31/08/2005	19675
DB96E1	Yes	16 bit	200	11:13:48	31/08/2005	64115
DB96Z2	Yes	16 bit	100	11:14:44	31/08/2005	-94156
DB96N2	Yes	16 bit	100	11:14:44	31/08/2005	72012
DB96E2	Yes	16 bit	100	11:14:44	31/08/2005	-110528

Figure 2.12 A view of the recording channels of the data acquisition system

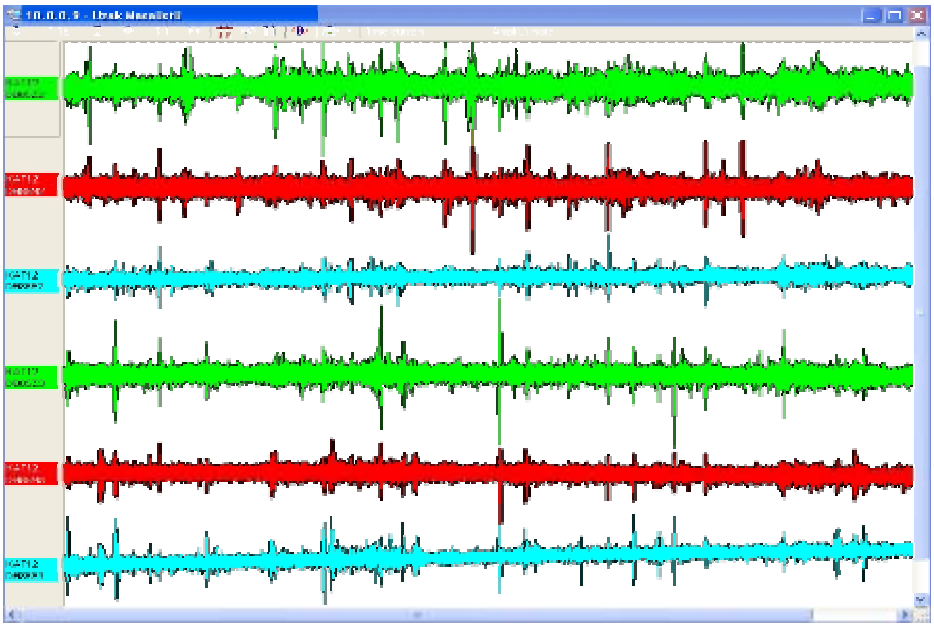

Figure 2.13 A graphical view of the continuous recording of the channels

During the project, continuous and triggered readings were recorded constantly in GCF file format. By using scream also UFF, SAC, MiniSEED, P-GSEGy, PEPP, SUDs, GSE formats can be chosen (DM24S12AMS manual). To use in the analysis methods, all the recorded data files which are not in UFF format must be converted to the UFF format at the end. According to that knowledge, recording the files in UFF format seems more logical. But files in UFF format must represent a continuous period of time and if a discontinuity is detected in the incoming data stream, then the file which is currently recording will be closed and a new file opened with a file name time stamp matching the start of the new file. While changing the configuration parameters, Scream automatically stops recording and that situation creates discontinuity in the received readings. Also other discontinuities can occur in triggered and continuous readings by the internal and external factors. During these situations, any time periods missing from the GCF file are presented by values of -2147483647 (the lowest possible negative number in the GCF file) (DM24S12AMS manual). Not to loose any received reading, all the data are recorded in GCF file format and then converted to UFF format in that project. The most convenient way to convert a GCF file into UFF format is using the "gcf2asc" program. "Gcf2asc" will create a file with the same name as the original, but in a text file. Then it is possible to rename the produced file with an .uff of .ufa extension. Text version of the produced file is sufficient for us in that study. Also original names of the every received data represent the date of their record. File names contain year number, month number, day number of the month, hour and minute of the recorded date. File names of the recorded data sets were seen in Figure 2.14.

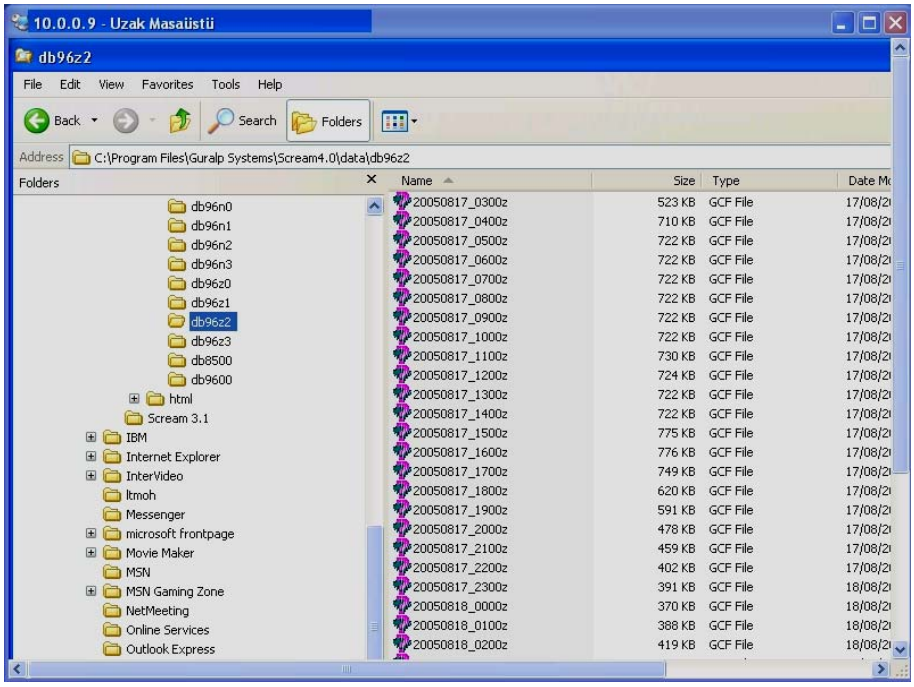

Figure 2.14 View of the recorded data files of one of the analogue channel in Scream Software

All recorded data are stored on the local hard disk. Scream controls that storing according to our choices. Total size of the laptop's "C" driver is 15.7 GB. To use its hard disk space, two options are provided by Scream. One of them is "Stop on Disk Full" option. If that option is selected, then Scream will stop recording data once it runs out of space in its directory. This way, the data recorded will have a known starting point. Second option is "Ring Buffer". In that option, Scream will start deleting the oldest files in the data directory in order to make space for new data, so the most recent recorded measurements are always protected. In that option a specific amount of free disk space must be leaved. 500Mb free disk space was leaved in that project.

Also old recorded readings can be seen as a graph without converting the file format by using Scream (Figure 2.15). By enlarging it, the changes can be seen clearly (Figure 2.16). This option provides us a chance to choose the best recording before download it for the subsequent analysis.

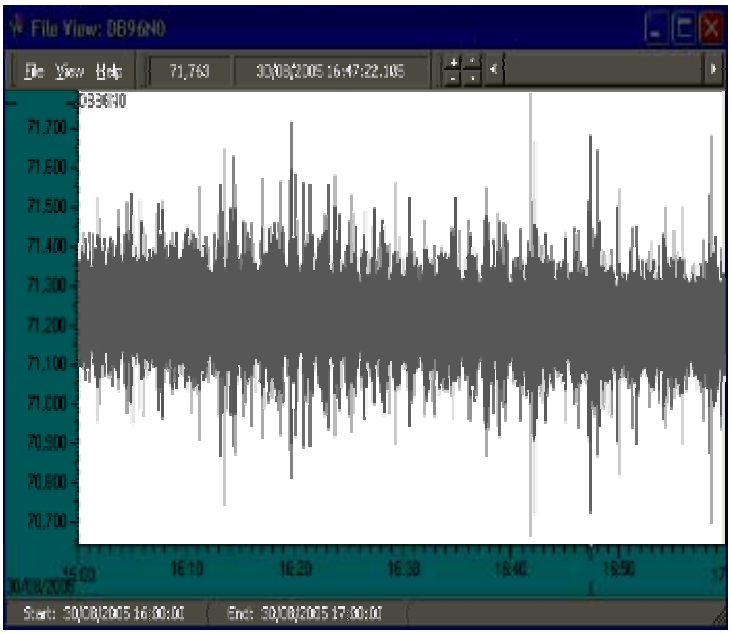

Figure 2.15 View of the old recorded data in a graph form

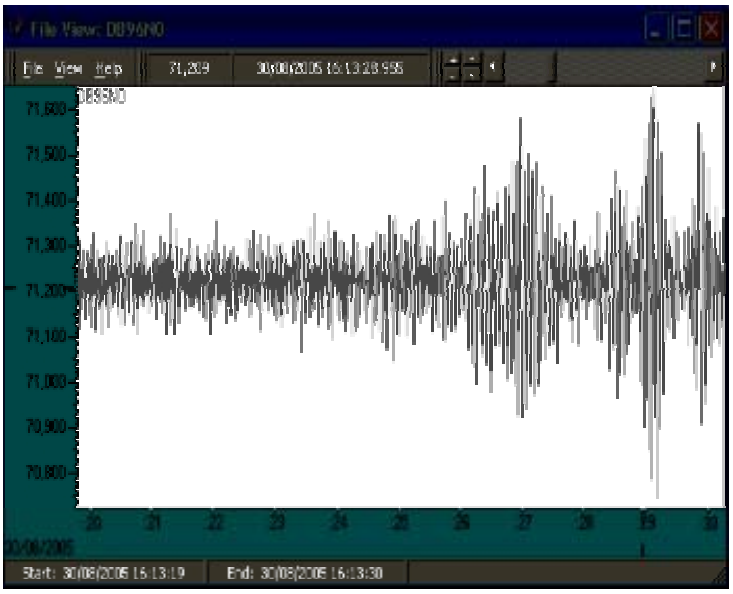

Figure 2.16 Enlarged view of the old recorded data in a graph form

Granularity option of the Scream allows us to decide how large files are allowed to become before a new one is started. A limit on a file's size or its duration can be set by using Scream. During that study, a limit on the duration of the recorded data is preferred to set and it is chosen one hour. This situation was preferred because of the Artemis software's work discipline.

In the Scream's configuration "Baud Rate" option is also important. Baud rate is a measure of the rate at which a modem can transmit data (DM24S12AMS manual). Scream creates Com Ports according to the channels. Such an example it refers first six analog accelerometers as Com Port10 and the rest six analog channels as Com Port11. Furthermore it sorts the digital channels of the triaxial accelerometer as Com Port9 (Figure 2.12). Also it creates Com Ports for "mux" channels. In that project "mux" channels are not used therefore choosing a baud rate for these Com Ports is unnecessary. For the Com Ports of analog and digital channels baud rate was chosen as 57600 since that baud rate is high enough to allow all the transmission of all data generated by the channels and also it is low enough to fit within the operating range of the telemetry equipment we are using.

2.2.5. Installation Process

The accelerometers are located in x and y directions of the stories to capture dominant bending modes in both directions. X-direction is selected to be parallel to the road in front of the building, and y-direction is perpendicular to the road axis. Except for the roof and ground floors, two analog accelerometers were placed in y-direction and one analog accelerometer was placed in x-direction. The two accelerometers in the y direction are placed at the two farthest sides of the floor to be able to capture torsional modes. The location of the accelerometers were selected similar for all floors. A triaxial accelerometer was placed on the ground floor and a GPS antenna was located at the roof level. At the roof floor no accelerometers were placed since only 12 channels were available.

Locations of the accelerometers on 2nd floor can be seen in Figure 2.17.

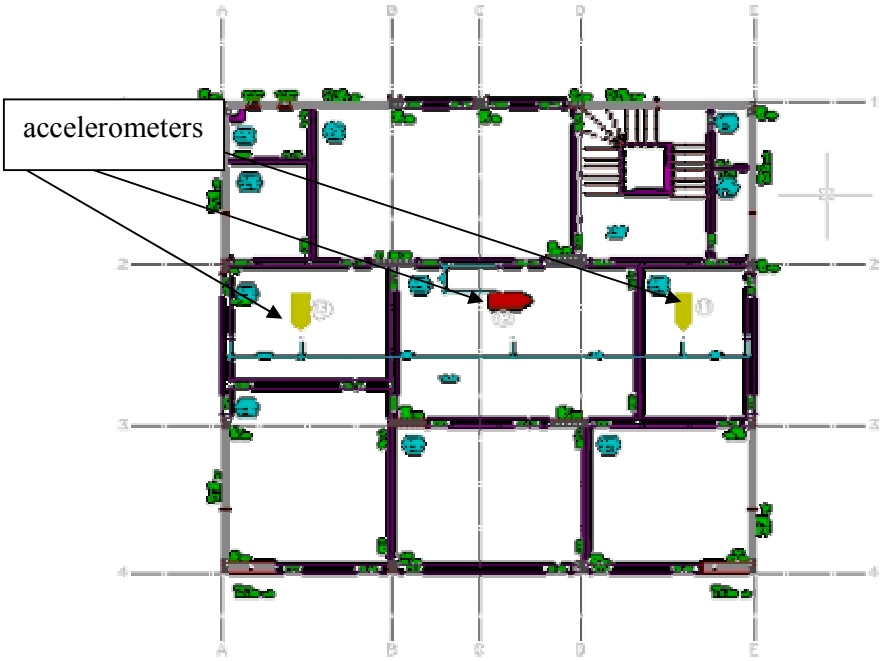

Figure 2.17 AutoCAD view of the located sensors on 2nd floor
(Sensors are not scaled in that drawing. They enlarged to be seen clearly.)

The locations of the accelerometers were decided first and then the design drawings were sent to Istanbul. Cable lengths were determined. Sufficient lengths of cables and GPS were sent to Istanbul. Cable ways (Figure 2.18) for every story were prepared and the GPS was located at roof by a technical team.

Figure 2.18 Prepared cable ways

For the instrumentation of the sensors and data acquisition system research team went to Istanbul. First step of the instrumentation process of that journey was the placement of the analog accelerometers. For that step, some boards of the suspended ceiling were moved for each story and an unexpected situation was perceived. Accelerometers had been planned to locate the adjacent to the outer walls of the building but a lot of pipes were placed adjacent to the outer walls inside the suspended ceiling. Therefore analog accelerometers were located possible closest points to the outer walls. Because of that situation, some assumptions were made while analyzing the mode shapes of the building in Artemis software.

To install the analog accelerometers, screw cells were opened by using a drill. Then using three screws, accelerometers were fastened to the ceiling and then connected to the prepared cable. Works which were done to install an accelerometer is seen in Figure 2.19.

Figure 2.19 Installation of an accelerometer

Installation process was repeated for twelve accelerometers. Except one of them, accelerometers were stayed inside the suspended ceiling. One was located in archive room and there was no suspended ceiling in that room (Figure 2.20).

Figure 2.20 The accelerometer in archive room

After the installation of analog accelerometers, triaxial accelerometer was located on the ground floor. Then every cable which was coming from the sensors was connected to the data acquisition system and necessary configurations were made in Scream software.

Most important problem was the connection between data acquisition system's laptop and our computers; therefore remote connection was established as the last step. In the network connections part of the notebook computer, dial-up options were created (Figure 2.21).

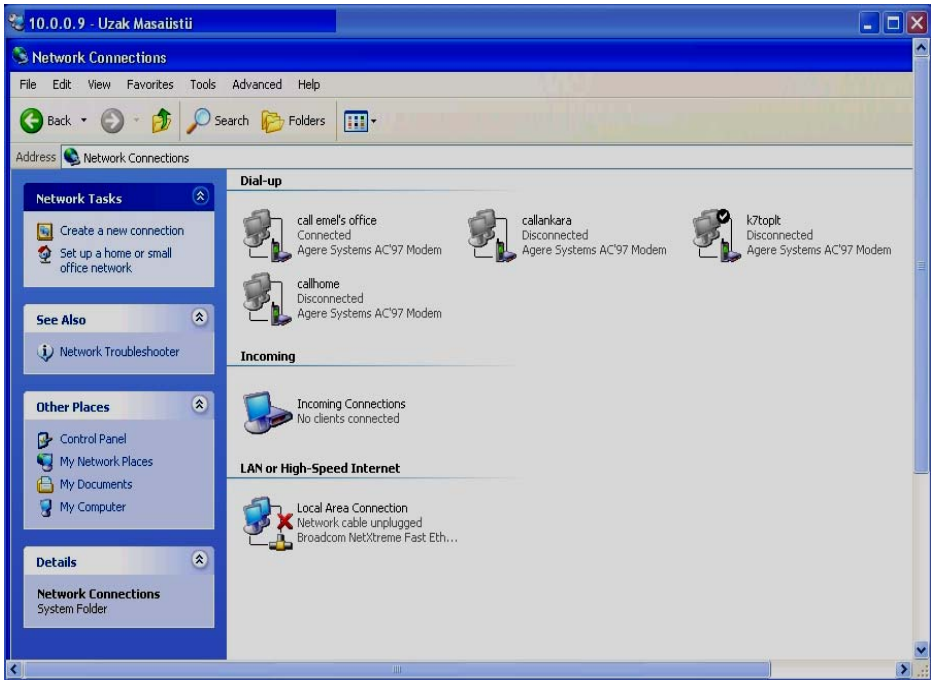

Figure 2.21 Network connections of the data acquisition system

During the connections, the data acquisition system was dialed up by our computer and then an order to the laptop of the data acquisition system to call back our connected computer was given and the connection was stopped. Lastly, when the laptop of the data logger dialed-up our computer, connection was accepted so the remote connection was completed. That procedure was repeated for every remote connection.

2.3. Post Processing of Measured Data

2.3.1. Artemis Software

The Artemis name stands for Ambient Response Testing and Modal Identification Software. Artemis Extractor software which used in that study includes both frequency and time domain techniques for estimation of all modal parameters (Artemis manual).

2.3.1.1. Configuration File

In the first step experimental structure and recorded data must be introduced to the Artemis Software. For that step Configuration File (SVS) is used. While creating a new project in a SVS File format of the Artemis Software, geometry of the experimental structure in line and node definitions, measured data as well as the sampling interval used in the data acquisition system, DOF information relating to the geometry and slave node equations (to make the complete geometry move in an animation when measurements have not been taken in all nodes of the geometry) are required (see Appendix A).

In the configuration file, firstly the sampling interval ($\Delta T=1/f$) must be given to the software then the skeleton of the building was introduced by defining the nodes and lines. Since each story was divided into two parts by the transducers, two surfaces were created for the skeleton of the building. If the transducers had been placed on the corners of the structure, the division would not have needed. Nodes were loaded to the configuration file according to their x, y and z coordinates and also lines were defined between the nodes. In the next step, surfaces were created inside the floor lines.

In the setups part, recorded data text file was loaded to the configuration file. In the scream software every channel's recorded data had been stored separately and also had been stored in GCF file format. As mentioned in the Scream Software part, all the data were converted from GCF file format to the UFF file format and saved as text file. But in the Artemis Software all the channel's readings which were recorded in the same time interval must be saved in a same text file. Consequently, the channel's readings were loaded to the MATLAB and combined in order as a matrix according to their channel numbers. After that, they were saved as a text file. The important point is that every channel's readings must be in an equal length; by the other say they must have equal numbers of columns.

Located nodes and the directions of the transducers were defined in the following line of the configuration file text format. The transducers in the

configuration file and the transducers in the recorded data text file must be in the same order. A project geometry which was created according to the inputs of the configuration file by Artemis was seen in Figure 2.22.

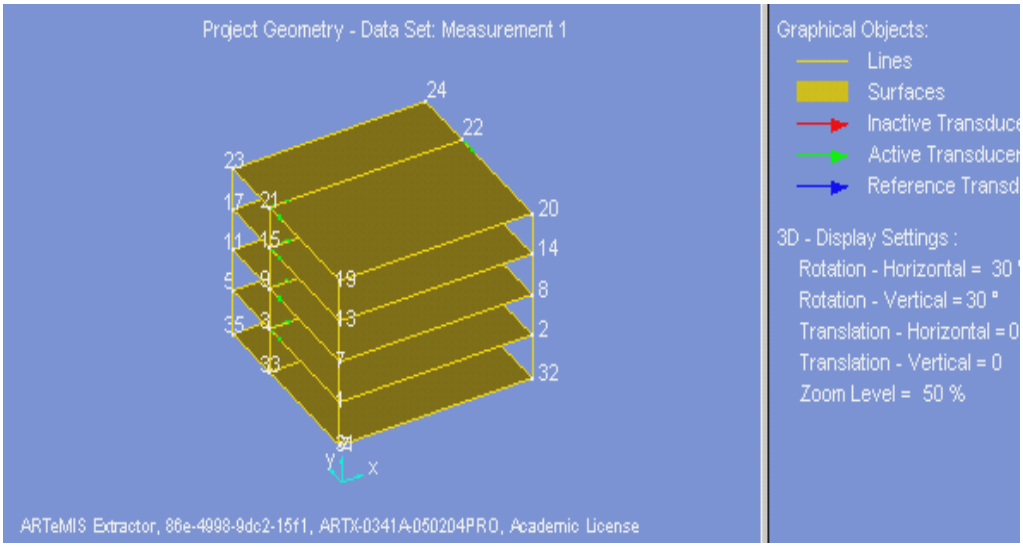

Figure 2.22 Project Geometry of the experimental building in Artemis

After all these steps, slave node equations were created. Slave node equations can be used for definitions of rigid body motions and slave nodes. This is very helpful when the mode shapes are animated. Since the measurements are only available in few nodes of the geometry, the equations are used to make the complete geometry move. During our experimental study, readings were taken only from the placed transducers' nodes therefore in Artemis Software the only known movements were gained in transducers' nodes. But for each story six nodes were exist in the configuration file and the movements of two nodes were known. Consequently slave node equations were used to combine every node's movements to each other. As seen from the Figure 2.22, the movements in x and y directions of the 21st, 15th, 9th, 3rd nodes and the movements in y direction of the 22nd , 16th ,10th , 4th modes were known by the experimental studies.

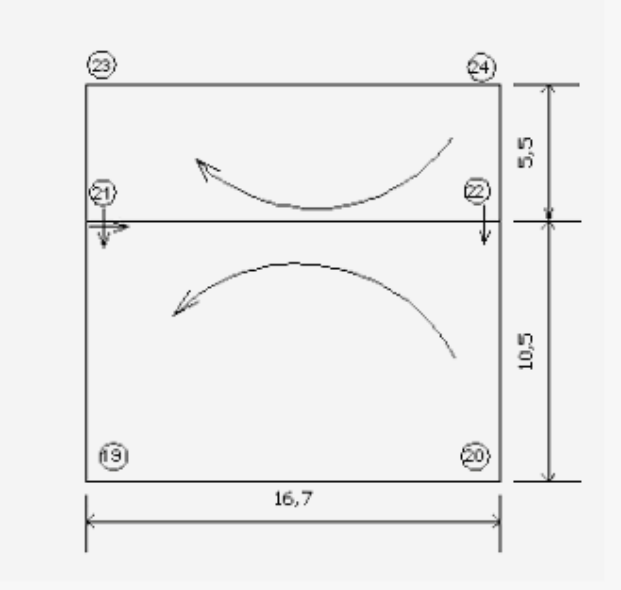

Figure 2.23 Skeleton of 4th story as AutoCAD drawing

Slave node equations will be explained by using the 4th floor's nodes. Accelerometers were located on the 21st joint and 22nd joint of the Figure 2.23. In the equation line of the configuration file, nodes were defined according to their number and direction. Direction x is represented as 1 and y is represented as 2. As seen from the Figure 2.23, the movement of 19th node in y direction is equal to the movement of 21st node in y direction and it was shown as node (19, 2) =node (21, 2) in the slave node equation line of the configuration file. By using the same assumption other equations in y direction were written as node(23,2)=node(21,2), node(20,2)=node(22,2), node (23,2)=node(22,2). Also the movement of 22nd node in x direction is equal to the movement of 21st node in x direction and it was shown as node (21, 1) =node (22, 1). Important point is that, while creating the slave node equations in the configuration file, unknown movement must be written to the left side of the equation and the known movement by the other say transducer's movement must be written at the right side of the equation. As seen from the Figure 2.23, more complicated equations were needed to gain the movements of 23rd, 24th, 19th and 20th nodes in x directions because in these lines no transducer in x direction was existed. Therefore in the first step deformation angle (θ) was defined;

$$\theta = ((node22,2) - node(21,2))/16.7 \qquad (2.1)$$

The deformation in the x-direction of the corners of the fourth floor was calculated in Eqn.2.2 and Eqn. 2.3 for 19th and 23rd joints ;

$$node(19,1) = node(21,1) + 10.5 \times \theta \qquad (2.2)$$

$$node(23,1) = node(21,1) - 5.5 \times \theta \qquad (2.3)$$

In the Eqn. 2.2 and 2.3, the movement was described by two displacements and one angle. In all these equations a simple logic was used. That logic is an assumption which accepts the floor movements as a rigid body movement.

As mentioned in the experimental study part, analog accelerometers were located on the possible closest points to the outer walls. But according to the Artemis software's work discipline they had been adjacent to the outer walls. Therefore two assumptions were made during the analysis. Firstly the accelerometers were assumed to be adjacent to the outer walls and the length of the longitudinal wall was remained as 16,7m, then the analysis was completed according to that assumption. Secondly, the length of the wall was reduced according to the accelerometer's locations and the longitudinal wall's length was assumed 13,7m. Both assumptions were applied on the experimental readings of 6th June and the analysis was done on a 0-10 Hz frequency range.

Table 2.1. MAC matrix between two assumptions

MAC	3,156459Hz	5,271049Hz	6,363461Hz	7,724195Hz	8,403810Hz
3,134151 Hz	**0,9989**	0,4268	0,9046	0,2792	0,7685
5,287706 Hz	0,4316	**0,9998**	0,6629	0,4657	0,08283
6,379996 Hz	0,8983	0,6318	**0,9973**	0,1488	0,5483
7,714590 Hz	0,3028	0,456	0,1462	**0,9976**	0,7049
8,418015 Hz	0,7789	0,07649	0,5522	0,6615	**0,9981**

Table 2.1 shows the modal vector comparisons of the two assumptions. In the comparison part, Modal Assurance Criteria (MAC) was used. Mode shape

vectors are taken from the joints which were determined in Artemis and compared with each other. MAC is a scalar value between 0 and 1. When it gets closer to the unity, that means the compared modes are well-matched. Highlighted values represents the matched modes and their values are nearly 1. That means they matched very well and there is no significant difference between two assumptions. Furthermore, any diversity between the frequency values of these analysis did not occurred. Frequency comparison of the captured modes from two analysis which were completed according to two different assumptions and the MAC values of the comparison are given in Figure 2.24 together as a summary.

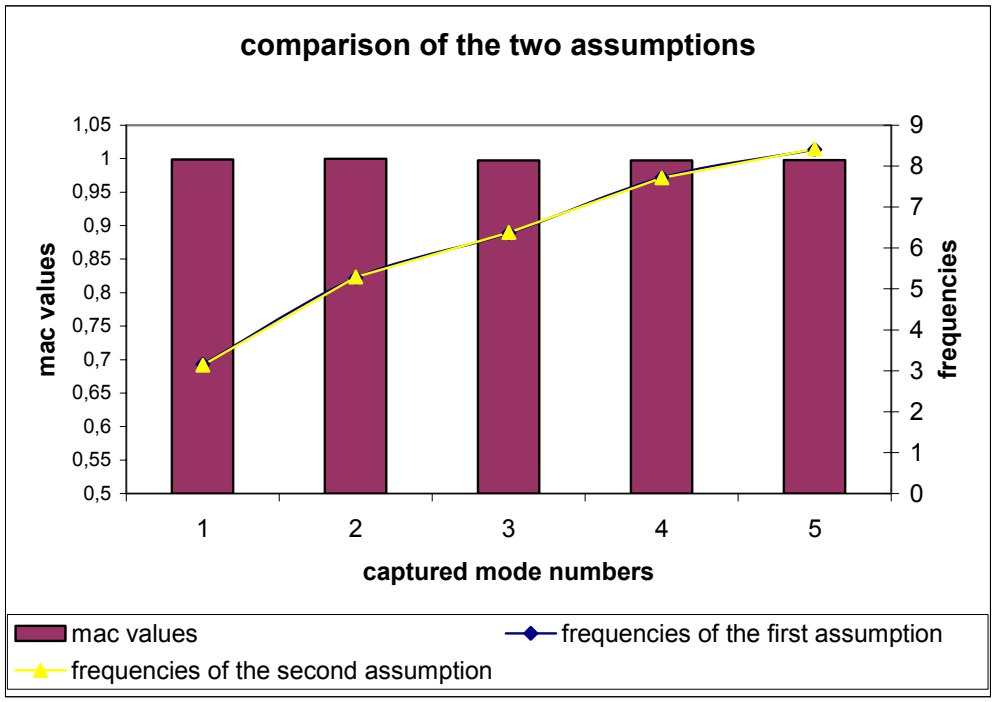

Figure 2.24 Comparison graphic of the two assumptions

2.3.2. Processing Measured Data

Before starting to work on the measured data in Artemis Software, data processing must be completed. Define Signal Processing Configuration option in the software is used to specify basic signal processing like decimation and filtering of the signals.

The first signal processing to perform on the measured data is the decimation. The purpose of decimation is to reduce the frequency range to the frequency range of interest (Artemis manual).

The second signal processing is filtering which used to shape the signal in the frequency domain. In the Artemis software low-pass, high-pass, band-pass and band-stop filter types are existed. These filter options are helpful to investigate the data on different frequency ranges. For example by using band-pass filter, 10-25Hz or 25-50Hz frequency ranges can be selected to work on.

The next step of the Signal Processing Configuration wizard is to configure the spectral density matrices estimation. By changing the number of frequency lines, frequency resolution parameter is selected. To get more smooth spectral densities and more accurate mode shape estimations, number of frequency lines must be chosen less. On the other hand, if more modes are wanted to identify, then much higher number of frequency lines must be chosen. In that study, our aim was identifying more modes therefore higher number of frequency lines (1024) were selected.

For the subsequent step, type and the maximum number of modes must be chosen. In that study, number of structural modes, harmonic modes and noise modes were chosen as 10, 0, and 30 in order. In the analyses captured mode numbers were below the given values. But if the estimation of the modes had turned out to be inaccurate then given numbers of the modes could have been changed.

2.3.3. Modal Identification

Three readings were recorded in separate time intervals during that study, each of them was investigated separately and then they were compared between each other. First reading was recorded on June 6th , second reading were recorded on June 16th and the third one was recorded on July 16th.

Every recorded data were investigated in three parts according to their frequency ranges. Our signal had been sampled at 100 Hz, i.e. 100 samples per second, then the Nyquist frequency was 50 Hz and the spectral density estimates would defined from 0-50 Hz. Then the investigations showed that first modes could not have captured clearly in a huge frequency range like 0-50 Hz. Consequently we were interested in the modal properties under 10 Hz, then we decimated the signal 10 times. Signal was decimated 10 times and that means every 10^{th} sample was kept the rest was discarded. As the result of decimation sampling frequency was 20Hz, nyquist frequency was 10Hz and sampling interval was 0,05s.

Investigations were done in 0-10 Hz frequency range and five modes were captured from that study. Since five modes are inadequate to understand the structure's behavior, another investigation was done in 10-25 Hz frequency range. To investigate the structure in the given frequency range, high-pass filter type was used and also decimation factor was chosen as 2. Another investigation was done in 25-50 Hz frequency range to see all the modes captured from the experimental study. At the end results of the three analyses were combined.

2.3.3.1. Modal Identification in 0-10Hz Frequency Range

In the Artemis software, two model identification techniques are available, one is Stochastic Subspace Identification and the other is Frequency Domain Decomposition. Frequency Domain Decomposition Technique is a peak picking method and in that study it did not used. During the analytical study Stochastic Subspace Identification Technique was used. In the SSI (Stochastic Subspace Identification) techniques a parametric model is fitted directly to the raw series data returned by the transducers. A parametric model is a mathematical model with some parameters that can be adjusted to change the way the model fits to the data. In general a set of parameters that will minimize the deviation between the predicted system response (predicted transducer signal) and measured system response (transducer signal) are looked for (Artemis manual). In Artemis Extractor there are three different implementations of SSI technique: Unweighted Principal Component

(UPC), Principal Component (PC), and Canonical Variate Analysis (CVA). All known time domain modal identification techniques can be formulated in a generalized form as an innovation state space formulation where the A-matrix contains the physical information, the C-matrix extracts the information that can be observed in the system response and the K-matrix contains the statistical information. The statistical information allows for a covariance equivalent modeling, so that the model can have the correct correlation function and thus also the correct spectral density functions (Artemis manual).

$$\tilde{x}_{t+1}=A.\tilde{x} + K.e_t \qquad (2.4)$$

Equation 2.4 refers the state equation and models the dynamic behavior of the physical system and equation 2.5 refers the observation (output) equation, since this equation controls which part of the dynamic system that can be observed in the output of the model.

$$\tilde{y}_t=C.\tilde{x} + e_t \qquad (2.5)$$

In order to estimate A and C, the extended observability matrix Γ_i must be estimated. The estimation of this matrix can be done in different ways and results in that several stochastic subspace identification techniques exist. The only significant difference between the three different stochastic subspace algorithms is the choice of the weight matrices $\boldsymbol{W}_1$ and $\boldsymbol{W}_2$ by the other say estimation of observability matrix Γ_i (Artemis manual).

As mentioned earlier, three algorithms (UPC, PC, CVA) of the SSI techniques aim to find the true model order by using parametric model estimation. A stabilization diagram (Figure 2.25) is created by these three algorithms. Estimation of the state space models is represented in frequency domain in the stabilization diagram. Frequency axis ranging from 0 to the Nyquist frequency of the selected frequency range is represented in the horizontal axis. Dimensions of the available

state space models are listed in the vertical axis. Maximum state space dimension was selected as 80 in all analysis of that study.

State space model is automatically generated by the Artemis software and manually selected. The software has windows that enable comparison of experimentally measured data and syntactically generated data based on the state space model selection. The regenerated curves should successfully match the experimentally measured curves as a measure of proper state space selection. Another state space model selection technique is examining the repeating structural mode trend at subsequent state spaces. If a repeated trend is observed at a resonant frequency, it is a strong indicator that a structural mode has been estimated.

Three kinds of modes were captured in the software: stable modes, unstable modes, and noise modes, which are seen in the stabilization diagram (Figure 2.25) with red plus sign, green cross, and yellow cross, respectively. If the maximum allowed deviation of the natural frequency, damping ratio, Modal Assurance Criteria (MAC) of the mode shape vector and MAC of the initial modal amplitude vector of the captured mode are less than the specified maximum allowed deviations when compared with one of the modes of the previous model, then the mode is called a stable mode and marked with red color. If the deviations of the above requirements are greater than the specified maximum allowed deviations then the mode is called unstable and marked with green color. Both of the mode types are called structural modes. However, noise modes are occurred in the analysis because of limited data records and the non-linearity of the system. Generally, noise modes are spread in a non-systematic and non-repeated way. Since they are usually very heavily damped and structural modes are usually lightly damped, noise modes are excluded from the analysis (Artemis manual).

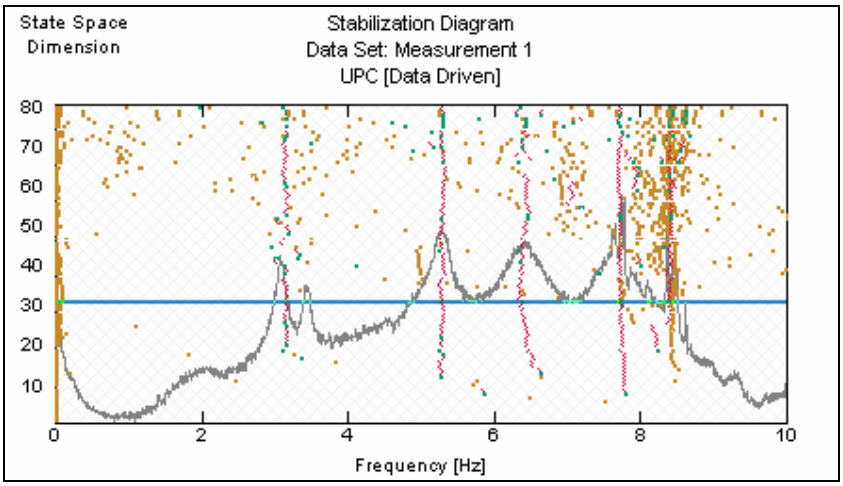

Figure 2.25 An example for the stabilization diagram of Artemis software

After estimating the state space model according to the repeated trend of the structural modes in stabilization diagram, selected state space model must be controlled by using Validate Response Prediction option in Artemis software (Figure 2.26). The magnitude of the spectral density of the measured data is represented by the green curve and the magnitude of the spectral density of the state space model is represented by the red curve in the diagram. When the red curve covers the green curve that means estimated state space model is the true model and the analysis can be continue by using that state space model.

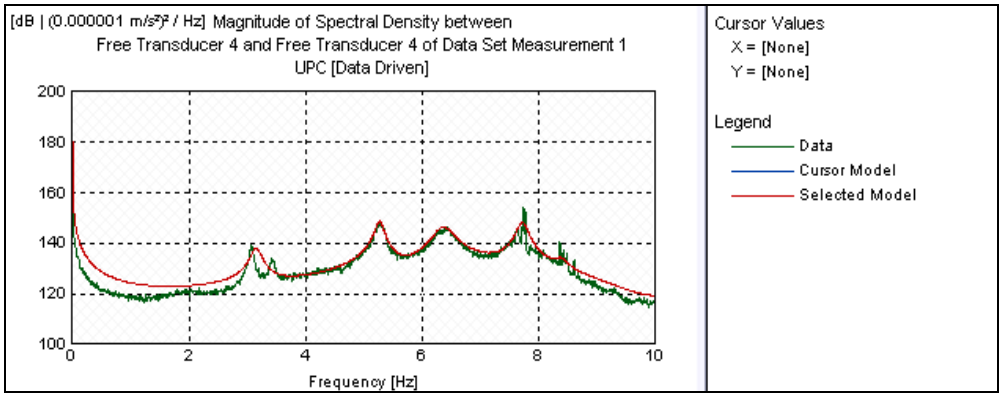

Figure 2.26 An example of Validate Response Prediction option

First recorded data (June 6th), second recorded data (June 16th) and the third recorded data (July 16th) were investigated separately in 0-10 Hz frequency range

and they were investigated by using three Stochastic Subspace Techniques (UPC, PC, and CVA). These three data sets were recorded in 2005.

Table 2.2. Frequency and damping values of captured modes from UPC,PC,CVA algorithms of the first recorded data

	UPC		PC		CVA	
	frequency(Hz)	*damping(%)*	*frequency(Hz)*	*damping(%)*	*frequency(Hz)*	*damping(%)*
mode1	**3,156**	2,75	**3,124**	2,138	**3,14**	2,956
mode2	**5,271**	1,277	**5,288**	1,289	**5,278**	1,27
mode3	**6,363**	2,502	**6,403**	2,645	**6,399**	2,842
mode4	**7,724**	1,087	**7,722**	0,9792	**7,721**	1,174
mode5	**8,404**	1,439	**8,442**	0,5481	**8,347**	2,166

Frequency and damping values of the captured modes from UPC, PC, CVA algorithm results of the first recorded data are given in the Table 2.2. Same modes were gained from three different algorithms since frequency and damping values of these modes are very close to each other. Comparison of the frequency values of the captured modes which were determined by using UPC, PC and CVA algorithms separately are seen in Figure 2.27.

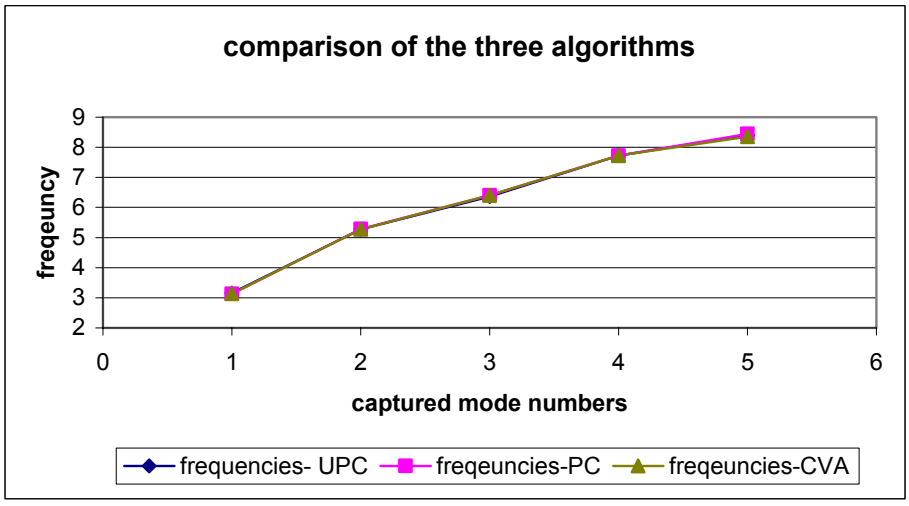

Figure 2.27 Comparison of the frequency values of the modes which were determined by analyzing first data set with UPC, PC and CVA algorithms

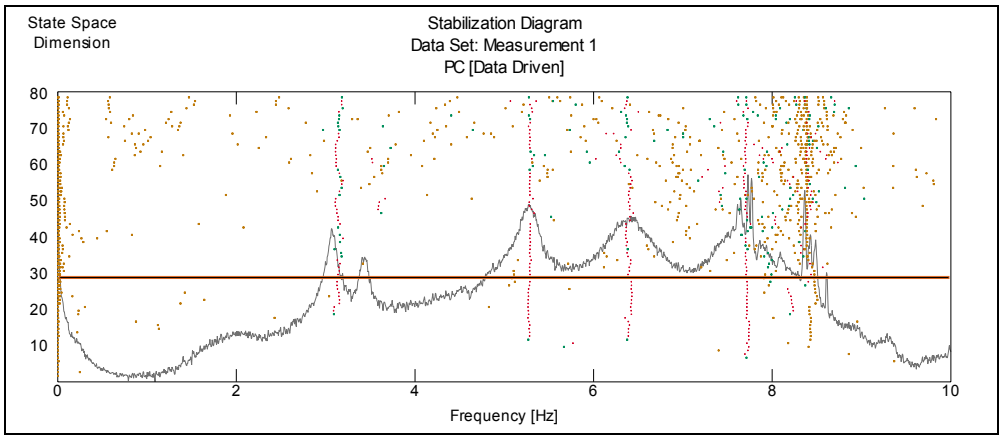

Figure 2.28 Captured modes from PC algorithm on first data set in the stabilization diagram

Repeated trend of the structural modes which were captured from PC algorithm by analyzing the first data set is seen in Figure 2.28.

In Figure 2.29, 2.30 and 2.31, the modes which were captured according to the state space model estimation are seen for three different algorithms. In these graphs, vertical axis represents the data set number and the horizontal axis refers to the interested frequency range. One data set was used in all the analysis of that study. If the records had been collected from two different data sets by using reference sensors, captured modes of the two data sets would have been compared with each other and the common captured modes should be selected as the results.

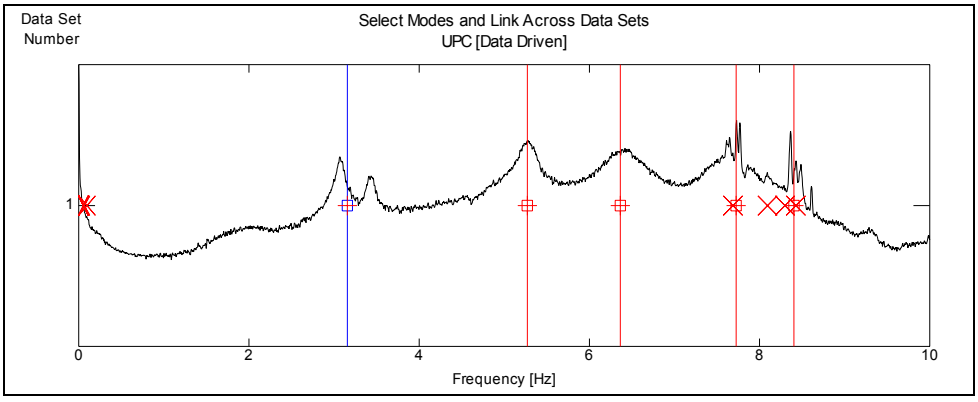

Figure 2.29 Captured modes from UPC algorithm on first data set

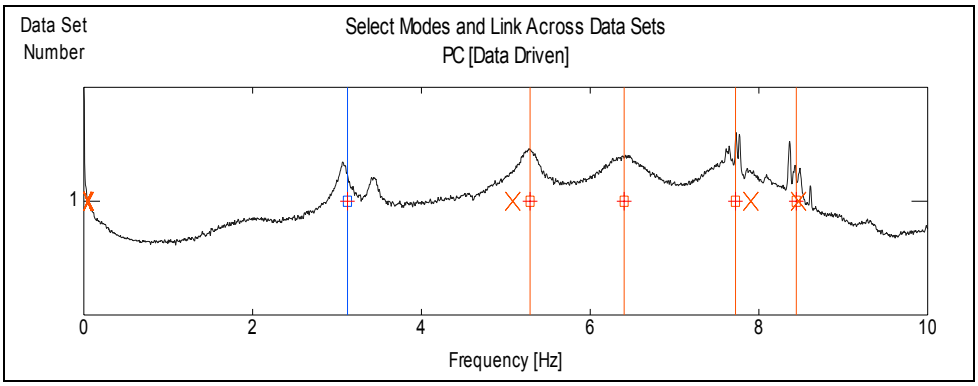

Figure 2.30 Captured modes from PC algorithm on first data set

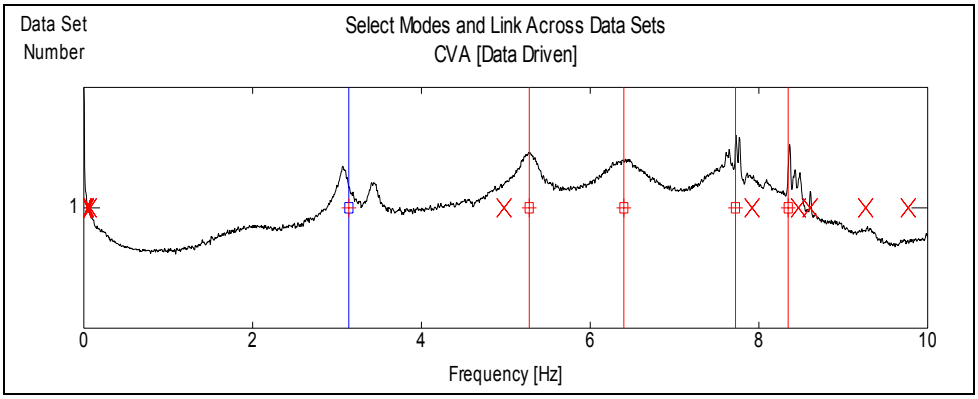

Figure 2.31 Captured modes from CVA algorithm on first data set

The mode shapes captured from the UPC, PC, CVA algorithms were compared between each other. In the comparison part, Modal Assurance Criteria (MAC) was used. MAC is based on a comparison between an experimentally measured mode shape from using one algorithm,$\{\psi x\}$, and an experimentally measured mode shape from using another algorithm, $\{\psi a\}$. MAC is defined in Equation 2.6.

$$MAC(a,x) = \frac{\left[(\psi x)^T \cdot (\Psi a)\right]^2}{\left[(\psi x)^T \cdot (\Psi x)\right] \cdot \left[(\psi a)^T \cdot (\Psi a)\right]} \qquad (2.6)$$

Table 2.3. MAC matrix between UPC algorithm and PC algorithm results of first data set

MAC	3,123943Hz	5,288132Hz	6,403211Hz	7,222117Hz	8,442327Hz
3,156459 Hz	**0.9996**	0.4251	0.9027	0.3453	0.7546
5,271049 Hz	0.4369	**0.9999**	0.6468	0.4419	0.07504
6,363461 Hz	0.8993	0.6554	**0.9998**	0.1168	0.4936
7,724195 Hz	0.2933	0.4632	0.1444	**0.9964**	0.729
8,403810 Hz	0.7656	0.08982	0.5445	0.7378	**0.9956**

MAC matrix between UPC and PC algorithm results of first data set are seen in Table 2.3. Five captured modes of the two algorithms are matched very well according to their MAC values and frequency comparison. Their frequency comparison according to the MAC values are seen in Figure 2.32. In the figure, horizontal axis refers to the matched mode numbers, left side vertical axis represents the MAC values and the right side vertical axis represents the frequency values in Hz.

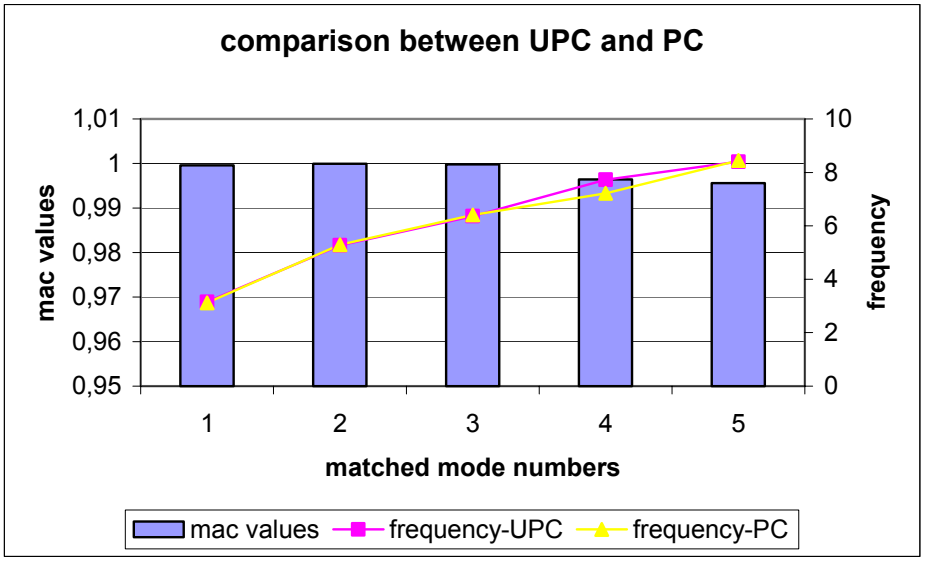

Figure 2.32 Comparison between frequencies of the matched modes of UPC and PC algorithms of first data set according to their MAC values

Same comparisons were repeated to compare the other algorithms between each other. Results are shown in Table 2.4 and Figure 2.33.

Table 2.4. MAC matrix between UPC algorithm and CVA algorithm results of first data set

MAC	3,140233Hz	5,277736Hz	6,398936Hz	7,721481Hz	8,347017Hz
3,156459 Hz	**0.9999**	0.4257	0.8983	0.3379	0.7602
5,271049 Hz	0.4307	**0.9999**	0.6581	0.4513	0.08356
6,363461 Hz	0.8992	0.6552	**1**	0.1075	0.5276
7,724195 Hz	0.293	0.4619	0.1537	**0.998**	0.6761
8,403810 Hz	0.7689	0.08707	0.5339	0.7018	**0.9994**

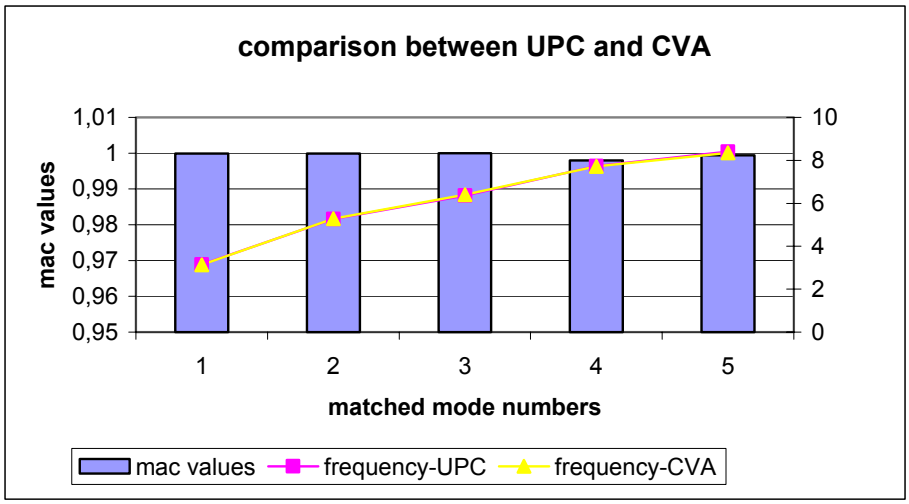

Figure 2.33 Comparison between frequencies of the matched modes of UPC and CVA algorithms of first data set according to their MAC values.

Five modes were captured in the modal identification of 0-10 Hz frequency range by using first data set. First data set is a two hours continuous reading which was recorded on June 6th at 11:00AM-01:00PM. June 6th was Monday and the minimum and maximum temperature levels reported by the meteorology was 15ºC and 25ºC, respectively. The modes which had damping ratios less that 5% were concerned during the analysis and five modes were captured from the analysis.

Since UPC, PC and CVA algorithms gave the same results, reliability of the captured modes were proved for the records which were taken on June 6th.

Same procedure was applied to the second data set. It is a one hour continuous reading which was recorded on June 16th at 5:25PM-6:25PM. June 16th was Thursday and the minimum and maximum temperature levels reported by the meteorology was 17ºC and 27ºC, respectively. In that analysis, the modes which had damping ratios less that 5% were concerned too and four modes were captured from the analysis.

Frequency and damping values of the captured modes from three algorithms for the second data set in 0-10Hz frequency range are given in Table 2.5 and the frequency comparison is plotted in Figure 2.34.

Table 2.5. Frequency and damping values of captured modes from UPC, PC,CVA algorithms of second data set

	UPC		**PC**		**CVA**	
	frequency(Hz)	*damping(%)*	*frequency(Hz)*	*damping(%)*	*frequency(Hz)*	*damping(%)*
mode1	**3,213**	3,63	**3,215**	3,231	**3,182**	2,737
mode2	**5,223**	1,483	**5,227**	1,501	**5,219**	1,442
mode3	**6,475**	3,235	**6,456**	3,16	**6,459**	3,129
mode4	**7,713**	1,493	**7,702**	1,672	**7,713**	1,55

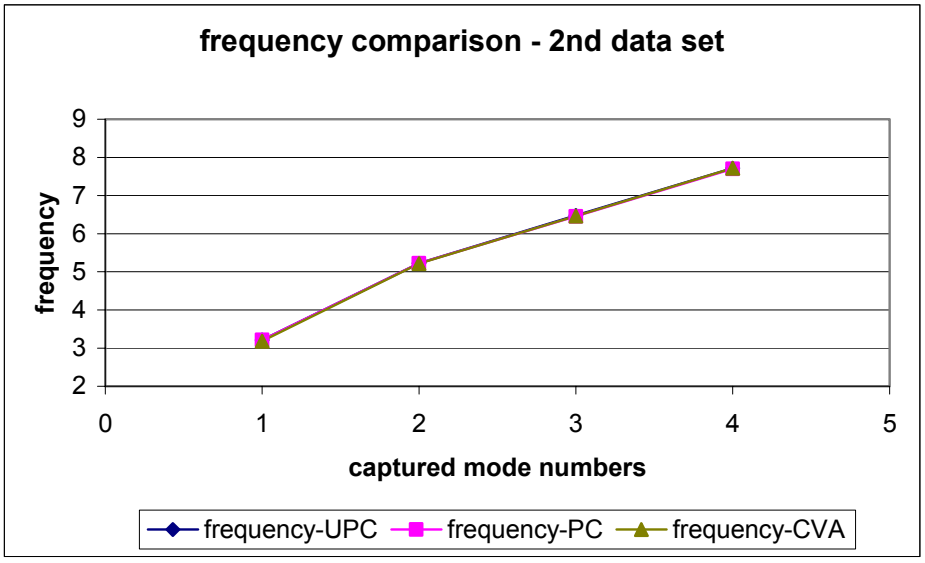

Figure 2.34 Comparison of the frequency values of the modes which were determined by analyzing second data set with UPC, PC and CVA algorithms

MAC matrix between UPC algorithm and PC algorithm results of second data set and UPC algorithm and CVA algorithm results were given in Table 2.6 and Table 2.7 respectively. Furthermore their frequency comparisons according to their MAC values are seen in Figure 2.35 and 2.36.

Table 2.6. MAC matrix between UPC algorithm and PC algorithm results of second data set

MAC	3,215Hz	5,227Hz	6,456Hz	7,702Hz
3,213Hz	**0.9998**	0.424	0.845	0.569
5,223Hz	0.4281	**1**	0.6734	0.3987
6,475Hz	0.8479	0.6717	**0.9997**	0.08589
7,713Hz	0.5844	0.386	0.1045	**0.9993**

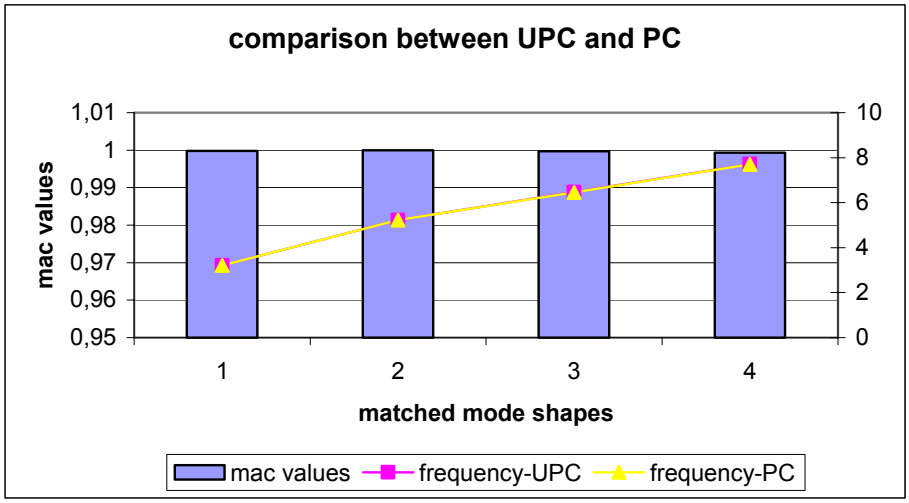

Figure 2.35 Comparison between frequencies of the matched modes of UPC and PC algorithms of second data set according to their MAC values

Table 2.7. MAC matrix between UPC algorithm and CVA algorithm results of second data set

MAC	3,182Hz	5,219Hz	6,459Hz	7,713Hz
3,213Hz	**0.9995**	0.4197	0.8413	0.5855
5,223Hz	0.4194	**0.9999**	0.6699	0.3842
6,475Hz	0.8516	0.6696	**0.9995**	0.1018
7,713Hz	0.5828	0.3884	0.09324	**0.9998**

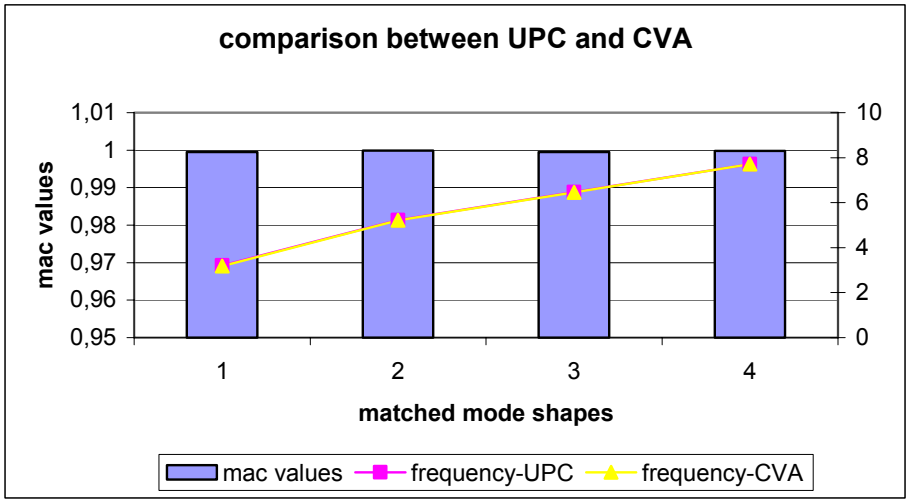

Figure 2.36 Comparison between frequencies of the matched modes of UPC and CVA algorithms of second data set according to their MAC values

Three different algorithms of the SSI technique captured the same modes with closer frequency and damping values for the second data set as seen from the below tables and figures. Consequently, result modes of second data set for 0-10 Hz frequency range were correlated by three algorithms.

Third data set was stored on July 16th and was two hours long. July 16th was Saturday and the weather was rainy on that day. The minimum and maximum temperature levels reported by the meteorology was 19ºC and 27ºC, respectively. The modes which had damping ratios less that 5% were take into consideration during the analysis of the third data set in 0-10 Hz frequency range since higher damping ratios are assumed to belong to noisy modes. Four modes were captured from the third data set. Frequency and damping values of the captured modes from the three algorithms and their frequency comparison graphic are given in Table 2.8 and Figure 2.37 respectively.

Table 2.8. Frequency and damping values of captured modes from UPC, PC,CVA algorithms of third data set

	UPC		PC		CVA	
	frequency(Hz)	*damping(%)*	*frequency(Hz)*	*damping(%)*	*frequency(Hz)*	*damping(%)*
Mode1	**3,266**	2,122	**3,263**	2,207	**3,264**	2,244
Mode2	**5,298**	1,255	**5,29**	1,032	**5,304**	1,308
Mode3	**6,543**	2,336	**6,492**	2,182	**6,539**	2,813
Mode4	**7,896**	1,671	**7,904**	1,902	**7,905**	1,939

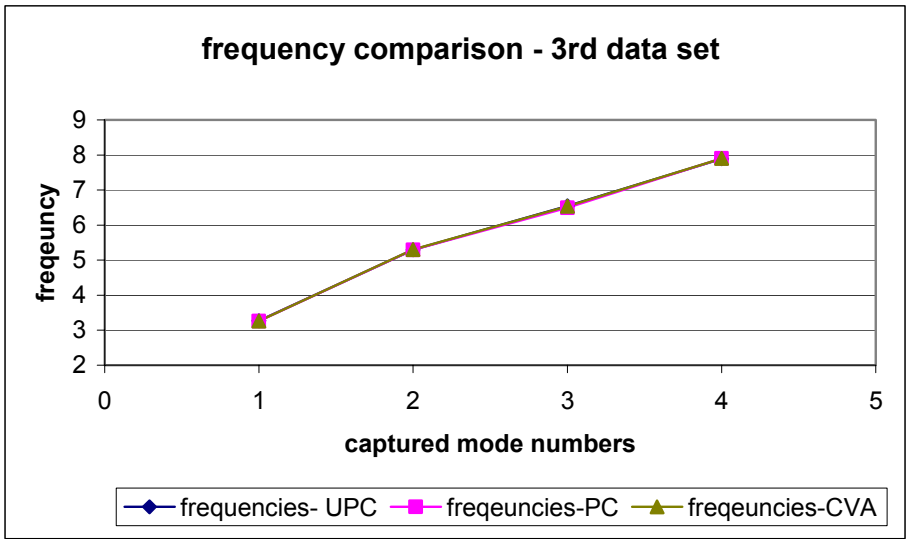

Figure 2.37 Comparison of the frequency values of the modes which were determined by analyzing third data set with UPC, PC and CVA algorithms

Table 2.9. MAC matrix between UPC algorithm and PC algorithm results of third data set

MAC	3,266Hz	5,298Hz	6,543Hz	7,896Hz
3,263Hz	**1**	0.4389	0.8474	0.4898
5,29Hz	0.4465	**0.9998**	0.6961	0.4803
6,492Hz	0.8523	0.6771	**0.9996**	0.04861
7,904Hz	0.4823	0.4955	0.03423	**0.9993**

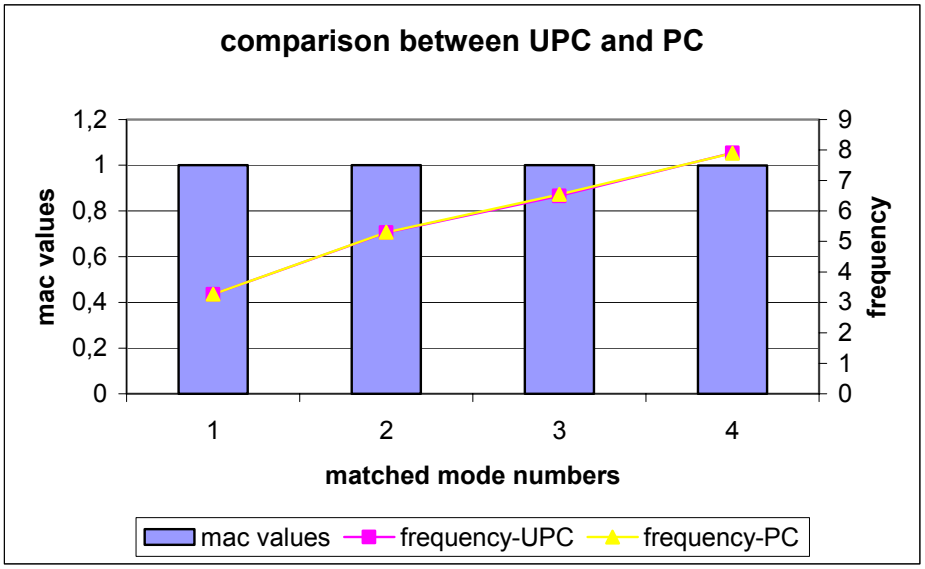

Figure 2.38 Comparison between frequencies of the matched modes of UPC and PC algorithms of third data set according to their MAC values

Table 2.10. MAC matrix between UPC algorithm and CVA algorithm results of third data set

MAC	3,266Hz	5,298Hz	6,543Hz	7,896Hz
3,264Hz	**0.9999**	0.4562	0.8579	0.4885
5,304Hz	0.4506	**0.9998**	0.6862	0.4801
6,539Hz	0.8542	0.6863	**0.9993**	0.05638
7,905Hz	0.4769	0.4799	0.02671	**0.9984**

MAC matrix between UPC algorithm and PC algorithm results of third data set and UPC algorithm and CVA algorithm results were given in Table 2.9 and Table 2.10 respectively. Furthermore, their frequency comparisons according to their MAC values are seen in Figure 2.38 and 2.39. As seen from the tables and the graphs, captured modes are matching with each other.

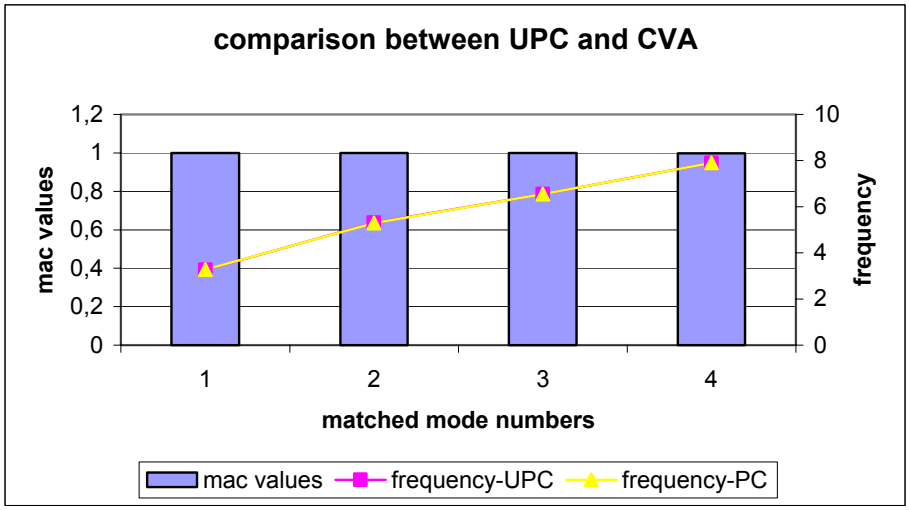

Figure 2.39 Comparison between frequencies of the matched modes of UPC and CVA algorithms of third data set according to their MAC values

After the comparison of data sets separately, PC algorithm results of three data sets were compared with each other to capture the accurate mode shapes in 0-10 Hz frequency range. PC algorithm modes in 0-10 Hz frequency range were determined as the result modes for every data set.

Table 2.11. MAC matrix between PC algorithm results of first and second readings

MAC	3,215Hz	5,227Hz	6,456Hz	7,702Hz
3,124Hz	**0.9991**	0.4145	0.8481	0.571
5,288Hz	0.4447	**0.9997**	0.6807	0.3814
6,403Hz	0.8998	0.6336	**0.9916**	0.203
7,722Hz	0.3512	0.4649	0.2242	**0.9351**
8,442Hz	0.7538	0.1029	0.4516	0.8297

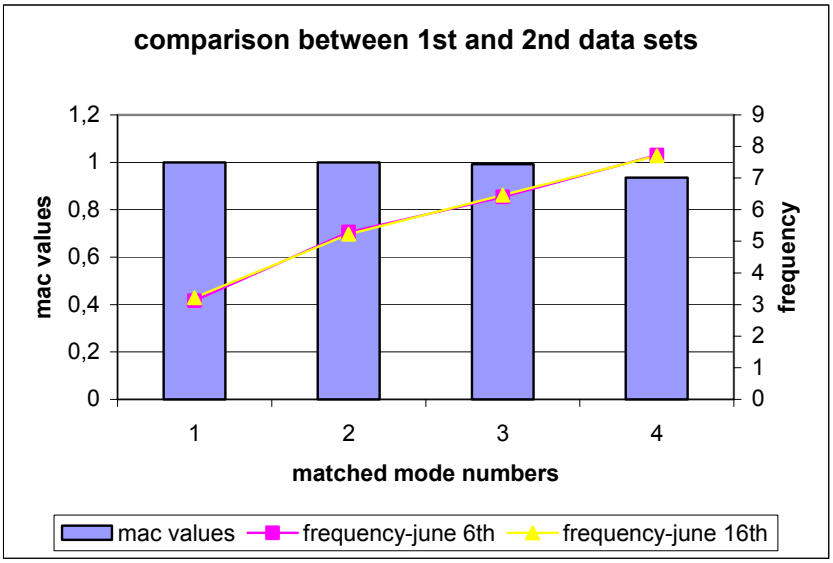

Figure 2.40 Comparison between matching modes of PC algorithms of first and second readings in 0-10 Hz frequency range

First, the captured modes of PC algorithms of first and second data set were compared. The comparison results are shown in Table 2.11 and Figure 2.40. Four modes are matched well. Their MAC values are greater than 0.9 and their frequency values are closer to each other. Graphical form of the MAC matrix is seen in Figure 2.41. The violet color in the graph refers the greater MAC values, that means it refers the well-matched modes of the data sets. Except the first four diagonal modes, third modes of the data sets are matched with the first modes.

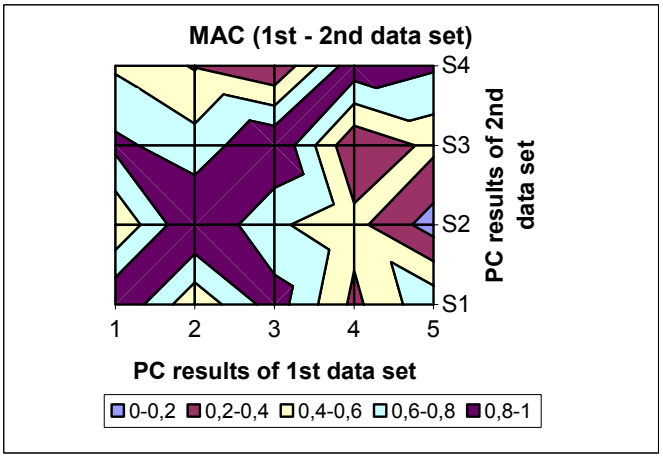

Figure 2.41 Graphical form of the MAC matrix between PC algorithm results of first and second data set

Second, the captured modes of PC algorithms of first and third data set were compared. MAC matrix between PC algorithm results of first and third readings are given in Table 2.12 and the graphical form of that MAC matrix is represented in Figure 2.42. Four modes of the two data sets are matched with higher MAC values. Furthermore, third modes of the data sets are matched with the first modes in that comparison, too. Third mode of the experimental model is similar with the first mode of the experimental mode.

Table 2.12. MAC matrix between PC algorithm results of first and third data set

MAC	3,263Hz	5,29Hz	6,492Hz	7,904Hz
3,124Hz	**0.9371**	0.3609	0.8224	0.4706
5,288Hz	0.3955	**0.9457**	0.6559	0.4761
6,403Hz	0.8583	0.6109	**0.9718**	0.119
7,722Hz	0.3128	0.5261	0.2325	**0.9338**
8,442Hz	0.7419	0.1439	0.4687	0.8038

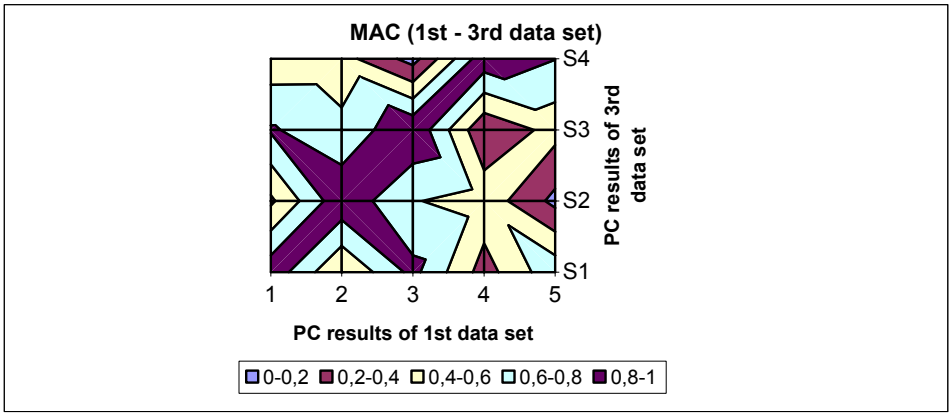

Figure 2.42 Graphical form of the MAC matrix between PC algorithm results of first and third data set

Frequency comparison of the matched modes of PC algorithms of first and third data set is given in Figure 2.43 according to their MAC values.

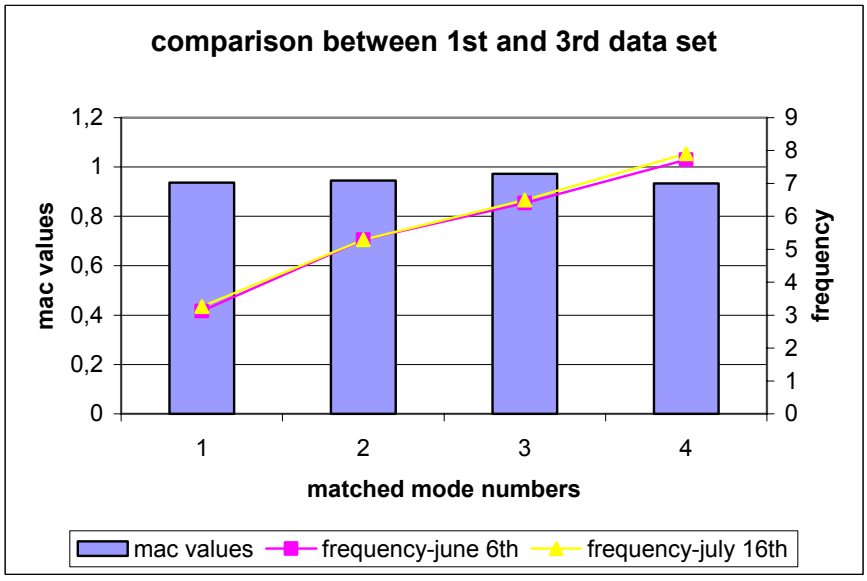

Figure 2.43 Comparison between matching modes of PC algorithms of first and third data set in 0-10 Hz frequency range

The captured modes of PC algorithms of second and third data set were compared as the third step. The comparison results are shown in Table 2.13 and

Figure 2.44. Four modes are matched well with higher MAC values. Graphical form of the MAC matrix is seen in Figure 2.45.

Table 2.13. MAC matrix between PC algorithm results of second and third data set

MAC	3,215Hz	5,227Hz	6,456Hz	7,702Hz
3,263Hz	**0.9341**	0.3723	0.8181	0.465
5,29Hz	0.384	**0.9487**	0.6518	0.491
6,492Hz	0.8125	0.6628	**0.9839**	0.05319
7,904Hz	0.534	0.4445	0.08144	**0.9776**

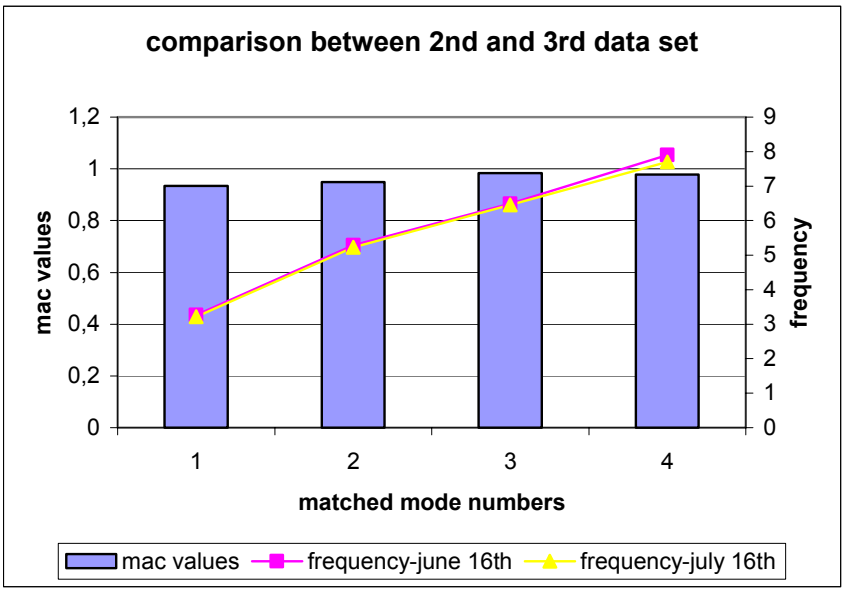

Figure 2.44 Comparison between matching modes of PC algorithms of second and third data set in 0-10Hz frequency range

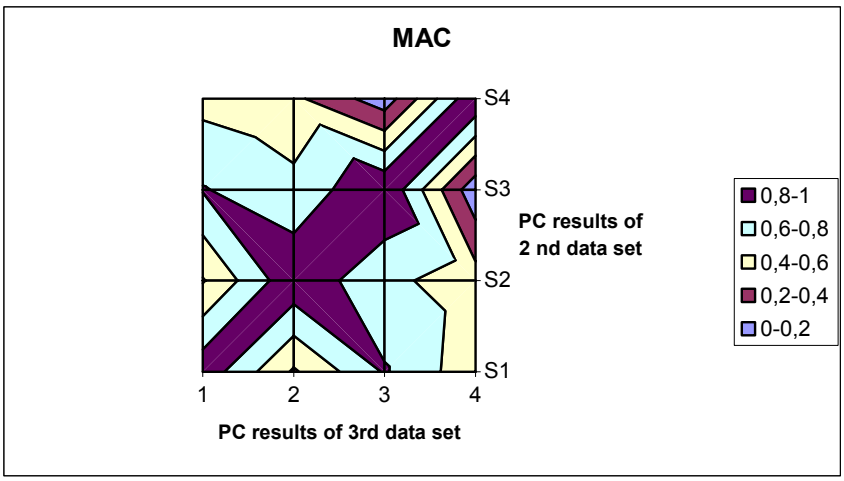

Figure 2.45 Graphical form of the MAC matrix between PC algorithm results of second and third data set

By using first data set, five modes were captured, also by using second and third data set, four modes were captured. And the comparison results showed that same modes were captured by three different data sets. As seen from the graphs and tables, comparisons of the data sets of first and second data set gave greater MAC values than the comparisons of these data sets with third data set. Furthermore, one more mode was captured from the analysis of first data set. Therefore, the mode shapes of the first readings of PC algorithm were accepted as the captured modes from the experimental study in 0-10 Hz frequency range.

2.3.3.2. Modal Identification in 10-25Hz Frequency Range

By working on the recorded data sets in 0-10Hz frequency range only the longitudinal modes were captured. Therefore recorded data on June 6th, June 16th and July 16th were investigated separately in 10-25Hz frequency range to capture the torsional and translational modes using three Stochastic Subspace Techniques (UPC, PC, and CVA).

When the data is processed using 5% and 10% damping ratio limits, majority of the modes that were found to be stable in 10% damping limit has been lost and become unstable for 5% damping ratio limit for the investigation of the first data set

(June 6th) in 10-25Hz frequency range. Therefore the modes which had damping ratios less than 10% were considered in the analysis. Same problem was also faced for the other recorded data sets (June16th, July16th) and the modes which had damping ratios less than 10% were are accepted in those analyses. The damping ratios of the accepted modes using three different SSI techniques are given in Table 2.14. The same table also presents a comparison between the mode numbers and frequencies obtained from the three techniques. Furthermore, each set of mode shapes obtained from UPC, PC, and CVA algorithms are compared using MAC matrices in Table 2.15, Table 2.16, and Table 2.17 for UPC versus PC, UPC verses CVA, and PC versus CVA comparisons, respectively. In MAC comparison tables, the high correlating MAC values are highlighted. Although the bolt color terms are generally larger than 0.8, the divergence of the terms from 1.00 is an indication that all of the modes are not identical, and in some cases, they are quite different. This raises concern on the dependability of different analysis algorithms.

Table 2.14. Frequency and damping values of captured modes from UPC, PC, CVA algorithms of first data set in 10-25Hz frequency range

	UPC		**PC**		**CVA**	
	frequency(Hz)	*damping(%)*	*frequency(Hz)*	*damping(%)*	*frequency(Hz)*	*damping(%)*
Mode6	**11,46**	3,759	**11,49**	4,658	**11,49**	4,62
Mode7	**12,35**	7,074	**12,94**	6,787	**14,22**	6,985
Mode8	**12,99**	6,596	**14,17**	6,259	**15,27**	7,524
Mode9	**14,57**	7,031	**15,22**	4,412	**16,82**	7,805
Mode10	**16,57**	5,935	**16,73**	6,986	**17,55**	8,562
Mode11	**17,64**	4,184	**17,24**	4,76	**18,06**	3,179
Mode12	**18,1**	4,098	**17,92**	2,277	**18,46**	8,54
Mode13	**19,45**	2,145	**19,45**	4,929	**19,49**	2,36
Mode14	**20,39**	2,981	**19,48**	2,397	**19,73**	5,443
mode15			**20,31**	4,136		
mode16			**20,8**	8,365		

Table 2.15. MAC matrix between UPC algorithm and PC algorithm results of first data set in 10-25Hz frequency range

MAC	11,49Hz	12,94Hz	14,17Hz	15,22Hz	16,73Hz	17,24Hz	17,92Hz	19,45Hz	19,48Hz	20,31Hz	20,8Hz
11,46Hz	**0.9931**	0.4632	0.08334	0.08005	0.3015	0.3561	0.2001	0.3635	0.3119	0.1691	0.4273
12,35Hz	0.6292	**0.8442**	0.1752	0.3147	0.5509	0.6552	0.611	0.06597	0.1502	0.2701	0.1947
12,99Hz	0.2441	0.6693	**0.8964**	0.3135	0.4055	0.2953	0.1115	0.3979	0.5524	0.1102	0.1848
14,57Hz	0.1223	0.1015	0.6512	**0.9425**	0.3616	0.2561	0.2947	0.1797	0.2091	0.3527	0.1763
16,57Hz	0.2096	0.2849	0.1951	0.6785	**0.8268**	0.5332	0.37	0.5132	0.2713	0.3623	0.0739
17,64Hz	0.3437	0.6053	0.1553	0.2404	0.5687	0.6638	0.907	0.3387	0.1861	0.2943	0.05318
18,1Hz	0.2323	0.2968	0.295	0.3381	0.5867	0.3392	**0.9419**	0.5604	0.3174	0.4252	0.04162
19,45Hz	0.1759	0.3576	0.5226	0.1058	0.2988	0.2106	0.2391	0.5914	**0.9302**	0.05851	0.2005
20,39Hz	0.05313	0.1777	0.08198	0.2324	0.3113	0.03029	0.4832	0.4672	0.1598	**0.819**	0.1816

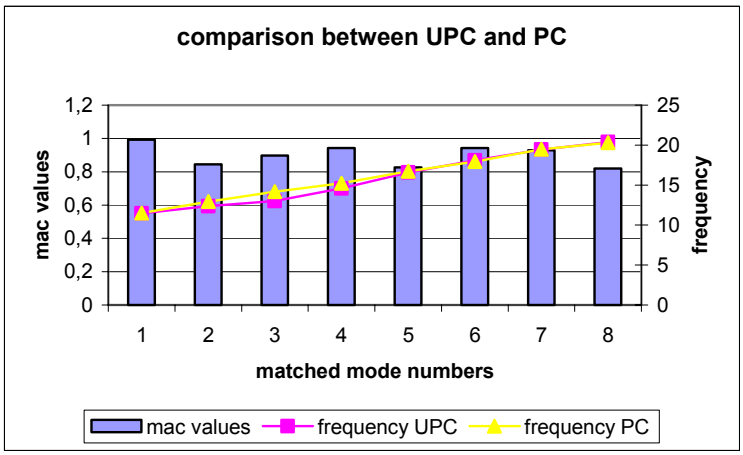

Figure 2.46 Comparison between frequencies of the matched modes of UPC and PC algorithms of first data set in 10-25 Hz frequency range according to their MAC values

Figure 2.46 represents the frequency comparison of the matched modes of UPC algorithm and PC algorithm of first data set in 10-25 Hz frequency range according to their MAC values. Nine modes were captured from UPC algorithm and eleven modes were captured from PC algorithm. Furthermore, eight of them are

matched with MAC values greater than 0.8. Captured mode frequencies are closer to each other.

Table 2.16. MAC matrix between UPC algorithm and CVA algorithm results of first data set in 10-25Hz frequency range

MAC	11,49Hz	14,22Hz	15,27Hz	16,82Hz	17,55Hz	18,06Hz	18,46Hz	19,49Hz	19,73Hz
11,46Hz	**0.9944**	0.09558	0.2216	0.1863	0.3271	0.1465	0.2474	0.2462	0.2472
12,35Hz	0.6145	0.2599	0.128	0.3391	0.5048	0.6083	0.4665	0.3019	0.08859
12,99Hz	0.3476	**0.8952**	0.4573	0.3574	0.5463	0.1367	0.2347	0.4852	0.2829
14,57Hz	0.09919	0.6108	**0.8016**	0.5306	0.2348	0.4275	0.5197	0.201	0.125
16,57Hz	0.2076	0.1465	0.6578	**0.9411**	0.2483	0.5168	0.7725	0.3984	0.4132
17,64Hz	0.2931	0.1446	0.1213	0.3584	0.5993	**0.8191**	0.2502	0.214	0.3677
18,1Hz	0.2216	0.2115	0.3267	0.4421	0.5032	**0.8873**	0.1524	0.03568	0.5535
19,45Hz	0.2418	0.5087	0.2064	0.3201	0.3308	0.1938	0.4256	**0.9012**	0.4596
20,39Hz	0.05791	0.05989	0.1539	0.2645	0.2541	0.5365	0.1439	0.3014	0.5281

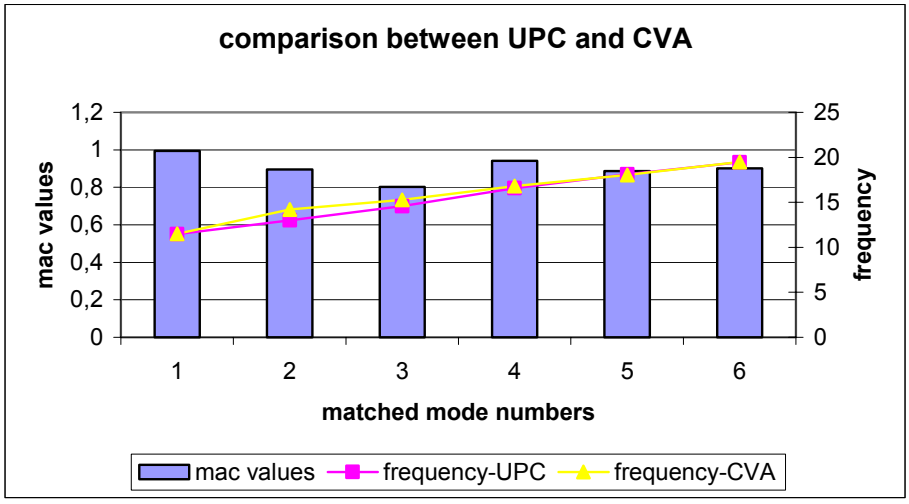

Figure 2.47 Comparison between frequencies of the matched modes of UPC and CVA algorithms of first data set in 10-25 Hz frequency range according to their MAC values

As seen from Table 2.16 and Figure 2.47, six modes are matched with the MAC values greater than 0.8 during the comparison of UPC and CVA algorithms of first data set in 10-25 Hz frequency range. Frequencies of the matched modes are closer to each other. In the comparison of UPC and PC algorithms, 1st, 2nd, 3rd, 4th,5th, 7th, 8th and 9th modes of the UPC algorithm were matched with the PC algorithm modes. However, 1st, 3rd, 4th, 5th, 6th, 7th, 8th modes of the UPC algorithm were matched with the captured modes of the CVA algorithm in the comparison. 6th mode of the UPC algorithm and 2nd mode of the UPC algorithm were not correlated by the two comparisons.

The comparison results between PC and CVA algorithms are given in Table 2.17 and Figure 2.48. Seven modes were well-matched in that comparison. 1st, 3rd, 4th, 5th, 6th ,7th and 8th modes were matched with the captured modes of the CVA algorithm.

Table 2.17. MAC matrix between PC algorithm and CVA algorithm results of first data set in 10-25Hz frequency range

MAC	11,49Hz	14,22Hz	15,27Hz	16,82Hz	17,55Hz	18,06Hz	18,46Hz	19,49Hz	19,73Hz
11,49Hz	**0.9844**	0.07293	0.1994	0.1701	0.2964	0.1835	0.1838	0.2225	0.2178
12,94Hz	0.4953	0.6051	0.2571	0.4389	0.559	0.4875	0.4805	0.4356	0.1132
14,17Hz	0.07563	**0.9596**	0.5079	0.2324	0.3219	0.3028	0.1033	0.3515	0.1735
15,22Hz	0.1148	0.4804	**0.9005**	0.6177	0.1929	0.4576	0.5279	0.1664	0.2671
16,73Hz	0.2516	0.4243	0.5244	**0.9043**	0.07065	0.7393	0.5131	0.3134	0.2781
17,24Hz	0.342	0.2263	0.4578	0.2952	0.7543	0.2472	0.6757	0.3904	0.4385
17,92Hz	0.1729	0.2628	0.2768	0.4993	0.3465	**0.9575**	0.2169	0.065	0.4048
19,45Hz	0.3551	0.2664	0.4217	0.5198	0.4558	0.4429	0.4848	0.4819	**0.8882**
19,48Hz	0.3346	0.4737	0.3399	0.2774	0.3631	0.2381	0.3668	**0.8549**	0.6077
20,31Hz	0.1608	0.2031	0.309	0.3784	0.2149	0.4953	0.4229	0.3293	0.4077
20,8Hz	0.437	0.1451	0.2169	0.1666	0.07254	0.09724	0.157	0.2477	0.4421

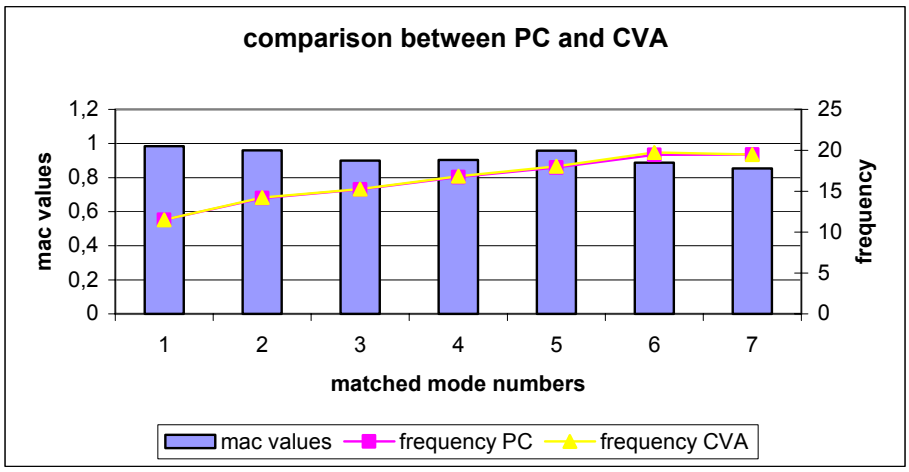

Figure 2.48 Comparison between frequencies of the matched modes of PC and CVA algorithms of first data set in 10-25 Hz frequency range according to their MAC values

As a result, PC algorithms of the first data set gave the greater MAC values in the comparisons and the number of the result modes which were matched with the captured modes of the other algorithms are greater than the number of the results modes of the other algorithms. Since PC algorithm modes of the first data set are accepted as the result modes of the first data set in 10- 25 Hz frequency range.

Table 2.18 presents a comparison between the mode numbers, damping ratios and frequencies obtained from the three techniques for the second data set in 10-25 Hz frequency range. Furthermore, each set of mode shapes obtained from UPC, PC, and CVA algorithms are compared using MAC matrices in Table 2.19, Table 2.20, and Table 2.21 for UPC versus PC, UPC versus CVA, and PC versus CVA comparisons, respectively. The graphical forms of these comparisons are seen in Figure 2.49, Figure 2.50 and Figure 2.51.

Table 2.18. Frequency and damping values of captured modes from UPC, PC,CVA algorithms of second data set in 10-25Hz frequency range

	UPC		**PC**		**CVA**	
	frequency(Hz)	*damping(%)*	*frequency(Hz)*	*damping(%)*	*frequency(Hz)*	*damping(%)*
Mode5	**10,92**	2,613	**11,52**	3,325	**11,55**	4,154
Mode6	**11,49**	4,085	**13,53**	5,476	**12,35**	9,902
Mode7	**12,64**	8,998	**14,51**	4,004	**14,44**	4,341
Mode8	**13,69**	6,578	**16,19**	4,821	**16,11**	9,47
Mode9	**14,52**	5,025	**17,53**	2,838	**17,36**	6,618
Mode10	**15,93**	6,646	**19,43**	2,599	**19,27**	3,972
Mode11	**17,3**	2,711	**20,4**	1,639	**19,92**	4,49
Mode12	**19,24**	2,555	**20,72**	7,12	**20,5**	2,611
Mode13	**20,7**	7,074			**20,8**	5,71

Nine modes were captured from UPC algorithm and CVA algorithm and eight modes were captured from PC algorithm in the analysis of second data set in 10-25 Hz frequency range.

Table 2.19. MAC matrix between UPC algorithm and PC algorithm results of second data set in 10-25Hz frequency range

MAC	11,52Hz	13,53Hz	14,51Hz	16,19Hz	17,53Hz	19,43Hz	20,4Hz	20,72Hz
10,92Hz	0.8929	0.1052	0.0596	0.3497	0.1506	0.2535	0.3763	0.2787
11,49Hz	**0.9838**	0.2996	0.123	0.2617	0.3066	0.1885	0.2854	0.2239
12,64Hz	0.3989	**0.8638**	0.6698	0.1795	0.2792	0.4025	0.2024	0.08608
13,69Hz	0.2042	0.558	0.4234	0.264	0.7264	0.1246	0.2635	0.2052
14,52Hz	0.0817	0.5933	**0.9002**	0.3913	0.3798	0.1404	0.274	0.06418
15,93Hz	0.237	0.6728	0.2161	**0.8506**	0.2279	0.2277	0.4589	0.03193
17,3Hz	0.2059	0.4309	0.2687	0.3746	**0.9485**	0.5305	0.2423	0.1549
19,24Hz	0.2142	0.4198	0.4237	0.2877	0.6848	0.7196	0.2089	0.1716
20,7Hz	0.2133	0.1549	0.07367	0.09959	0.2179	0.177	0.1145	**0.9958**

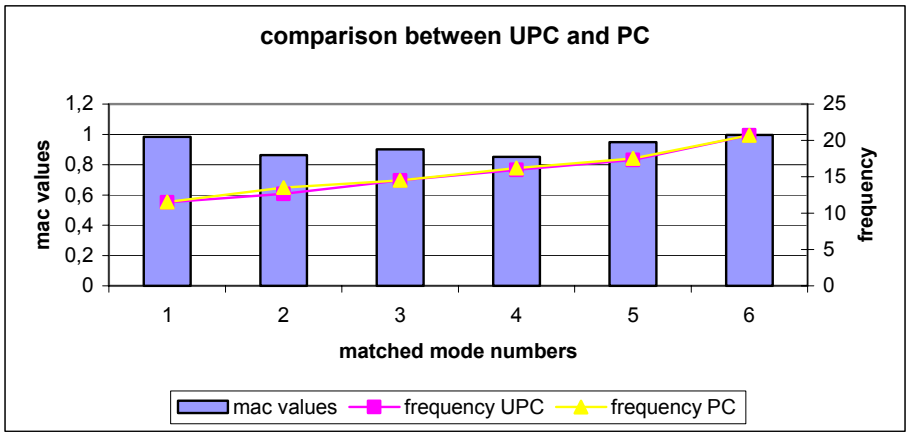

Figure 2.49 Comparison between frequencies of the matched modes of UPC and PC algorithms of second data set in 10-25 Hz frequency range according to their MAC values

In the comparison of UPC and PC algorithms of second data set in 10-25 Hz frequency range, six modes were matched. $2^{nd,}$ 3^{rd}, 5^{th}, 6^{th}, 7^{th} and 9^{th} modes of the UPC algorithm were matched with the result modes of the PC algorithm.

Table 2.20. MAC matrix between UPC algorithm and CVA algorithm results of second data set in 10-25Hz frequency range

MAC	11,55Hz	12,35Hz	14,44Hz	16,11Hz	17,36Hz	19,27Hz	19,92Hz	20,5Hz	20,8Hz
10,92Hz	0.8655	0.2247	0.1245	0.3465	0.1699	0.1006	0.3865	0.5017	0.2745
11,49Hz	**0.9928**	0.4749	0.1803	0.2621	0.3847	0.2436	0.2727	0.4408	0.2369
12,64Hz	0.3872	0.7579	0.6145	0.2995	0.3484	0.6075	0.2427	0.2217	0.07632
13,69Hz	0.1253	0.3867	0.5281	0.5244	0.6762	0.4994	0.1413	0.2117	0.207
14,52Hz	0.1166	0.2225	**0.9827**	0.4865	0.3441	0.4326	0.3582	0.2343	0.06374
15,93Hz	0.3517	0.813	0.4715	**0.8672**	0.2521	0.1782	0.1777	0.4193	0.04876
17,3Hz	0.253	0.3241	0.2904	0.2204	**0.947**	0.6053	0.149	0.3598	0.1404
19,24Hz	0.2255	0.204	0.4495	0.08528	0.6403	**0.83**	0.2991	0.3334	0.1581
20,7Hz	0.129	0.1065	0.05978	0.1445	0.1824	0.2755	0.1034	0.03515	**0.9917**

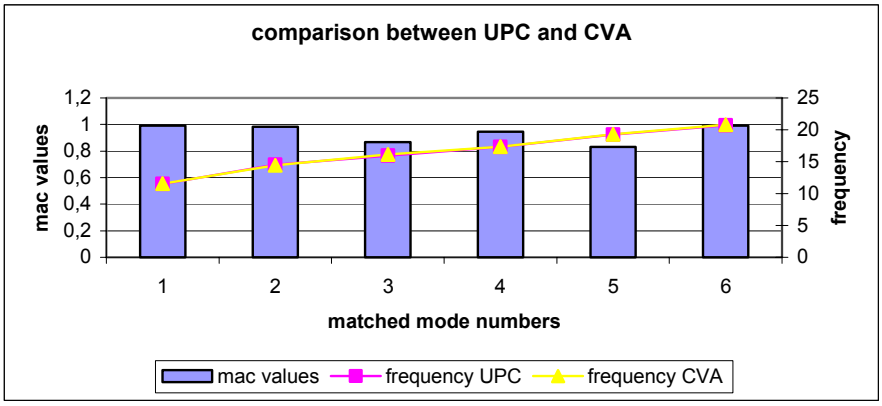

Figure 2.50 Comparison between frequencies of the matched modes of UPC and CVA algorithms of second data set in 10-25 Hz frequency range according to their MAC values

Six modes were matched in the comparison of UPC and CVA algorithms of second data set. 2nd, 5th, 6th, 7th, 8th and 9th modes of the UPC algorithm were well matched with the result modes of the CVA algorithm.

Table 2.21. MAC matrix between PC algorithm and CVA algorithm results of second data set in 10-25Hz frequency range

MAC	11,55Hz	12,35Hz	14,44Hz	16,11Hz	17,36Hz	19,27Hz	19,92Hz	20,5Hz	20,8Hz
11,52Hz	**0.9854**	0.3241	0.1522	0.1383	0.3329	0.1781	0.284	0.4505	0.2568
13,53Hz	0.2706	**0.8066**	0.6716	0.4194	0.4063	0.6118	0.3367	0.0871	0.1369
14,51Hz	0.09448	0.3827	**0.9352**	0.1889	0.3063	0.4156	0.442	0.1432	0.05989
16,19Hz	0.2878	0.5838	0.3465	**0.8229**	0.2531	0.1463	0.2059	0.4939	0.08239
17,53Hz	0.314	0.3288	0.3199	0.2515	**0.9711**	0.568	0.1691	0.4136	0.15
19,43Hz	0.1967	0.2072	0.1489	0.2728	0.4063	0.5479	0.4972	0.3808	0.1543
20,4Hz	0.3008	0.1055	0.2606	0.3573	0.267	0.4089	0.2645	**0.9473**	0.05862
20,72Hz	0.1635	0.07262	0.05508	0.1375	0.1208	0.2478	0.1401	0.07999	**0.9987**

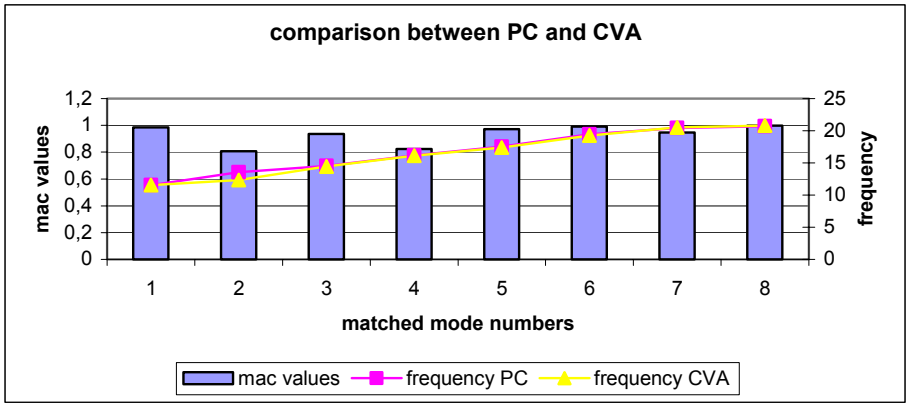

Figure 2.51 Comparison between frequencies of the matched modes of PC and CVA algorithms of second data set in 10-25 Hz frequency range according to their MAC values

Eight modes were matched in the comparison of PC and CVA algorithms of second data set in 10-25 Hz frequency range. Except the six mode, all the captured modes of PC algorithm were matched with the result modes of the CVA algorithm.

As a result, PC algorithm captured more well-matched than the others. Therefore, PC algorithm modes are accepted as the result modes of the second data set in 10-25 Hz frequency range.

The comparison between the mode numbers, damping ratios and frequencies obtained from the three techniques for the third data set in 10-25 Hz frequency range is shown in Table 2.22. Furthermore, each set of mode shapes obtained from UPC, PC, and CVA algorithms are compared using MAC matrices in Table 2.23, Table 2.24, and Table 2.25 for UPC versus PC, UPC verses CVA, and PC versus CVA comparisons, respectively. The graphical forms of these comparisons are seen in Figure 2.52, Figure 2.53 and Figure 2.54.

Table 2.22. Frequency and damping values of captured modes from UPC, PC,CVA algorithms on third data set in 10-25 frequency range

	UPC		PC		CVA	
	frequency(Hz)	*damping(%)*	*frequency(Hz)*	*damping(%)*	*frequency(Hz)*	*damping(%)*
Mode5	**10,67**	2,811	**10,59**	2,064	**10,46**	2,355
Mode6	**11,61**	3,022	**11,47**	5,638	**10,98**	3,919
Mode7	**12,31**	5,512	**12,52**	5,72	**11,67**	7,01
Mode8	**13,26**	9,285	**13,21**	4,649	**12,8**	5,128
Mode9	**14,16**	4,215	**15**	3,751	**13,81**	6,58
Mode10	**15,09**	3,609	**17,43**	2,943	**14,87**	4,641
Mode11	**16,36**	4,15	**19,17**	2,817	**17,08**	6,137
Mode12	**17,21**	3,527	**20,34**	3,847	**18,12**	8,433
Mode13	**19,23**	3,486	**20,6**	2,378	**19,12**	2,967
mode14	**19,91**	3,617			**20,08**	4,557
mode15	**20,63**	2,626			**20,63**	2,535
mode16	**20,92**	5,98			**20,81**	5,866

In the analysis of third data set in 10-25 Hz frequency range, twelve modes were captured by UPC and CVA algorithms and nine modes were captured by PC algorithm.

Eight modes were matched in the comparison of UPC and PC algorithm results of third data set in 10-25 Hz frequency range. 1^{st}, 2^{nd}, 3^{rd}, 6^{th}, 8^{th}, 9^{th},10^{th} and 11^{th} modes of the UPC algorithm were well-matched with the result modes of the PC algorithm according to their MAC and frequency values.

Table 2.23. MAC matrix between UPC algorithm and PC algorithm results of third data set in 10-25Hz frequency range

MAC	10,59Hz	11,47Hz	12,52Hz	13,21Hz	15Hz	17,43Hz	19,17Hz	20,34Hz	20,6Hz
10,66Hz	**0.9791**	0.6223	0.6945	0.6182	0.3952	0.2337	0.2917	0.5444	0.2372
11,61Hz	0.4796	**0.9635**	0.7292	0.5257	0.0596	0.2955	0.1572	0.4333	0.07657
12,31Hz	0.6248	0.3832	**0.8986**	0.8984	0.6583	0.4908	0.4584	0.2619	0.1556
13,26Hz	0.3345	0.5783	0.3464	0.6119	0.414	0.7163	0.4159	0.4268	0.1243
14,16Hz	0.3172	0.5248	0.5571	0.67	0.5037	0.2916	0.4673	0.2406	0.04538
15,09Hz	0.4222	0.3541	0.5422	0.3873	**0.9771**	0.3851	0.6025	0.1785	0.09208
16,36Hz	0.4336	0.209	0.3235	0.04015	0.4314	0.2849	0.1967	0.4662	0.4215
17,21Hz	0.2072	0.2268	0.2198	0.537	0.2464	**0.9868**	0.2017	0.5188	0.05851
19,23Hz	0.5306	0.09711	0.2888	0.4396	0.4451	0.5179	**0.8178**	0.5398	0.3121
19,91Hz	0.5688	0.3088	0.2786	0.4439	0.05803	0.5978	0.2872	**0.9073**	0.3542
20,63Hz	0.3795	0.05477	0.1641	0.2059	0.05817	0.1603	0.2947	0.5907	**0.9666**
20,92Hz	0.2721	0.32	0.2494	0.2278	0.02752	0.08415	0.1693	0.1323	0.1511

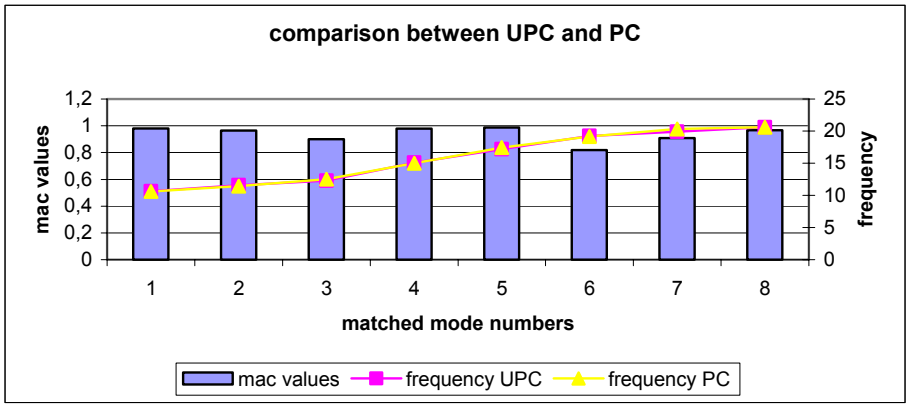

Figure 2.52 Comparison between frequencies of the matched modes of UPC and PC algorithms of third data set in 10-25 Hz frequency range according to their MAC values

In the comparison of UPC and CVA algorithms of third data set in 10-25 Hz frequency range, seven modes were matched. 1st, 2nd, 6th,8th, 9th,11th and 12th modes of the UPC algorithm are these matched modes.

Table 2.24. MAC matrix between UPC algorithm and CVA algorithm results of third data set in 10-25Hz frequency range

MAC	10,46 Hz	10,98 Hz	11,67 Hz	12,8Hz	13,81 Hz	14,87 Hz	17,08 Hz	18,12 Hz	19,21 Hz	20,08 Hz	20,63 Hz	20,81 Hz
10,66Hz	**0.9664**	0.5909	0.2302	0.5526	0.4062	0.306	0.1904	0.3503	0.4659	0.2275	0.4338	0.226
11,61Hz	0.6316	0.8735	0.7057	**0.9151**	0.2359	0.0397	0.4909	0.5054	0.0902	0.246	0.2112	0.2749
12,31Hz	0.5748	0.2847	0.73	0.5502	0.7552	0.6721	0.3848	0.5727	0.5417	0.3564	0.2309	0.1432
13,26Hz	0.4559	0.4611	0.7644	0.8562	0.2777	0.4724	0.7429	0.6984	0.4418	0.1661	0.2221	0.2447
14,16Hz	0.417	0.4137	0.8815	0.8662	0.7334	0.5816	0.3365	0.3211	0.2946	0.0970	0.0972	0.2549
15,09Hz	0.2846	0.5107	0.524	0.2513	0.7847	**0.9648**	0.415	0.2253	0.4764	0.2273	0.0289	0.1009
16,36Hz	0.3825	0.3036	0.2603	0.1358	0.254	0.4811	0.2072	0.117	0.3647	0.29	0.4231	0.0635
17,21Hz	0.1883	0.1153	0.4685	0.3807	0.0919	0.2375	0.9128	**0.932**	0.509	0.2746	0.2568	0.0985
19,23Hz	0.4707	0.1226	0.2938	0.3356	0.2968	0.4088	0.4536	0.4497	**0.9108**	0.0533	0.4452	0.2485
19,91Hz	0.5876	0.3251	0.0511	0.2747	0.2295	0.108	0.5083	0.619	0.6575	0.3552	0.6537	0.193
20,63Hz	0.3674	0.0116	0.0920	0.0912	0.1323	0.0919	0.2034	0.1832	0.4494	0.5433	**0.9543**	0.1504
20,92Hz	0.2811	0.2723	0.1628	0.2965	0.1049	0.0361	0.0647	0.0477	0.1261	0.0441	0.1656	**0.9852**

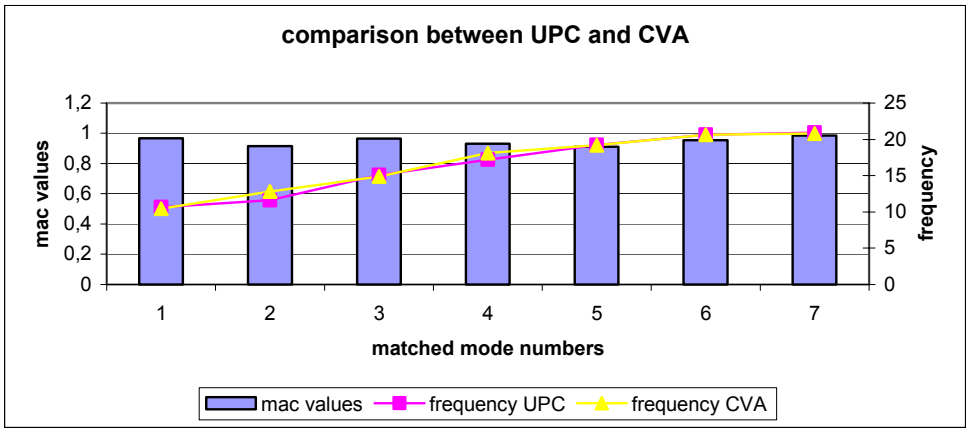

Figure 2.53 Comparison between frequencies of the matched modes of UPC and CVA algorithms of third data set in 10-25 Hz frequency range according to their MAC values

In the comparison between PC and CVA algorithm results of the third data set in 10-25 Hz frequency range, six modes were matched. 1st, 2nd, 5th, 6th, 7th and 9th modes of the PC algorithm were matched with the result modes of the CVA algorithm.

Table 2.25. MAC matrix between PC algorithm and CVA algorithm results of third data set in 10-25Hz frequency range

MAC	10,46 Hz	10,98 Hz	11,67 Hz	12,8 Hz	13,81 Hz	14,87 Hz	17,08 Hz	18,12 Hz	19,21 Hz	20,08 Hz	20,63 Hz	20,81 Hz
10,59Hz	**0.9658**	0.4788	0.149	0.4842	0.4681	0.3468	0.0874	0.2402	0.5063	0.1972	0.4516	0.2073
11,47Hz	0.6249	**0.9547**	0.5538	0.8229	0.0260	0.2155	0.4643	0.4779	0.0759	0.2966	0.2072	0.3126
12,52Hz	0.6728	0.5908	0.558	0.6013	0.6766	0.5981	0.2435	0.4254	0.3791	0.3564	0.2543	0.2023
13,21Hz	0.5821	0.2262	0.6358	0.5946	0.7161	0.4641	0.4959	0.6042	0.4974	0.3681	0.2748	0.1829
15Hz	0.3055	0.4169	0.4923	0.1656	0.8704	**0.9856**	0.3672	0.1679	0.421	0.2349	0.0462	0.0544
17,43Hz	0.1541	0.0911	0.5154	0.4107	0.0169	0.2795	0.9395	**0.9476**	0.5438	0.2951	0.249	0.1163
19,17Hz	0.2177	0.2965	0.3806	0.2953	0.5568	0.5783	0.2813	0.2016	**0.8424**	0.0866	0.2497	0.2597
20,34Hz	0.5942	0.4275	0.2128	0.4203	0.1659	0.2484	0.5261	0.6061	0.4733	0.3692	0.7234	0.0811
20,6 Hz	0.2475	0.1211	0.0824	0.0960	0.0813	0.1079	0.1869	0.1744	0.3482	0.6266	**0.896**	0.0978

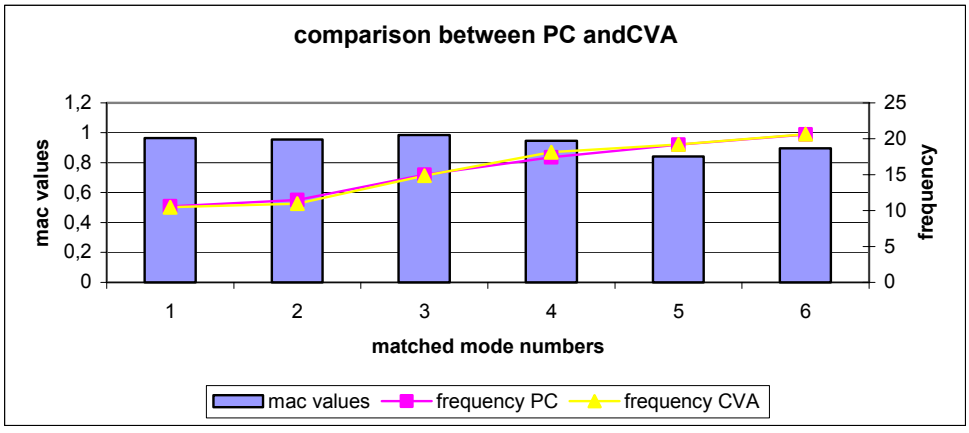

Figure 2.54 Comparison between frequencies of the matched modes of PC and CVA algorithms of third data set in 10-25 Hz frequency range according to their MAC values

Since the captured modes of the PC algorithm had less damping ratios then the modes which were captured from the other algorithms, PC algorithm results are accepted as the result modes of the third data set in 10-25 Hz frequency range. Furthermore, the result modes of the PC algorithm were matched with the other captured modes as good as the modes of the other algorithms.

The captured modes of PC algorithms of first data set (June 6th) and second data set (June 16th) were compared with each other in 10-25 Hz frequency range. The comparison results are shown in Table 2.26 and Figure 2.55. Five modes are matched well. Their MAC values are greater than 0.8 and their frequency values are closer to each other. Furthermore, some of the diagonal modes were matched with MAC values between 0.6 and 0.8. Graphical form of the MAC matrix is seen in Figure 2.56.

Table 2.26. MAC matrix between PC algorithm results of first and second data set in 10-25Hz frequency range

MAC	11,52Hz	13,53Hz	14,51Hz	16,19Hz	17,53Hz	19,43Hz	20,4Hz	20,72Hz
11,49Hz	**0.985**	0.2562	0.06797	0.1634	0.1749	0.2111	0.2982	0.2651
12,94Hz	0.5231	0.7818	0.5363	0.3595	0.346	0.2815	0.04037	0.08882
14,17Hz	0.1034	0.4974	**0.9121**	0.1097	0.4312	0.2382	0.2292	0.0546
15,22Hz	0.1398	0.3887	0.6416	0.7727	0.2043	0.3418	0.3894	0.0462
16,73Hz	0.39	0.4012	0.2509	**0.8567**	0.1358	0.3725	0.3026	0.07208
17,24Hz	0.413	0.4929	0.2258	0.2409	**0.82**	0.4946	0.3126	0.1138
17,92Hz	0.286	0.3828	0.1927	0.6939	0.5897	0.1454	0.5398	0.0729
19,48Hz	0.2827	0.3808	0.453	0.1982	0.3574	0.4546	0.343	0.223
20,31Hz	0.1751	0.06951	0.119	0.4345	0.1195	0.534	0.7104	0.2111
20,8Hz	0.411	0.05656	0.1422	0.07145	0.1224	0.1645	0.1948	**0.9409**

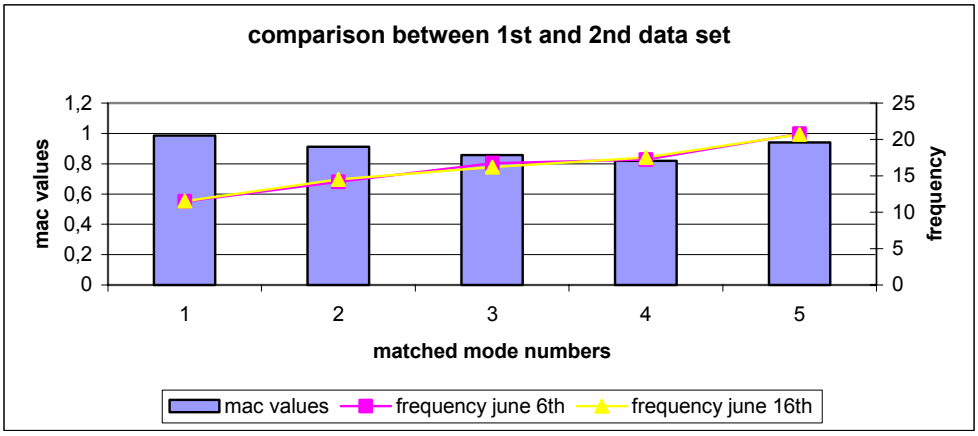

Figure 2.55 Comparison between matching modes of PC algorithms of first and second data set in 10-25 Hz frequency range

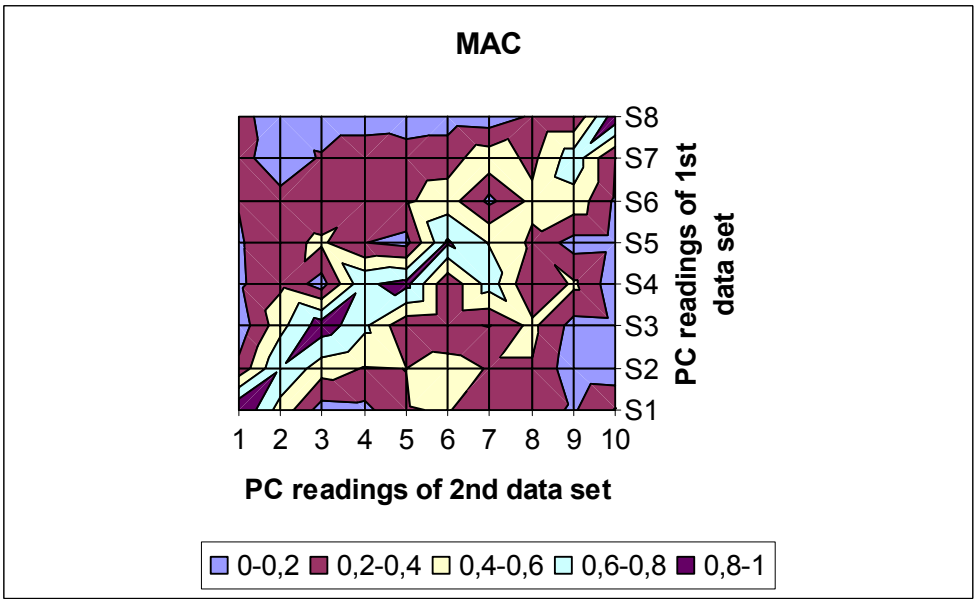

Figure 2.56 MAC matrix between PC algorithm results of first and second data set

As the second step, the captured modes of PC algorithms of first (June 6th) and third data set (July 16th) were compared with each other in 10-25 Hz frequency range. Table 2.27, Figure 2.57 and Figure 2.58 represents the comparison results. In that comparison five modes are matched. Their MAC values are not as greater as the MAC values of the compared modes between PC algorithms of first and second data set.

Table 2.27. MAC matrix between PC algorithm results of first and third data set in 10-25Hz frequency range

MAC	10,59Hz	11,47Hz	12,52Hz	13,21Hz	15Hz	17,43Hz	19,17Hz	20,34Hz	20,6Hz
11,49Hz	0.5316	**0.8989**	0.8224	0.5491	0.1896	0.24	0.06375	0.4808	0.1104
12,94Hz	0.5986	0.5081	0.545	0.5526	0.5792	0.2739	0.4446	0.1097	0.2281
14,17Hz	0.5004	0.3719	0.4255	0.5163	**0.8552**	0.2241	0.5947	0.1571	0.1054
15,22Hz	0.1178	0.08278	0.4487	0.3541	0.6156	0.41	0.1308	0.4066	0.3037
16,73Hz	0.3085	0.5121	0.2333	0.1859	0.3228	0.2581	0.4701	0.3462	0.4303
17,24Hz	0.2615	0.3059	0.2766	0.5004	0.1147	**0.8028**	0.08177	0.4934	0.08785
17,92Hz	0.2999	0.2468	0.2818	0.3192	0.04857	0.509	0.3281	0.4364	0.5468
19,48Hz	0.4767	0.1545	0.4557	0.5232	0.4355	0.3651	**0.7949**	0.3895	0.05811
20,31Hz	0.2453	0.1762	0.1425	0.1841	0.05941	0.1134	0.3148	0.4107	**0.8685**
20,8Hz	0.3717	0.4331	0.3002	0.198	0.1499	0.09356	0.2771	0.2562	0.1153

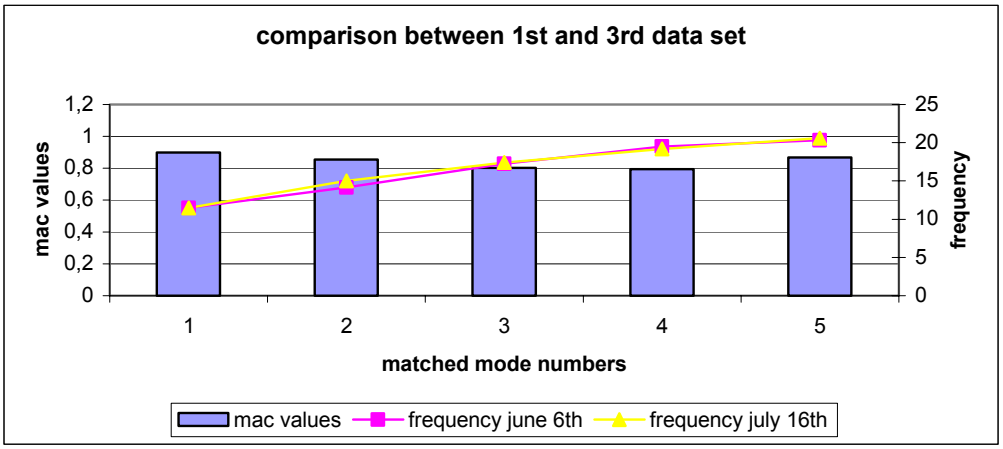

Figure 2.57 Comparison between matching modes of PC algorithms of first and third data set in 10-25 Hz frequency range

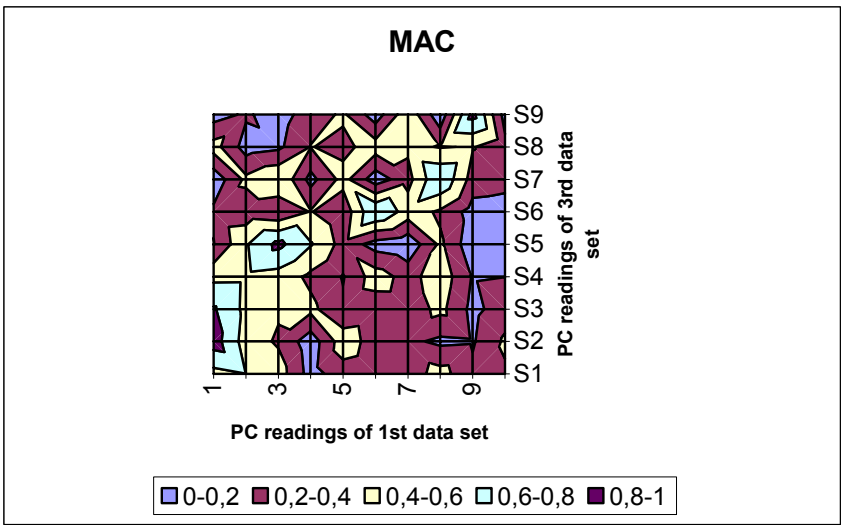

Figure 2.58 MAC matrix between PC algorithm results of first and third data set

In the analysis of the data sets in 10-25 Hz frequency range, damping ratio was chosen less than % 10. The aim of that choice was to capture the repeated trend of the structural modes and not to miss any stable mode. On the other hand, software assigned some of the unstable modes (which were not in a repeated trend) as the stable modes because of the higher damping ratio. These modes gave MAC results between 0.6 and 0.8 near the well-matched modes (Figure 2.58).

As the third step, the result modes of PC algorithms of second and third data set were compared with each other in 10-25 Hz frequency range. Table 2.28, Figure 2.59 and Figure 2.60 represents the comparison results. Five modes are matched in that comparison. Their MAC values are not as greater as the MAC values of the compared modes between PC algorithms of first and second data set, too.

Table 2.28. MAC matrix between PC algorithm results of second and third data set in 10-25Hz frequency range

MAC	10,59Hz	11,47Hz	12,52Hz	13,21Hz	15Hz	17,43Hz	19,17Hz	20,34Hz	20,6Hz
11,52Hz	0.531	**0.9138**	0.8466	0.5623	0.2367	0.3036	0.00799 7	0.473	0.1197
13,53Hz	0.4643	0.07577	0.557	0.6915	0.6436	0.2138	0.5333	0.09229	0.1521
14,51Hz	0.5313	0.2918	0.5177	0.462	**0.9494**	0.302	0.5768	0.1915	0.01165
16,19Hz	0.283	0.2866	0.2728	0.2962	0.2866	0.4972	0.266	0.5269	0.4341
17,53Hz	0.1063	0.1766	0.2664	0.5176	0.3155	**0.8988**	0.3035	0.3262	0.2084
19,43Hz	0.3215	0.03095	0.2167	0.3219	0.2398	0.5483	0.5299	0.302	0.4416
20,4Hz	0.3159	0.2586	0.2576	0.346	0.1574	0.4099	0.2356	**0.816**	0.8253
20,72Hz	0.2635	0.3165	0.22	0.2379	0.07036	0.1536	0.2528	0.05967	0.1132

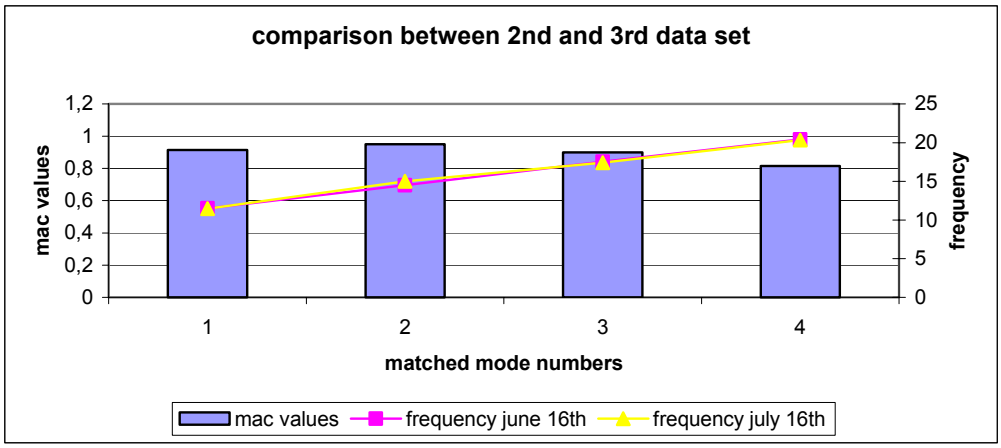

Figure 2.59 Comparison between matching modes of PC algorithms of second and third data set in 10-25 Hz frequency range

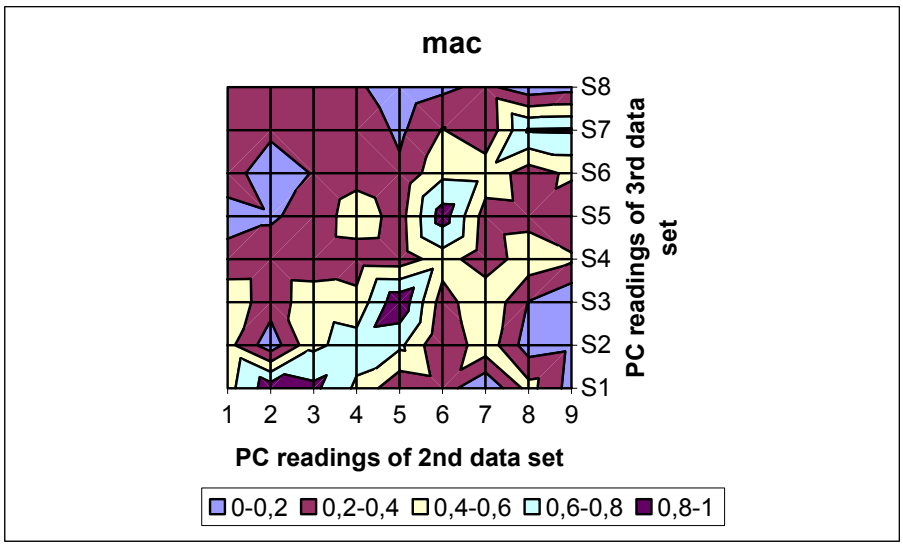

Figure 2.60 MAC matrix between PC algorithm results of second and third data set

In the 10-25Hz frequency range different number of modes was captured in the analysis of the readings which had been taken in different time intervals. These captured modes were mostly the bending and torsion modes. Also these captured modes have less accuracy when they compared with the modes which had captured in 0-10Hz frequency range. PC algorithm results of the first data set gave more matched modes than the others. Furthermore, the MAC values of the matched modes of that data set was greater and their damping ratios was less when compared with the result modes of the other algorithms. Therefore, the captured modes of the PC algorithm of the June 6th data set is accepted as the result modes for 10-25 Hz frequency range.

2.3.3.3. Modal Identification in 25-50Hz Frequency Range

First, second and third data sets were investigated in 25-50Hz frequency range by using UPC, PC and CVA algorithms. To capture all the modes their damping ratio was chosen as %10.

Table 2.29 represents the comparison between the mode numbers, frequencies and damping ratios obtained from the three techniques of first data set in 25-50 Hz frequency range. Nine modes were captured from PC and CVA algorithms and eight modes were captured from UPC algorithm.

Table 2.29. Frequency and damping values of captured modes from UPC, PC,CVA algorithms on first data set in 25-50Hz frequency range

UPC			PC			CVA		
	freq.(Hz)	*damping(%)*		*freq.(Hz)*	*damping(%)*		*freq.(Hz)*	*damping(%)*
Mode15	**25,32**	3,083	*Mode17*	**25,49**	2,415	*Mode15*	**25,16**	2,058
Mode16	**26,28**	7,003	*Mode18*	**27,1**	6,068	*Mode16*	**26,56**	6,414
Mode17	**27,12**	7,325	*Mode19*	**29,95**	2,348	*Mode17*	**29,73**	2,666
Mode18	**29,6**	2,537	*Mode20*	**33,25**	4,643	*Mode18*	**32,74**	9,675
Mode19	**40,87**	3,78	*Mode21*	**33,77**	3,667	*Mode19*	**33,76**	9,702
Mode20	**42,07**	4,02	*Mode22*	**37,83**	3,968	*Mode20*	**35,04**	6,857
Mode21	**43,96**	2,19	*Mode23*	**41,15**	3,364	*Mode21*	**42,47**	3,825
Mode22	**44,93**	4,749	*Mode24*	**42,31**	3,385	*Mode22*	**43,98**	2,07
			Mode25	**43,75**	1,955	*Mode23*	**44,92**	2,837

Furthermore, each set of mode shapes obtained from UPC, PC, and CVA algorithms of the first data set are compared using MAC matrices in Table 2.30 and Table 2.31 for UPC versus PC and UPC verses CVA comparisons, respectively. The comparison between frequencies of the matched modes of UPC, PC and CVA algorithms of first data set in 25-50 Hz frequency range according to their MAC values are also given in Figure 2.61 and 2.62.

Table 2.30. MAC matrix between UPC algorithm and PC algorithm results of first data set in 25-50Hz frequency range

MAC	25,49Hz	27,1Hz	29,95Hz	33,25Hz	33,77Hz	37,83Hz	41,15Hz	42,31Hz	43,75Hz
25,32Hz	**0.9602**	0.1944	0.3171	0.3217	0.5045	0.1706	0.2196	0.4598	0.6213
26,28Hz	0.1451	0.4146	0.09519	0.07698	0.1191	0.2252	0.3655	0.5293	0.3113
27,12Hz	0.3325	0.7446	0.3091	0.2862	0.08394	0.338	0.08361	0.2341	0.05102
29,6Hz	0.3322	0.3207	**0.9949**	0.1385	0.229	0.3575	0.1054	0.3193	0.2858
40,87Hz	0.2748	0.2685	0.1491	0.08309	0.2262	0.3449	0.7702	0.5046	0.4931
42,07Hz	0.4916	0.3221	0.2627	0.123	0.2822	0.2919	0.5141	**0.9164**	0.5889
43,96Hz	0.5364	0.1649	0.2467	0.06822	0.2156	0.1625	0.3559	0.3576	**0.9782**
44,93Hz	0.05411	0.2923	0.04175	0.1088	0.03457	0.2656	0.2907	0.7188	0.1565

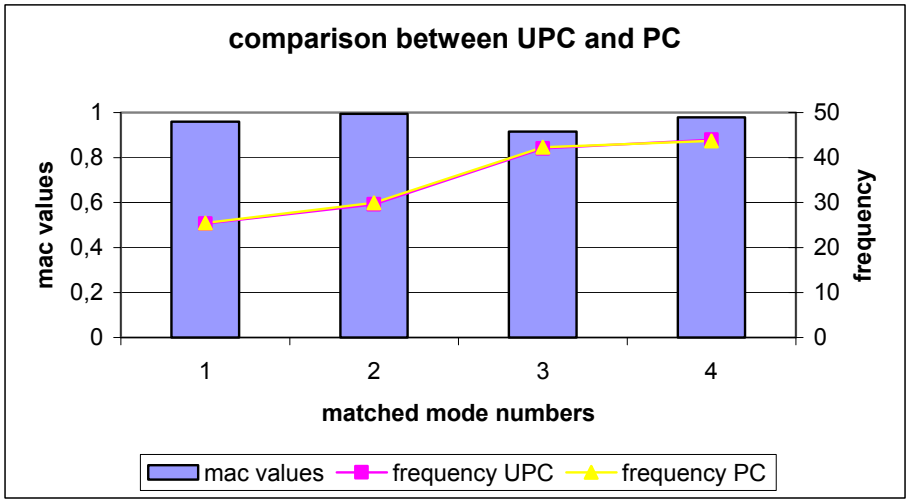

Figure 2.61 Comparison between frequencies of the matched modes of UPC and PC algorithms of first data set in 25-50 Hz frequency range according to their MAC values

As represented in the above figure and graph, only four modes were matched with the MAC values greater than 0.8. 1st, 4th, 6th and 7th modes are the matched modes of the UPC algorithm.

Table 2.31. MAC matrix between UPC algorithm and CVA algorithm results of first data set in 25-50Hz frequency range

MAC	25,16Hz	26,56Hz	29,73Hz	32,74Hz	33,76Hz	35,04Hz	42,47Hz	43,98Hz	44,92Hz
25,32Hz	**0.9818**	0.216	0.337	0.3691	0.2634	0.2269	0.5762	0.5248	0.5554
26,28Hz	0.2242	0.3259	0.09913	0.02755	0.1547	0.1572	0.4609	0.04919	0.539
27,12Hz	0.1666	**0.9363**	0.3581	0.2357	0.07845	0.156	0.2295	0.09042	0.1579
29,6Hz	0.3538	0.3397	**0.9969**	0.4951	0.2188	0.4254	0.2623	0.1889	0.1713
40,87Hz	0.3699	0.06235	0.1706	0.08832	0.1287	0.01314	0.6208	0.3218	0.5101
42,07Hz	0.6789	0.1383	0.2959	0.2556	0.08142	0.2286	**0.9678**	0.2668	0.6721
43,96Hz	0.6092	0.07837	0.2691	0.08493	0.1312	0.1701	0.4952	**0.8828**	0.715
44,93Hz	0.2159	0.08294	0.04084	0.1533	0.1386	0.1135	0.6111	0.283	0.6411

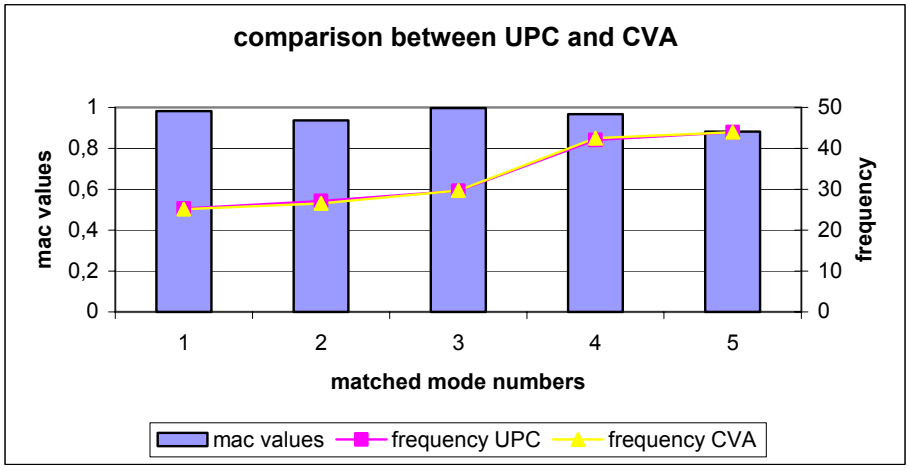

Figure 2.62 Comparison between frequencies of the matched modes of UPC and CVA algorithms of first data set in 25-50 Hz frequency range according to their MAC values

The MAC matrix between the UPC and CVA algorithms of the first data set in 25-50 Hz frequency range is given in Table 2.31. Furthermore, comparison between frequencies of the matched modes of UPC and CVA algorithms of first data set in 25-50 Hz frequency range according to their MAC values is represented

in Figure 2.62. 1st, 3rd, 4th,6th and 7th modes of the UPC algorithm were matched with the captured modes of the CVA algorithm.

Clear results were not gained from the comparisons of the first data set in 25-50 Hz frequency range. Only the half of the modes were matched with each other. Furthermore, the damping ratios of the modes which were captured from UPC and CVA algorithms are great. Therefore, PC algorithm modes are accepted as the result modes of the first data set in 25-50 Hz frequency range.

Frequency and damping ratio of the modes obtained from UPC,PC and CVA algorithms of the second data set are given in Table 2.32 for the 25-50Hz frequency range. Nine modes were captured from all these algorithms.

Table 2.32. Frequency and damping values of captured modes from UPC, PC,CVA algorithms of second data set in 25-50Hz frequency range

UPC			PC			CVA		
	freq.(Hz)	*damping(%)*		*freq.(Hz)*	*damping(%)*		*freq.(Hz)*	*damping(%)*
Mode14	**24,96**	1,695	*Mode13*	**25,01**	1,742	*Mode14*	**22,73**	4,268
Mode15	**25,55**	4,659	*Mode14*	**26,14**	2,972	*Mode15*	**24,82**	1,572
Mode16	**26,94**	4,316	*Mode15*	**27,82**	5,577	*Mode16*	**26,25**	3,341
Mode17	**29,15**	7,946	*Mode16*	**30,15**	5,632	*Mode17*	**26,71**	4,992
Mode18	**32,84**	4,252	*Mode17*	**32,86**	3,222	*Mode18*	**29,48**	4,062
Mode19	**35,32**	6,445	*Mode18*	**35,44**	3,866	*Mode19*	**32,46**	6,64
Mode20	**41,71**	4,047	*Mode19*	**39,52**	4,16	*Mode20*	**42,83**	5,876
Mode21	**43,67**	4,214	*Mode20*	**42,01**	4,32	*Mode21*	**44,54**	2,966
Mode22	**44,15**	2,755	*Mode21*	**44,2**	4,017	*Mode22*	**44,93**	5,184

Additionally, each set of mode shapes obtained from UPC, PC, and CVA algorithms of the second data set are compared using MAC matrices in Table 2.33, Table 2.34 for UPC versus PC and UPC verses CVA comparisons, respectively. The comparison between frequencies of the matched modes of UPC, PC and CVA algorithms of second data set in 25-50 Hz frequency range according to their MAC values are also given in Figure 2.63 and 2.64.

In the comparison between UPC and PC algorithms of the second data set in 25-50 Hz frequency range, four modes are matched with the MAC values greater

than 0.8 and the frequencies of the matched modes are closer to each other. Matched modes are the 1st, 5th, 6th and 9th modes of the UPC algorithm.

Table 2.33. MAC matrix between UPC algorithm and PC algorithm results of second data set in 25-50Hz frequency range

MAC	25,01Hz	26,14Hz	27,82Hz	30,15Hz	32,86Hz	35,44Hz	39,52Hz	42,01Hz	44,2Hz
24,96Hz	**0.9919**	0.1148	0.2497	0.1782	0.4271	0.2991	0.2058	0.1691	0.3016
25,55Hz	0.3839	0.7889	0.5276	0.1167	0.1499	0.1532	0.3093	0.1475	0.2097
26,94Hz	0.2926	0.7149	0.7277	0.2499	0.1734	0.5148	0.2616	0.1592	0.3097
29,15Hz	0.2751	0.2385	0.6214	0.7904	0.3611	0.6674	0.2145	0.1581	0.4072
32,84Hz	0.3313	0.09001	0.1619	0.2097	**0.9784**	0.1497	0.1639	0.1522	0.1437
35,32Hz	0.1208	0.4194	0.4018	0.3308	0.3443	**0.8414**	0.2988	0.2685	0.109
41,71Hz	0.2235	0.06676	0.0612	0.1775	0.3624	0.06372	0.2127	0.7709	0.2856
43,67Hz	0.2493	0.232	0.0568	0.1887	0.1006	0.2541	0.2474	0.5151	0.3019
44,15Hz	0.3388	0.2091	0.4447	0.1511	0.3231	0.3478	0.2191	0.3375	**0.8034**

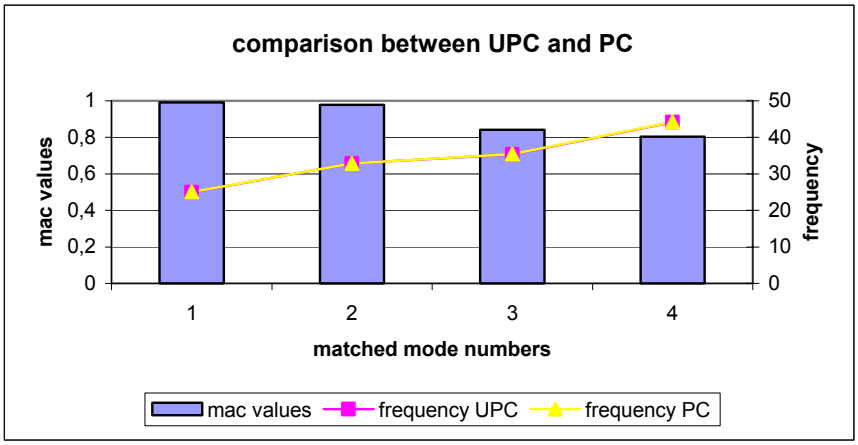

Figure 2.63 Comparison between frequencies of the matched modes of UPC and PC algorithms of second data set in 25-50 Hz frequency range according to their MAC values

From the comparison between UPC and CVA algorithm results of second data set in 25-50 Hz frequency range, four modes were determined as matching modes. These are the 1st, 3rd, 5th and 9th modes of the UPC algorithm (Table 2.34).

Table 2.34. MAC matrix between UPC algorithm and CVA algorithm results of second data set in 25-50Hz frequency range

MAC	22,73Hz	24,82Hz	26,25Hz	26,71Hz	29,48Hz	32,46Hz	42,83Hz	44,54Hz	44,93Hz
24,96Hz	0.2436	**0.9711**	0.3825	0.2943	0.1859	0.3543	0.1038	0.411	0.3396
25,55Hz	0.4953	0.4603	0.6831	0.615	0.2916	0.07689	0.2908	0.3837	0.4719
26,94Hz	0.4161	0.3043	0.8632	**0.935**	0.1525	0.2346	0.2251	0.4333	0.5084
29,15Hz	0.2165	0.2354	0.2749	0.2695	0.781	0.3391	0.1679	0.4368	0.3215
32,84Hz	0.2748	0.3847	0.01174	0.09405	0.3088	**0.9521**	0.06945	0.3603	0.4033
35,32Hz	0.2874	0.1864	0.3759	0.233	0.3372	0.3921	0.2756	0.2601	0.2124
41,71Hz	0.297	0.2102	0.1048	0.04658	0.1115	0.3549	0.6101	0.2257	0.2971
43,67Hz	0.3567	0.2539	0.2309	0.2091	0.2427	0.0547	0.4486	0.2813	0.313
44,15Hz	0.4351	0.3253	0.3718	0.3037	0.2028	0.3169	0.1413	**0.8335**	0.5533

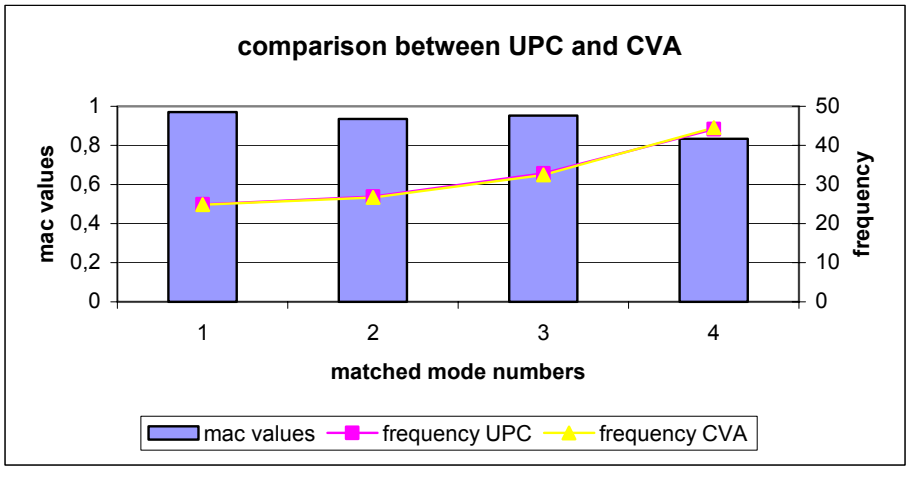

Figure 2.64 Comparison between frequencies of the matched modes of UPC and CVA algorithms of second data set in 25-50 Hz frequency range according to their MAC values

PC algorithm modes of the data set was chosen as the result modes for second data set in 25-50 Hz frequency range.

Table 2.35 represents the frequency and damping values of captured modes from UPC, PC,CVA algorithms on third data set in 25-50Hz frequency range. Seven modes were captured from UPC and PC algorithms and also six modes were captured from CVA algorithm.

Table 2.35. Frequency and damping values of captured modes from UPC, PC,CVA algorithms of third data set in 25-50Hz frequency range

UPC			PC			CVA		
	freq.(Hz)	*damping(%)*		*freq.(Hz)*	*damping(%)*		*freq.(Hz)*	*damping(%)*
Mode17	**26,11**	4,127	*Mode14*	**26,3**	4,256	*mode17*	**26,21**	4,031
Mode18	**29,73**	9,906	*Mode15*	**27,28**	4,901	*Mode18*	**27,07**	6,199
Mode19	**34,71**	6,394	*Mode16*	**31,24**	6,355	*Mode19*	**35,1**	7,782
Mode20	**40,37**	5,794	*Mode17*	**34,52**	4,628	*Mode20*	**38,61**	8,076
Mode21	**41,12**	4,284	*Mode18*	**37,78**	5,388	*Mode21*	**40,29**	4,002
Mode22	**42,87**	3,682	*Mode19*	**40,51**	3,188	*Mode22*	**43,92**	1,688
Mode23	**43,98**	1,691	*Mode20*	**44,07**	1,473			

Table 2.36. MAC matrix between UPC algorithm and PC algorithm results of third data set in 25-50Hz frequency range

MAC	26,3Hz	27,28Hz	31,24Hz	34,52Hz	37,78Hz	40,51Hz	44,07Hz
26,11Hz	**0.9442**	0.5218	0.1531	0.2526	0.1364	0.11	0.1089
29,73Hz	0.3879	0.05145	0.7857	0.4281	0.5692	0.2724	0.5284
34,71Hz	0.1616	0.3034	0.3395	**0.9332**	0.2806	0.103	0.2171
40,37Hz	0.2092	0.2257	0.236	0.1512	0.7814	0.7239	0.2496
41,12Hz	0.2123	0.2987	0.2365	0.116	0.5692	**0.8387**	0.2136
42,87Hz	0.1527	0.2616	0.2613	0.05736	0.3273	0.1921	0.4991
43,98Hz	0.1756	0.1151	0.3332	0.221	0.2939	0.1984	**0.9736**

MAC matrix between UPC algorithm and PC algorithm results of third data set in 25-50Hz frequency range is represented in Table 2.36. 1st, 3rd,5th and 7th modes of the UPC algorithm are matched with the captured modes of the PC algorithm. In Figure 2.65 comparison between frequencies of the matched modes of UPC and PC algorithms of third data set in 25-50 Hz frequency range according to their MAC values is seen.

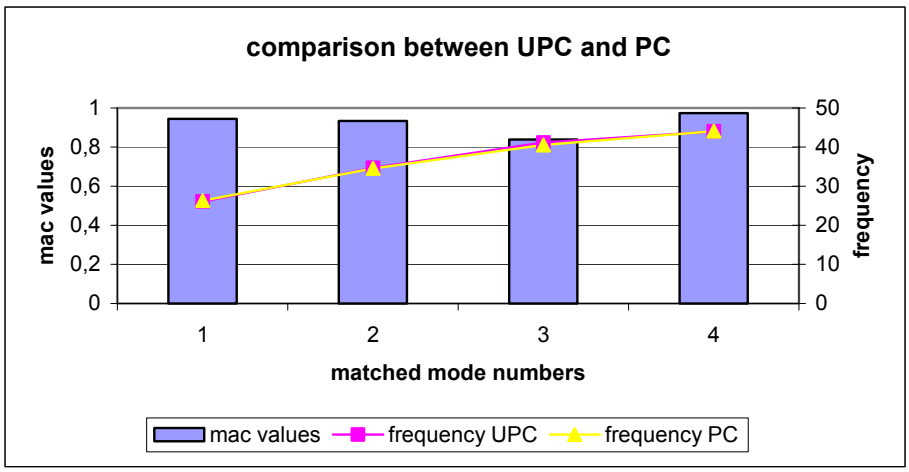

Figure 2.65 Comparison between frequencies of the matched modes of UPC and PC algorithms of third data set in 25-50 Hz frequency range according to their MAC values

Table 2.37. MAC matrix between UPC algorithm and CVA algorithm results of third data set in 25-50Hz frequency range

MAC	26,21Hz	27,07Hz	35,1Hz	38,61Hz	40,29Hz	43,92Hz
26,11Hz	**0.9816**	0.4349	0.2914	0.08068	0.1531	0.1221
29,73Hz	0.2598	0.222	0.4211	0.4286	0.268	0.4721
34,71Hz	0.2057	0.3721	**0.8925**	0.1539	0.253	0.1924
40,37Hz	0.1354	0.2455	0.3398	0.8123	**0.8745**	0.26
41,12Hz	0.153	0.3236	0.2834	0.7437	0.7179	0.2616
42,87Hz	0.09019	0.3133	0.02389	0.5577	0.4088	0.4733
43,98Hz	0.1153	0.1416	0.1088	0.3484	0.275	**0.9897**

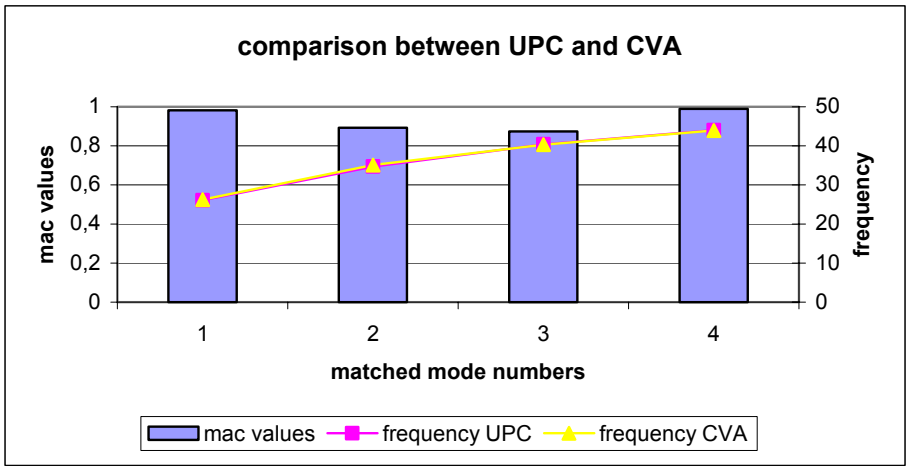

Figure 2.66 Comparison between frequencies of the matched modes of UPC and CVA algorithms of third data set in 25-50 Hz frequency range according to their MAC values

Comparison between the modes of the UPC and CVA algorithms of third data set in 25-50 Hz frequency range is given in Table 2.37 and Figure 2.66. 1st, 3rd,4th and 7th modes of the UPC algorithm are the matched modes.

Captured modes of the PC algorithm are accepted as the result modes of the third data set in 25-50 Hz frequency range. Damping ratios of these modes played a major role in that acceptance.

The result modes of the different time intervals were compared with each other. Table 2.38 represents the MAC matrix between the PC algorithm results of first and second data set in 25-50 Hz frequency range and their graphical comparison is given in Figure 2.67 and 2.68. As seen from the below table and figures, that comparison did not gave consistent results. Accepted minimum MAC value is reduced to the 0.5 and still only four modes were matched with each other.

Table 2.38. MAC matrix between PC algorithm results of first and second data sets in 25-50Hz frequency range

MAC	25,49Hz	27,1Hz	29,95Hz	33,25Hz	33,77Hz	37,83Hz	41,15Hz	42,31Hz	43,75Hz
25,01Hz	0.2481	0.1859	0.2533	0.05539	0.1034	0.1302	0.2427	0.2423	0.2308
26,14Hz	0.1369	0.3363	0.3852	0.1196	0.2746	0.3301	0.1413	0.1215	0.28
27,82Hz	0.1898	**0.5013**	0.04841	0.2231	0.4666	0.18	0.4338	0.1761	0.05833
30,15Hz	0.2446	0.2627	0.2206	**0.5577**	0.38	0.4171	0.2008	0.1179	0.05537
32,86Hz	0.1273	0.3172	0.4558	0.5314	0.4018	0.09929	0.206	0.2026	0.1767
35,44Hz	0.1454	0.4559	0.2967	0.1008	0.1811	**0.6218**	0.4185	0.2384	0.1242
39,52Hz	0.01254	0.1899	0.1975	0.1983	0.1604	0.07321	0.4788	0.446	0.1735
42,01Hz	0.0922	0.2255	0.3167	0.2456	0.2972	0.2706	0.3401	**0.65**	0.3792
44,2Hz	0.059	0.3855	0.4479	0.3309	0.2513	0.1908	0.1217	0.2259	0.3546

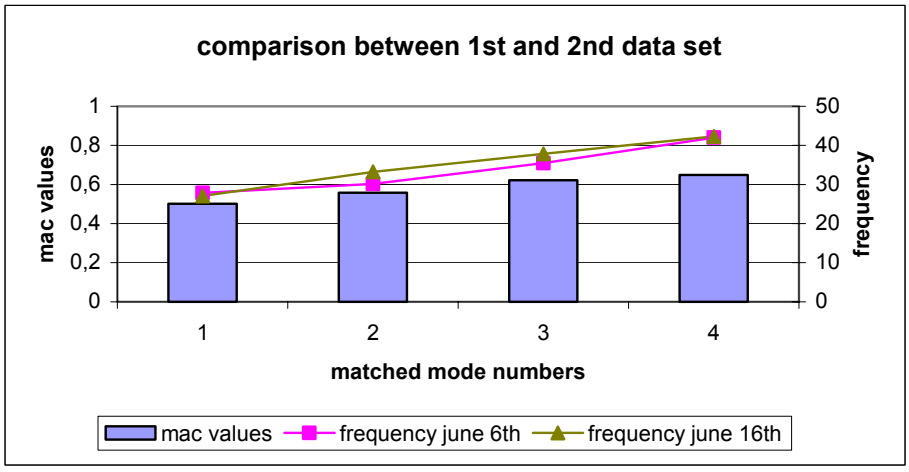

Figure 2.67 Comparison between frequencies of the matched modes of PC algorithms of first and second data sets in 25-50 Hz frequency range according to their MAC values

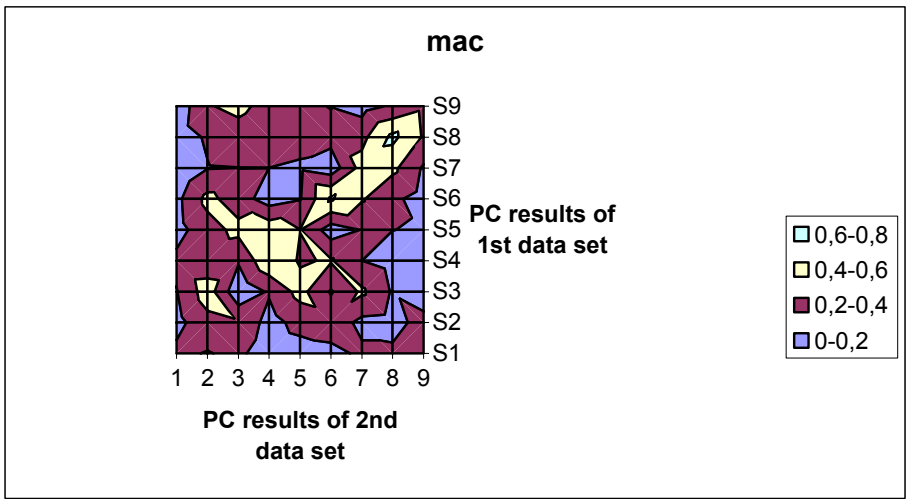

Figure 2.68 MAC matrix between PC algorithm results of first and second data sets

Table 2.39 represents the MAC matrix between the PC algorithm results of first and third data sets in 25-50 Hz frequency range and their graphical comparison is given in Figure 2.69 and 2.70. Accepted minimum MAC value is reduced to the 0.5 for that comparison, too. Only three modes were matched with each other with less MAC values and the frequency values of the matched modes are not closer to each other.

Table 2.39. MAC matrix between PC algorithm results of first and third data sets in 25-50Hz frequency range

MAC	26,3Hz	27,28Hz	31,24Hz	34,52Hz	37,78Hz	40,51Hz	44,07Hz
25,49Hz	0.1768	0.3309	0.2222	0.1208	0.07329	0.04845	0.2222
27,1Hz	0.2558	0.1618	0.497	0.1619	0.4993	0.2435	0.4222
29,95Hz	0.3279	0.108	0.01724	0.3181	0.3473	0.3169	0.4535
33,25Hz	0.03407	0.05855	0.3022	**0.7442**	0.2537	0.2318	0.3646
33,77Hz	0.2053	0.352	0.3332	0.5119	0.2513	0.08237	0.07688
37,83Hz	0.2052	0.2722	0.2452	0.112	0.4873	0.2596	**0.5334**
41,15Hz	0.2169	0.103	0.3644	0.117	**0.5155**	0.2687	0.07096
42,31Hz	0.2693	0.1987	0.1178	0.05244	0.2992	0.442	0.1476
43,75Hz	0.3564	0.3201	0.1115	0.2415	0.04297	0.07338	0.1626

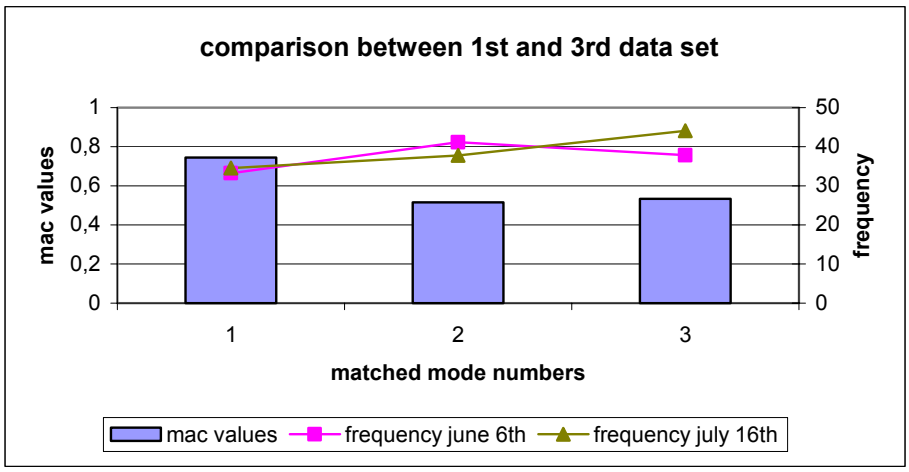

Figure 2.69 Comparison between frequencies of the matched modes of PC algorithms of first and third data sets in 25-50 Hz frequency range according to their MAC values

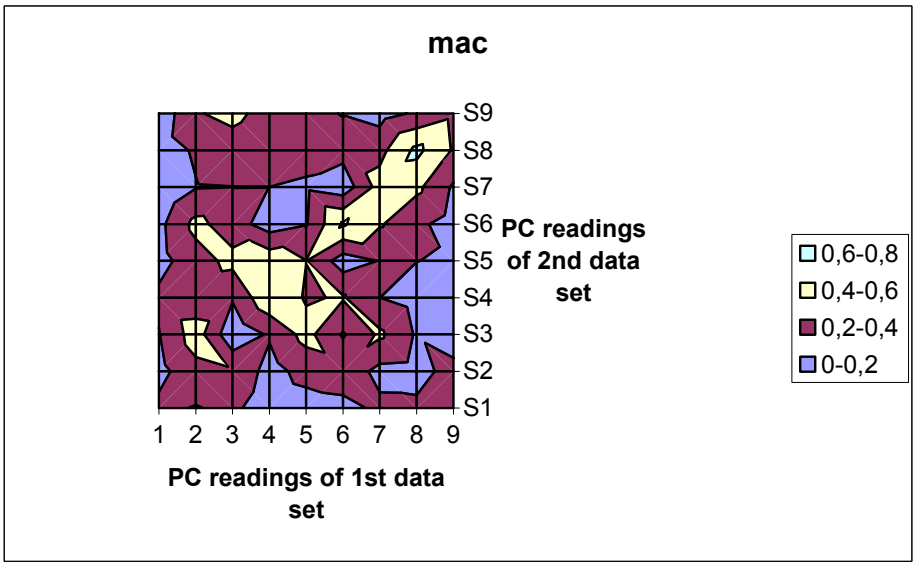

Figure 2.70 MAC matrix between PC algorithm results of first and third data sets

Most accurate results of the data sets comparison in 25-50 Hz frequency range were gained from the comparison of PC algorithm results of the first and third data sets. Seven modes were matched with each other (Figure 2.71) . Furthermore, their MAC values are more logical than the MAC values of the previous comparisons of the data sets in 25-50Hz frequency range (Table 2.40 and Figure 2.72).

Table 2.40. MAC matrix between PC algorithm results of second and third data sets in 25-50Hz frequency range

MAC	26,3Hz	27,28Hz	31,24Hz	34,52Hz	37,78Hz	40,51Hz	44,07Hz
25,01Hz	**0.8346**	0.5565	0.2	0.311	0.2348	0.06508	0.1294
26,14Hz	0.5705	**0.6294**	0.223	0.1068	0.4555	0.385	0.3004
27,82Hz	0.4437	0.2522	**0.793**	0.2303	0.397	0.1355	0.2807
30,15Hz	0.2356	0.2051	0.5342	0.2339	0.3617	0.3109	0.3594
32,86Hz	0.3639	0.2238	0.2777	**0.8535**	0.2748	0.1774	0.288
35,44Hz	0.3859	0.2005	0.662	0.1482	**0.8072**	0.3964	0.4424
39,52Hz	0.1396	0.2885	0.163	0.135	0.3379	**0.7446**	0.1099
42,01Hz	0.04022	0.1716	0.111	0.1287	0.3771	0.2087	0.1838
44,2Hz	0.3734	0.09978	0.3379	0.2049	0.07843	0.1556	**0.6675**

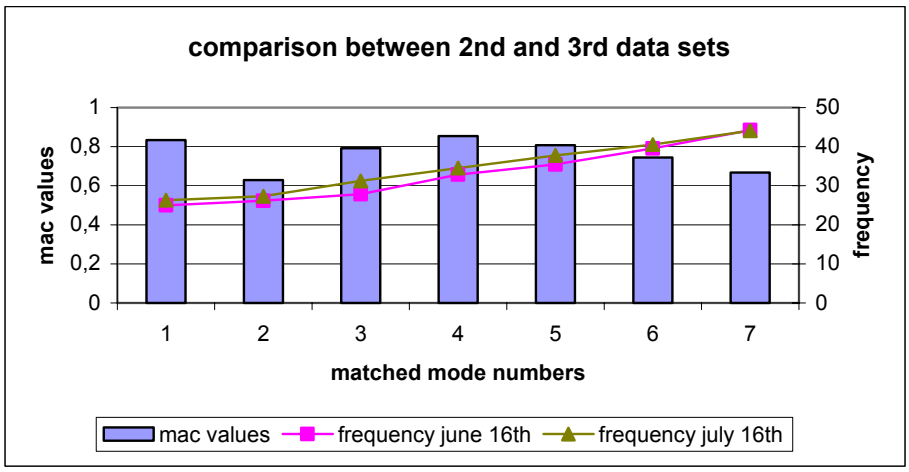

Figure 2.71 Comparison between frequencies of the matched modes of PC algorithms of second and third data sets in 25-50 Hz frequency range according to their MAC values

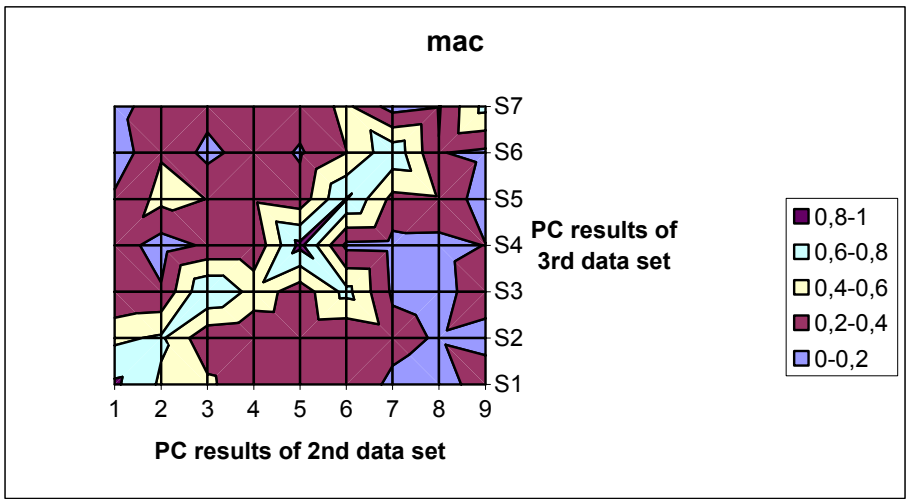

Figure 2.72 MAC matrix between PC algorithm results of second and third data sets

PC algorithm modes of the second data set is accepted as the result modes for the data sets in 25-50 Hz frequency range.

These analysis showed that results obtained in higher frequency range are less reliable and causes a decrement in the accuracy of the results. The dependability of the mode shapes and frequencies are better for the low frequency range intervals.

2.4. Discussion of Experimental Results

The recorded data were investigated in three different frequency ranges to better capture the modes. The comparison of the modes are further made by using three different data sets recorded at different times.

In the 0-10Hz frequency range, the same modes were gained from all three algorithms and using three different record sets. Modes obtained from the PC algorithm of first data set were accepted and used since the largest number of modes were obtained and four of the modes were nicely matching with the results of other data sets.

In the 10-25 Hz frequency range, captured modes were not matching as good as the modes of the 0-10 Hz frequency range. More modes were captured from the

algorithm of first data set, UPC and CVA algorithms of second data set than the other algorithms. Modes of the first data set were nicely correlating with the other algorithm's modes giving higher MAC values. Furthermore, PC algorithm modes of first data set had less damping ratios than the other algorithm modes. Therefore, PC algorithm of the first data set was chosen as a result in 10-25Hz frequency range.

In the 25-50Hz frequency range, PC algorithm of the second data set was chosen as the final result. 9 modes were captured by using this algorithm and they were nicely matching with the modes of the third data set than the other algorithms.

The modes which were matched in all comparisons are given in Table 2.41 with their mode numbers, MAC and frequency values as a summary. According to that table, nine modes were matched with each other in 0-50 Hz frequency range.

Table 2.41. Frequency and damping values of matching modes in all comparisons

6th June (PC)					*16th June (PC)*				*16th July (PC)*		
Mode Num.	Freq.	*Damp. (%)*	*Mac 16 jn*	*Mac 16jly*	Mode Num.	Freq.	*Damp. (%)*	*Mac 16jly*	Mode Num.	Freq.	*Damp. (%)*
1	**3,124**	2,138	0,999	0,937	1	**3,215**	3,231	0,934	1	**3,263**	2,207
2	**5,288**	1,289	0,997	0,946	2	**5,227**	1,501	0,9487	2	**5,29**	1,032
3	**6,403**	2,645	0,992	0,972	3	**6,456**	3,16	0,984	3	**6,492**	2,182
4	**7,772**	0,979	0,935	0,934	4	**7,702**	1,672	0,977	4	**7,904**	1,902
6	***11,49***	4,658	0,985	0,898	5	**11,52**	3,325	0,9138	6	**11,47**	5,638
8	***14,17***	6,259	0,9121	0,8552	7	**14,51**	4,004	0,9494	9	**15**	3,751
11	***17,24***	4,76	0,82	0,8028	9	**17,53**	2,838	0,8988	10	**17,43**	2,943
15	***20,31***	4,136	0,71	0,8685	11	**20,4**	1,639	0,816	13	**20,6**	2,378
20	**33,25**	4,643	0.5577	0,5577	17	**32,86**	3,222	0.8535	17	**34,52**	4,628

On the other hand, it is thought that some of the stable modes which were captured from one algorithm could not be captured by another algorithm. Therefore, the modes which were matched in all comparisons were not selected as the final result. The algorithm of the one data set which gave more accurate results in the comparisons was selected with their all modes as the final result for three different frequency range and twenty five modes were selected by using that logic.

The modes accepted as the final set which were obtained from all three tests are listed in Table 2.42.

Table 2.42. Final modes captured from all data sets

	Modes	
	frequency(Hz)	*damping(%)*
mode1	**3,124**	2,138
mode2	**5,288**	1,289
mode3	**6,403**	2,645
mode4	**7,722**	0,9792
mode5	**8,442**	0,5481
mode6	**11,49**	4,658
mode 7	**12,94**	6,787
mode 8	**14,17**	6,259
mode9	**15,22**	4,412
mode 10	**16,73**	6,986
mode 11	**17,24**	4,76
mode 12	**17,92**	2,277
mode 13	**19,45**	4,929
mode 14	**19,48**	2,397
mode 15	**20,31**	4,136
mode 16	**20,8**	8,365
mode 17	**25,01**	1,742
mode 18	**26,14**	2,972
mode 19	**27,82**	5,577
mode 20	**30,15**	5,632
mode 21	**32,86**	3,222
mode 22	**35,44**	3,866
mode 23	**39,52**	4,16
mode 24	**42,01**	4,32
mode 25	**44,2**	4,017

2.5. Recorded Reading on December 22nd

A last set of readings were recorded on December 22nd, 2005 to compare the analysis results between winter and summer. The stabilization diagram obtained for December 22nd reading is given in Figure 2.73. It is seen that, the 3.198 and 3.517 Hz modes in this data set were identified as two separate modes whereas the two peaks were identified as a single mode in the previous data set analysis results. When the June 6th data stabilization diagram (Figure 2.74) is compared with the December 22nd set, the difference can be easily seen for the first mode at 3.124 Hz.

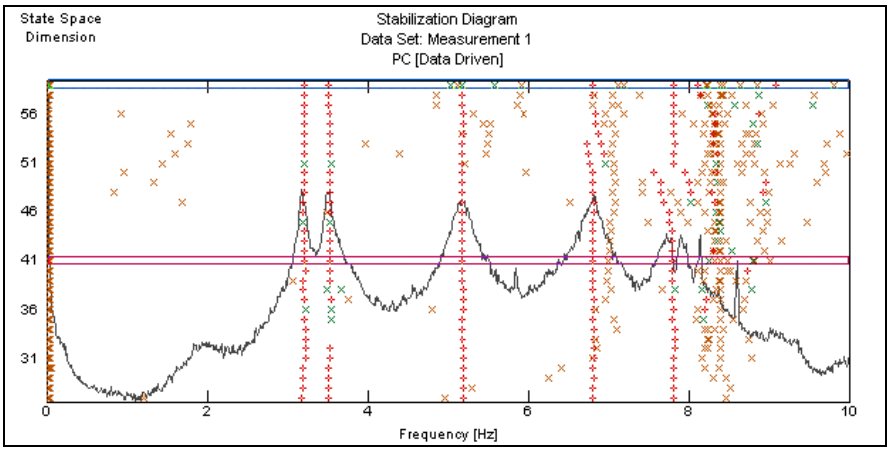

Figure 2.73 Captured modes from PC algorithm on r 22nd record in 0-10Hz frequency range

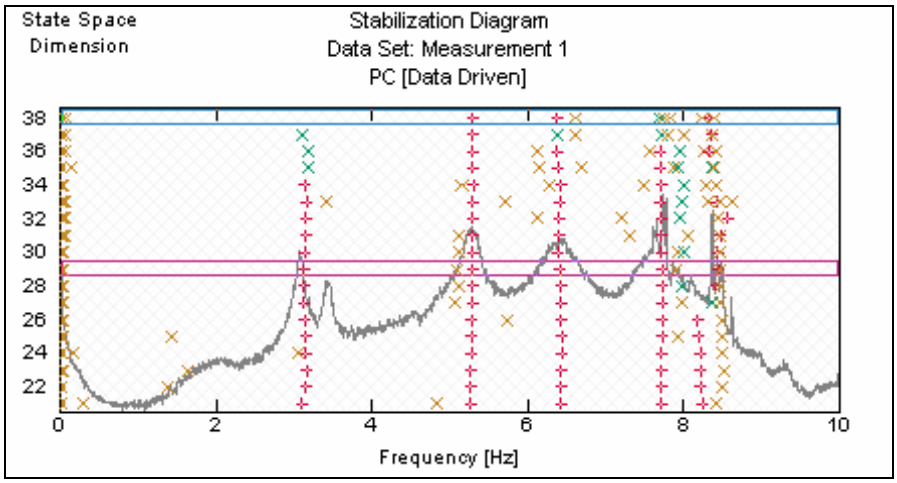

Figure 2.74 Captured modes from PC algorithm on June 6th record in 0-10Hz frequency range

First longitudinal mode in the x-direction has a natural vibration frequency of 3,198Hz and 3,517Hz in 22nd December readings. Both of the modes were well-matched with the first mode of the 6th June records (Table 2.44). Comparison of the mode shapes also reveals small differences as shown in Figure 2.75. Figure represents the eigen vector comparison of the first two modes of the December 22nd. As seen from the graph, Artemis captured nearly the same modes with different frequency values for that record.

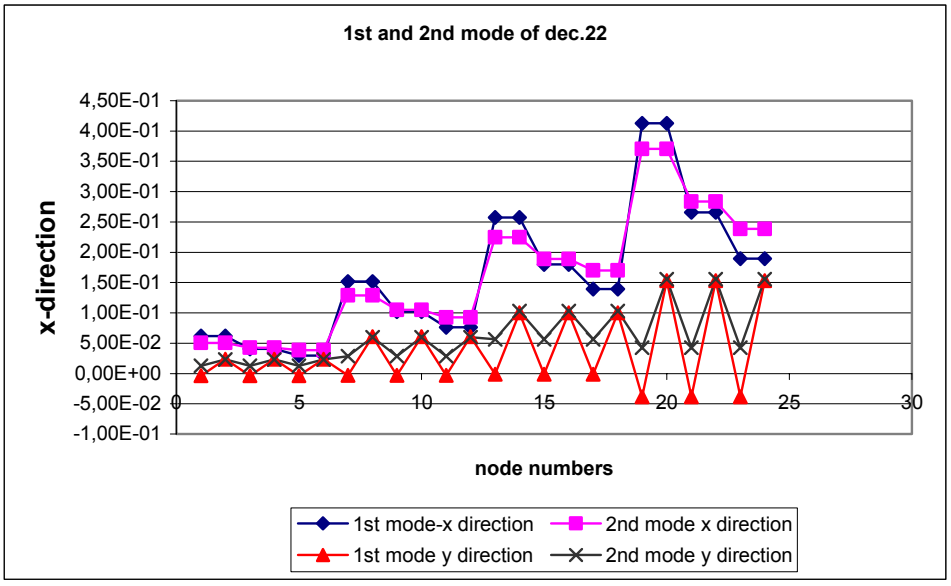

Figure 2.75 Eigen vector comparison of the 1st and 2nd modes of the December 22nd readings

The results of different SSI algorithms for the December 22nd data set is given in Table 2.46. It is observed that the natural frequencies obtained using all three algorithms are close to each other, similar to the stable modes obtained for 0-10 Hz range in the previous data sets. However, the damping ratios obtained for the December 22nd data set are relatively low compared to the results of the previous data set results. The change in the damping ratio may be related to the low ambient temperature.

Table 2.43. Frequency and damping values of captured modes from UPC,PC,CVA algorithms on December 22nd record

	UPC		PC		CVA	
	frequency(Hz)	*damping(%)*	*frequency(Hz)*	*damping(%)*	*frequency(Hz)*	*damping(%)*
Mode1	**3,208**	1,586	**3,198**	1,566	**3,187**	1,058
Mode2	**3,532**	0,896	**3,517**	1,001	**3,507**	0,792
Mode3	**5,181**	1,87	**5,171**	1,824	**5,184**	1,719
Mode4	**6,803**	1,649	**6,796**	1,525	**6,8**	1,702
Mode5	**7,801**	1,564	**7,783**	1,536	**7,803**	1,651

MAC matrix between PC algorithm results of December 22nd and the final result modes of the previous three data sets is given in Table 2.44. Four modes of the final result modes in 0-10 Hz frequency range were matched with the modes of the December 22nd.

Table 2.44. MAC matrix between PC algorithm results of December 22nd and June 6th readings on 0-10Hz frequency range

MAC	3,124Hz	5,288Hz	6,398936Hz	7,721481Hz	8,347017Hz
3,198 Hz	**0.9945**	0.3673	0.899	0.3468	0.7668
3,517 Hz	**0.9895**	0.4733	0.8679	0.3902	0.7492
5,171 Hz	0.3601	**0.9945**	0.596	0.513	0.1661
6,796 Hz	0.7366	0.7195	**0.9503**	0.3854	0.3467
7,783 Hz	0.201	0.5831	0.2331	**0.9752**	0.6717

Furthermore, the fifth mode of the June 6th record was not matched with any modes obtained from December 22nd data set similar to the other readings which were recorded on 16th June and 16th July which have the same mode missing.

Figure 2.76 represents the comparison between frequencies of the matched modes of PC algorithms of December 22nd and final result modes in 0-10 Hz frequency range according to their MAC values.

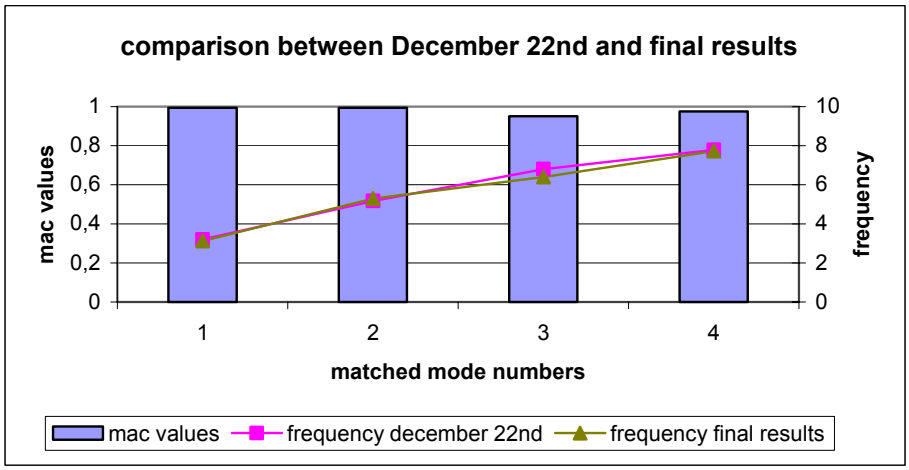

Figure 2.76 Comparison between frequencies of the matched modes of PC algorithms of December 22nd and final result modes in 0-10 Hz frequency range according to their MAC values

As the second step, reading recorded on December 22nd was compared with the final results in 10- 25 Hz frequency range. Stabilization diagram of the UPC algorithm on December 22nd in 10-25 Hz frequency range is represented in Figure 2.77. Furthermore, stabilization diagram of the final result modes in 10-25 Hz frequency range is seen in Figure 2.78. By comparing both figures, different captured modes from the data sets can be determined.

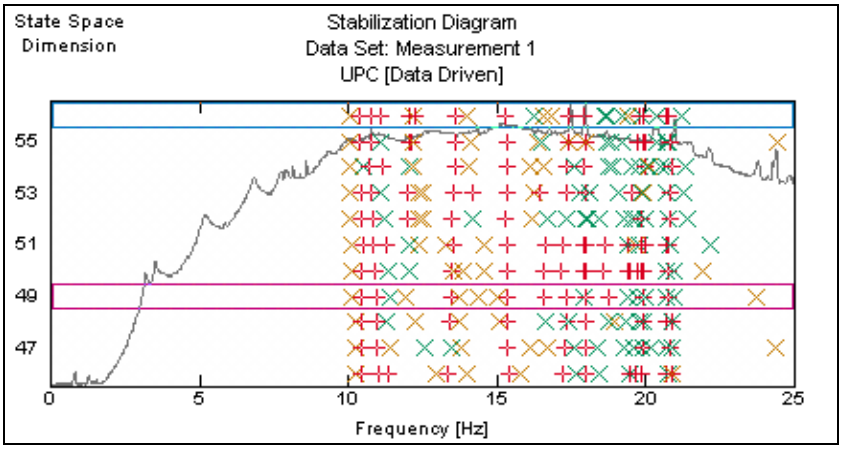

Figure 2.77 Captured modes from UPC algorithm on December 22nd record in 10-25 Hz frequency range

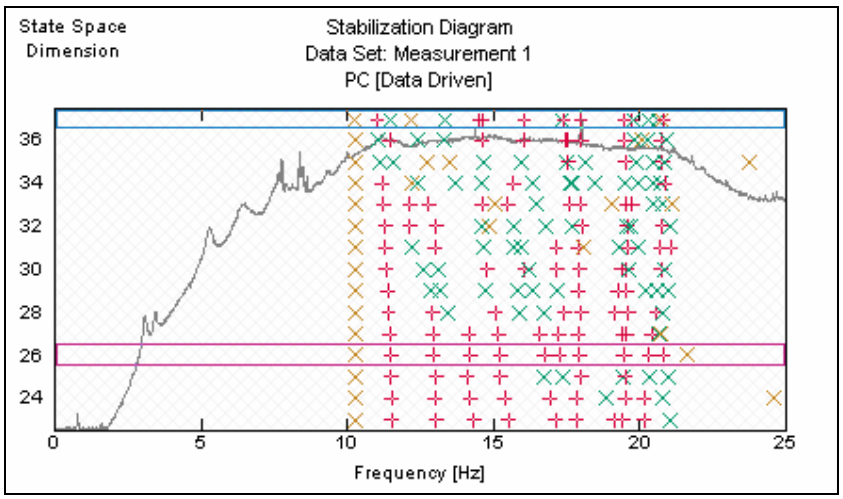

Figure 2.78 Captured modes from PC algorithm on June 6th record in 10-25 Hz frequency range

As the other recorded readings, the data of the December 22nd did not gave very clear results in the 10-25Hz frequency range. The first 10 modes which had damping ratios less than % 10 were captured from December 22nd data set using PC algorithm. Further detail of the first mode obtained from December 22nd data set are listed in Table 2.45. Corresponding MAC values comparing different algorithms are given in Table 2.46. The summary of the matching mode MAC values and frequencies are shown in Figure 2.79.

Table 2.45. Frequency and damping values of captured modes from UPC,PC,CVA algorithms on December 22nd record

	UPC		PC		CVA	
	frequency(Hz)	*damping(%)*	*frequency(Hz)*	*damping(%)*	*frequency(Hz)*	*damping(%)*
Mode6	**10,41**	5,481	**11,26**	5,644	**10,86**	1,575
Mode7	**10,92**	3,39	**12,42**	9,796	**12,97**	3,874
Mode8	**13,45**	4,784	**13,99**	5,338	**15,14**	6,38
Mode9	**15,34**	4,76	**15,55**	3,274	**17,58**	2,062
Mode10	**16,58**	6,408	**17,42**	0,9195	**17,99**	1,439
Mode11	**17,32**	0,8125	**17,92**	0,8387	**19,86**	1,804
Mode12	**17,95**	0,3549	**18,14**	3,91	**20,89**	2,03
Mode13	**18,71**	6,251	**19,92**	1,45		
Mode14	**19,88**	2,04	**20,6**	3,703		
Mode15	**20,74**	2,065	**20,92**	6,317		

Table 2.46. MAC matrix between UPC algorithm results of December 22nd and PC algorithm results of first data set in 10-25Hz frequency range

MAC	11,49Hz	12,94Hz	14,17Hz	15,22Hz	16,73Hz	17,24Hz	17,92Hz	19,45Hz	19,48Hz	20,31Hz	20,08Hz
10,41Hz	**0.9349**	0.3409	0.1915	0.1861	0.397	0.307	0.213	0.3555	0.2647	0.1907	0.3854
10,92Hz	0.7159	0.7996	0.5775	0.1915	0.2497	0.4237	0.1721	0.4047	0.4253	0.2768	0.369
13,45Hz	0.6222	0.2428	0.6017	0.4519	0.22	0.3771	0.1075	0.1173	0.07595	0.3639	0.2845
15,34Hz	0.2099	0.5412	**0.8803**	0.5981	0.1643	0.1679	0.09803	0.4036	0.5635	0.2565	0.2578
16,58Hz	0.09255	0.3929	0.2979	0.678	0.4502	0.6326	0.453	0.329	0.03662	0.2463	0.08263
17,32Hz	0.1966	0.5707	0.193	0.5609	**0.8686**	0.1996	0.7102	0.3929	0.201	0.327	0.05709
17,95Hz	0.3839	0.224	0.1751	0.7585	0.5385	0.4992	0.3094	0.515	0.179	0.5323	0.1975
18,71Hz	0.2202	0.3137	0.1786	0.6106	0.7977	0.1977	0.5524	0.4672	0.2188	0.3153	0.1027
19,88Hz	0.09094	0.403	0.5044	0.2054	0.271	0.2533	0.2393	0.5489	**0.8817**	0.0232	0.3073
20,74Hz	0.4426	0.4385	0.2859	0.2647	0.6278	0.3405	0.3099	0.2037	0.173	0.223	0.1954

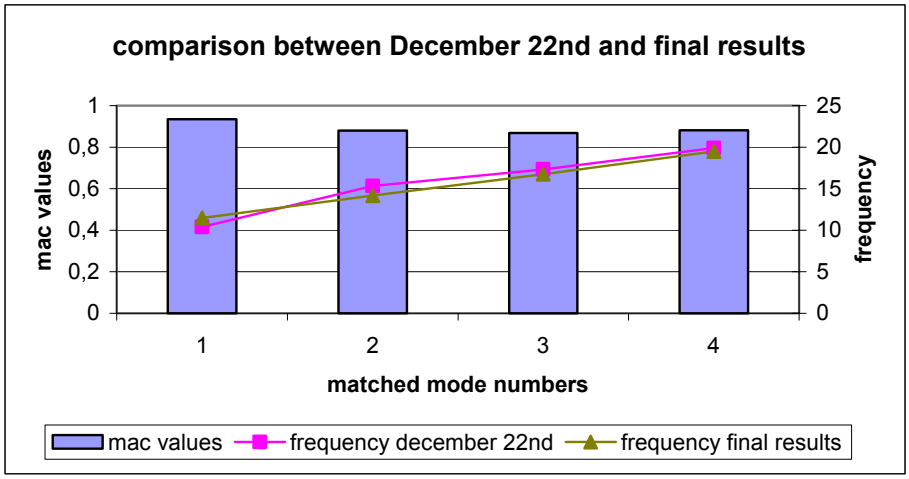

Figure 2.79 Comparison between frequencies of the matched modes of PC algorithms of December 22nd and final result modes in 10-25 Hz frequency range according to their MAC values

Four modes of the UPC algorithm of December 22nd in 10-25 Hz frequency range were matched with the final result modes in the same frequency range. The modes which had MAC values greater than the 0.8 was accepted as the matched modes. Matched mode numbers are less and it was an expected situation since the matched mode numbers of the previous data sets were also less. Furthermore, except the first matched mode, all the matched modes of the December 22nd data set in 10-25 Hz frequency range gave greater frequency values and less damping ratios than the matched final result modes.

As the third step, the data set which was recorded on December 22nd was investigated in 25-50 Hz frequency range. Frequency, mode numbers and damping ratios of captured modes from December 22nd in 25-50Hz frequency range is represented in Table 2.47. Furthermore, stabilization diagram of the December 22nd in 25-50 Hz frequency range is given in Figure 2.80 and the stabilization diagram of the final result modes is seen in Figure 2.81.

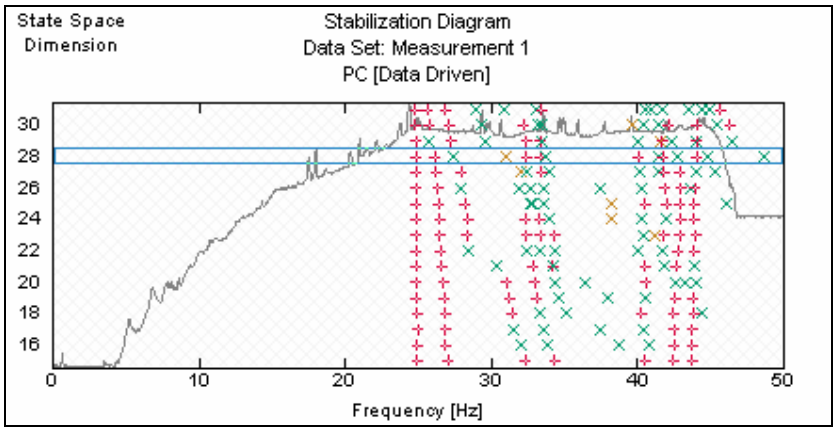

Figure 2.80 Captured modes from PC algorithm on December 22nd record in 25-50 Hz frequency range

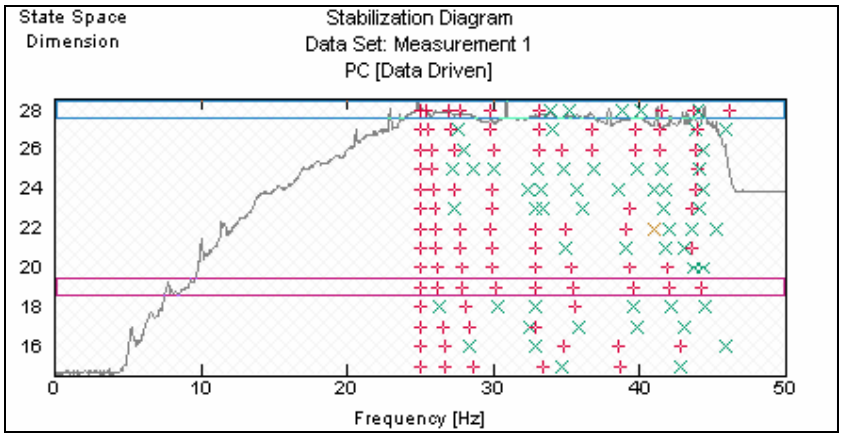

Figure 2.81 Captured modes from PC algorithm of first data set in 25-50 Hz frequency range

Table 2.47. Frequency and damping values of captured modes from UPC,PC,CVA algorithms on December 22nd record in 25-50Hz frequency range

UPC			PC			CVA		
	freq.(Hz)	*damping(%)*		*freq.(Hz)*	*damping(%)*		*freq.(Hz)*	*damping(%)*
Mode16	**24,6**	0,8805	*Mode16*	**24,82**	1,427	*Mode13*	**24,4**	1,107
Mode17	**25,5**	4,636	*Mode17*	**26,08**	4,597	*Mode14*	**24,74**	5,984
Mode18	**33,49**	9,993	*Mode18*	**32,35**	5,444	*Mode15*	**25**	3,986
Mode19	**44,58**	1,999	*Mode19*	**33,31**	4,256	*Mode16*	**31,85**	9,24
			Mode20	**40,05**	5,504	*Mode17*	**33**	8,226
			Mode21	**41,73**	3,528	*Mode18*	**40,69**	5,611
			Mode22	**44,05**	2,463	*Mode19*	**43,78**	5,081
						Mode20	**44,68**	1,636

The comparison of MAC values for December 22nd and June 16th (second data set) are given in Table 2.48 in matrix format for 25-50 Hz range. Similar to the results obtained before, no correlation between mode shapes were obtained for 25-50 Hz range. The poor correlation can be an indication of unstable mode shapes and frequencies in 25-50 Hz range due to temperature, or it may be an indication of improper ambient excitation for the given range.

Table 2.48. MAC matrix between PC algorithm results of December 22nd and second data set in 25-50Hz frequency range

MAC	25,01Hz	26,14Hz	27,82Hz	30,15Hz	32,86Hz	35,44Hz	39,52Hz	42,01Hz	44,2Hz
24,82Hz	0.3846	0.4015	0.01721	0.06929	0.242	0.008829	0.105	0.09529	0.1104
26,08Hz	0.1425	0.4158	0.1758	0.2473	0.2018	0.2964	0.175	0.3694	0.2183
32,35Hz	0.186	0.353	0.212	0.2951	0.224	0.2402	0.2878	0.2661	0.3128
33,31Hz	0.4467	0.2892	0.3502	0.09651	0.3212	0.1224	0.1296	0.3067	0.1662
40,05Hz	0.2753	0.3229	0.3077	0.1701	0.3033	0.3625	0.209	0.2037	0.2551
41,73Hz	0.3426	0.4344	0.1291	0.1758	0.2033	0.3325	0.3961	0.223	0.1351
44,05Hz	0.06582	0.2172	0.2021	0.281	0.08672	0.2859	0.05442	0.1176	0.3727

CHAPTER 3

ANALYTICAL STUDY

3.1. Introduction

In Chapter 3, two types of analytical models were used to simulate the measured dynamic properties of Kabatas İstanbul building. Two types of analytical models were calibrated in order to match the measured properties. The two types of models are briefly explained in bullet list format:

- Shear walls modeled using thick columns which were connected using rigid beams at floor levels.
- Shear walls modeled using thick columns which were connected using end-length offsets with rigid zone factor. Rigid zone factor was determined as 1. (i.e., all of the beam length is rigid offset.)

The major calibrated parameters were selected to be floor mass, elastic modulus of concrete and infill walls, spring stiffness, member locations. Details about each type of modeling, calibration and related pushover studies are explained below under separate headings.

3.2. Finite Element Models

Finite Element Modeling studies of the Kabatas İşbank building were started before the instrumented monitoring/testing. By analyzing finite element model of the building, the behavior and possible structural problems associated with the building were expected to be known.

Some important structural information about the building was missing in the structural plans and because of that situation necessitated assumptions were made for the two models. Reinforcements of the beams and columns were not known; therefore the minimum required beam and column reinforcements were used in the analysis. Furthermore, the slab weights of the floors were also not exactly known since the floor surface tiling type was not clear. Only the thickness of the slabs existed in the structural plan of the building. In the analysis, slab concrete thickness was taken as 15cm and thickness of the bedding concrete, surface tiling and plaster were chosen as 5cm, 2cm, 2cm respectively. Mosaic covering was used as surface tiling in the dead load calculations of the floors. However, total floor mass was used as a variable for the calibration studies. For the wall weight calculations, density of the hollow bricks was used.

General view of the thick column model is shown in Figure 3.1.

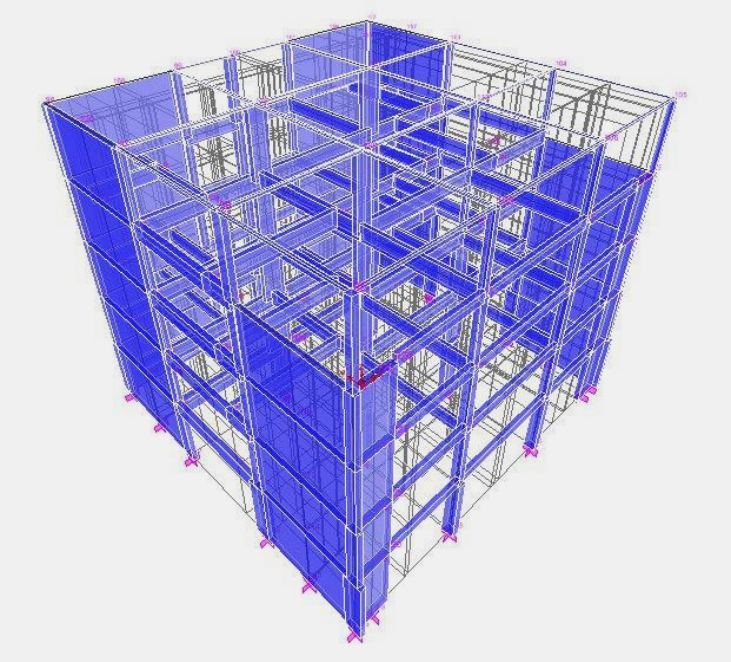

Figure 3.1 First FEM of the experimented structure

3.3. Comparison between analytical FEM and experimental measurement results

In the comparison part, Modal Assurance Criteria (MAC) was used. The modal vectors obtained from finite element model analyses can be compared against the experimentally determined modal vectors by using MAC. The point is that the mode shape vectors for the analytical models are taken from the DOFs which were used in the experimental model. MAC is based on a comparison between an experimentally measured mode shape, $\{\psi x\}$, and a theoretically predicted one, $\{\psi a\}$. MAC is defined in Equation 3.1.

$$MAC(a,x) = \frac{\left[(\psi x)^T \cdot (\Psi a)\right]^2}{\left[(\psi x)^T \cdot (\Psi x)\right] \cdot \left[(\psi a)^T \cdot (\Psi a)\right]} \qquad 3.1$$

Two options exist in Artemis Software to export the mode vectors of the tested building. The deformations can be exported in SVS and UFF formats. When SVS file form is used, absolute values of the deformations can only be seen. But using UFF format, directions of the displacements can also be determined. Positive x and positive y directions and related displacements are calculated according to their definitions in SAP2000 computer software. Therefore for the comparison between Artemis software and SAP2000, UFF format was used. Exported joint displacements of the mode vectors from Artemis and SAP2000 software were collected and a MAC matrix was created to compare the mode shapes in Excel environment.

Then, comparisons between the mode shapes and modal frequencies obtained from the experimental and analytical studies conducted. The comparison of analytical and experimental results formed the basis for model calibration. The fundamental assumptions before the calibration and during the calibration process are described below under each heading referring to different models.

3.3.1. First Model

The major properties and assumptions of the first model, which was constructed to represent the strengthened building without any calibration works are listed below. This model would represent the case if no experimental data were available.

- Rigid beams were used to connect columns to the shear wall column in the first model. Shear walls were determined as large columns in SAP2000 software. Moment of inertia about 3 axis and shear area in 2 direction were assigned very large values to create the rigid beams. Cross sectional area of the rigid beams were insignificant (and taken as 1cm²) since the floor diaphragm definition dominates the motion.
- Shear walls were designed as seen in the key (structural) plan of the building. Therefore, no shear walls were created on the front face of the building at roof level.
- According to the strengthening project, modulus of elasticity value were taken as 28500MPa (C20) for the shear walls and 27000MPa (C16) for the columns and beams.
- Reinforcement of the shear walls was selected StIII (S420) and the reinforcement of the column and beams were chosen StI (S220) as determined in the key plan of the building.
- Shear wall mass and weight values were automatically calculated by the software. Slab mass values were manually calculated and incorporated to the FEM using mass source joints after making assumptions for the surface tiling due to lack of the key plans.
- According to the structural plan; steel columns were used on some part of the roof story (Figure 3.2). Sections of these steel columns were not exist in the key plan. Therefore, they were modeled as concrete columns in the model; however, their modulus of elasticity value were chosen as steel's elasticity value.

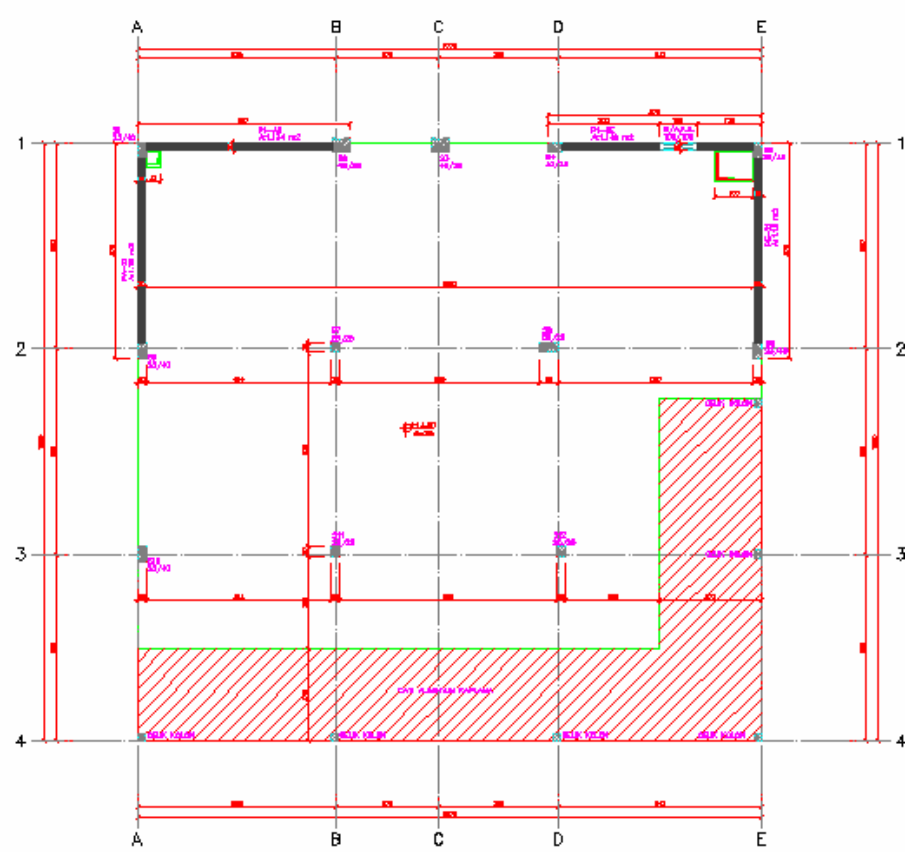

Figure 3.2. Structural plan of the roof story

Figure 3.3. shows the MAC comparison matrix of the first model. Circles in the figure represents the MAC matrix values and a series of small circles following a path in the diagonal direction as a function of mode numbers shows the frequency correlation. When the large circles that show good correlation between experimental and analytical modes match with frequency correlation path, the results are said to be matching both in frequency and mode shapes. Four modes are matched in the Figure 3.3. First one of the well-matched mode is in x direction and longitudinal, second one of them is a longitudinal mode and in y direction and the third mode is the second translational mode in x direction. Last mode represents a translation-torsion movement in both x and y directions (Table 3.1).

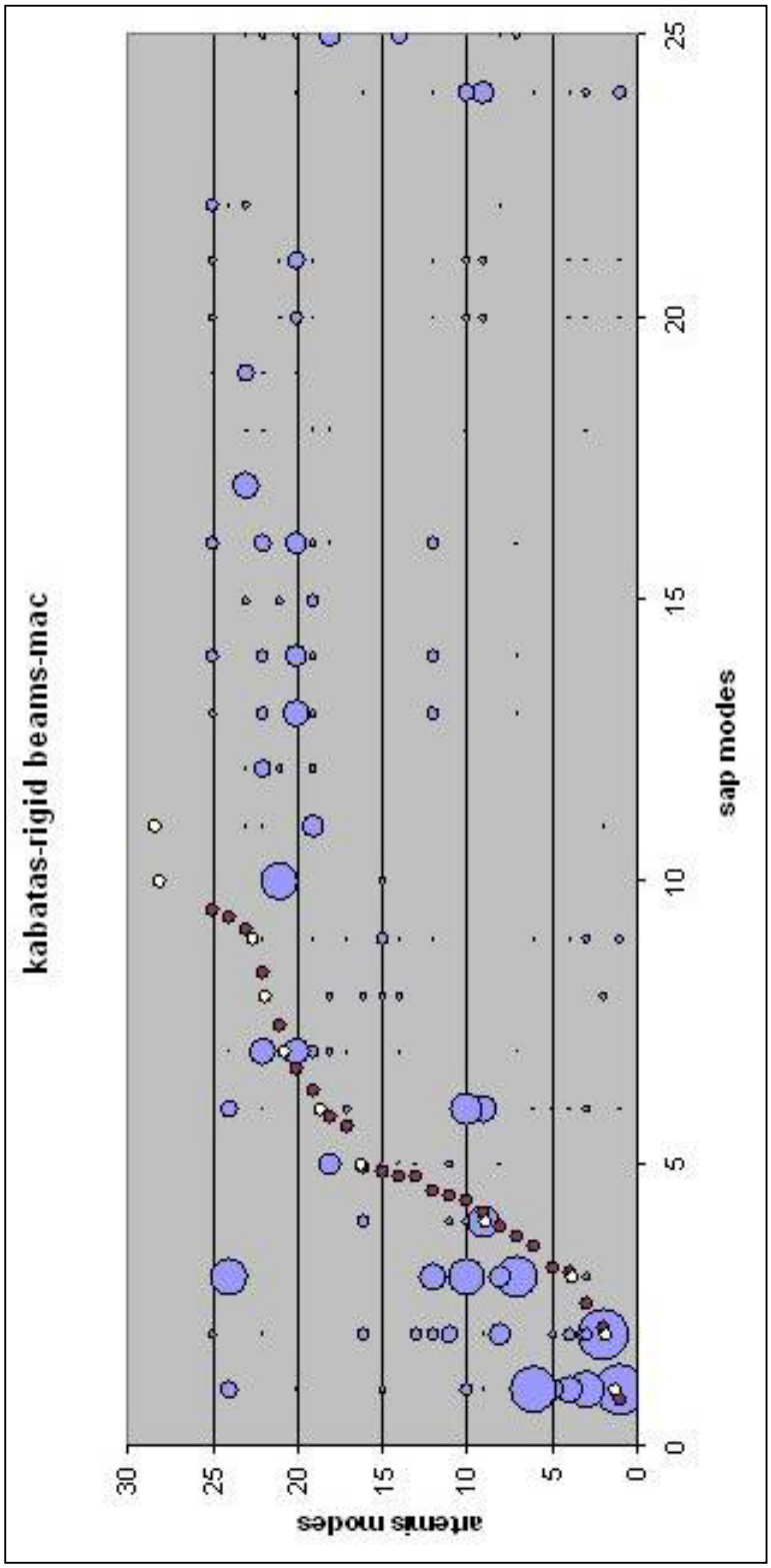

Figure 3.3 MAC comparison and frequency correlation between first analytical and experimental model

Table 3.1. Mode values of the first analytical model and experimental model

artemis			sap		mac	description
mode number	frequency	damping(%)	mode number	frequency		
1	3,124	2,138	1	3,6565	0,894	x-longitudinal
2	5,288	1,289	2	5,0077	0,947	y-longitudinal
9	15,22	4,412	4	14,987	0,565	2nd translational-x
20	30,15	5,632	7	31,926	0,480	translational-torsion

Figure 3.4 represents the frequency comparison of the matched modes of the first analytical model and experimental model according to the MAC values. As seen from the graphic, frequencies of the matched modes are closer to each other.

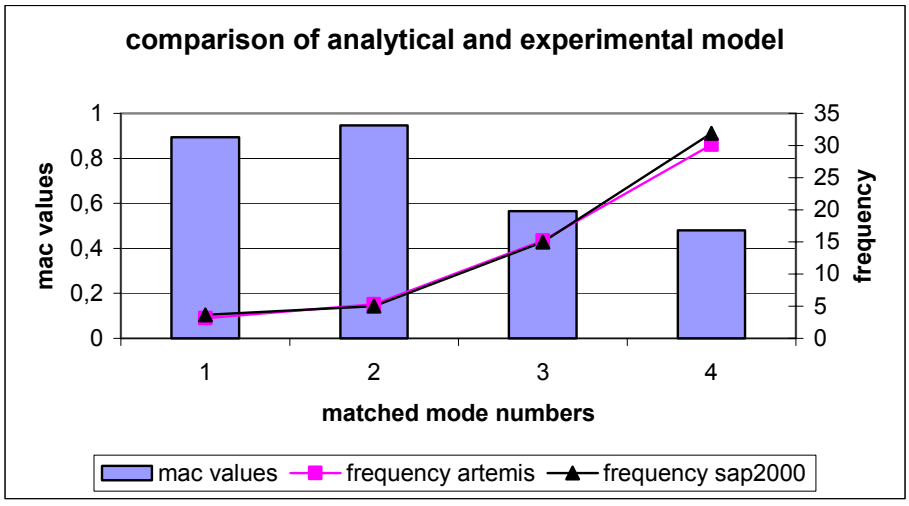

Figure 3.4 Frequency comparison of the matched modes of the first analytical model and experimental model according to the MAC values

3.3.2. Second Model

The second analytical model is quite similar to the first model with the exception that rigid links defined in the first model as frames with large moment of inertia and shear stiffness are replaced with end length offsets. The rigid zone factor for the offsets are taken as 1.0 which is infinitely rigid. The properties of the second model are listed below in bullet list format.

- Shear walls were created as large columns and end length offsets were defined on the beams to connect them to the shear walls. Rigid zone factor of the end-length offsets were taken as one.
- Shear walls were modeled between the existing columns in the original building according to the strengthening project.
- Shear wall mass and weight values were automatically calculated by the software. Slab mass values were manually calculated and incorporated to the FEM using mass source joints after making assumptions for the surface tiling due to lack of the key plans.
- Shear walls were designed as seen in the key plan of the building. Therefore, no shear walls were created on the front face of the building at roof level.
- According to the key plan; steel columns were used on some part of the roof story. The sections these steel columns were not exist in the key plan. Therefore, they were modeled as concrete columns in the model; however, their modulus of elasticity value were chosen as steel's elasticity value.
- According to the strengthening project, modulus of elasticity value were taken as 28500MPa (C20) for the shear walls and 27000MPa (C16) for the columns and beams.
- Reinforcement of the shear walls was selected StIII (S420) and the reinforcement of the column and beams were chosen StI (S220) as determined in the structural plan of the building.

Figure 3.5 represents MAC comparison and frequency correlation between second analytical and experimental model. Four modes were matched according to their MAC values and frequency correlation in the comparison.

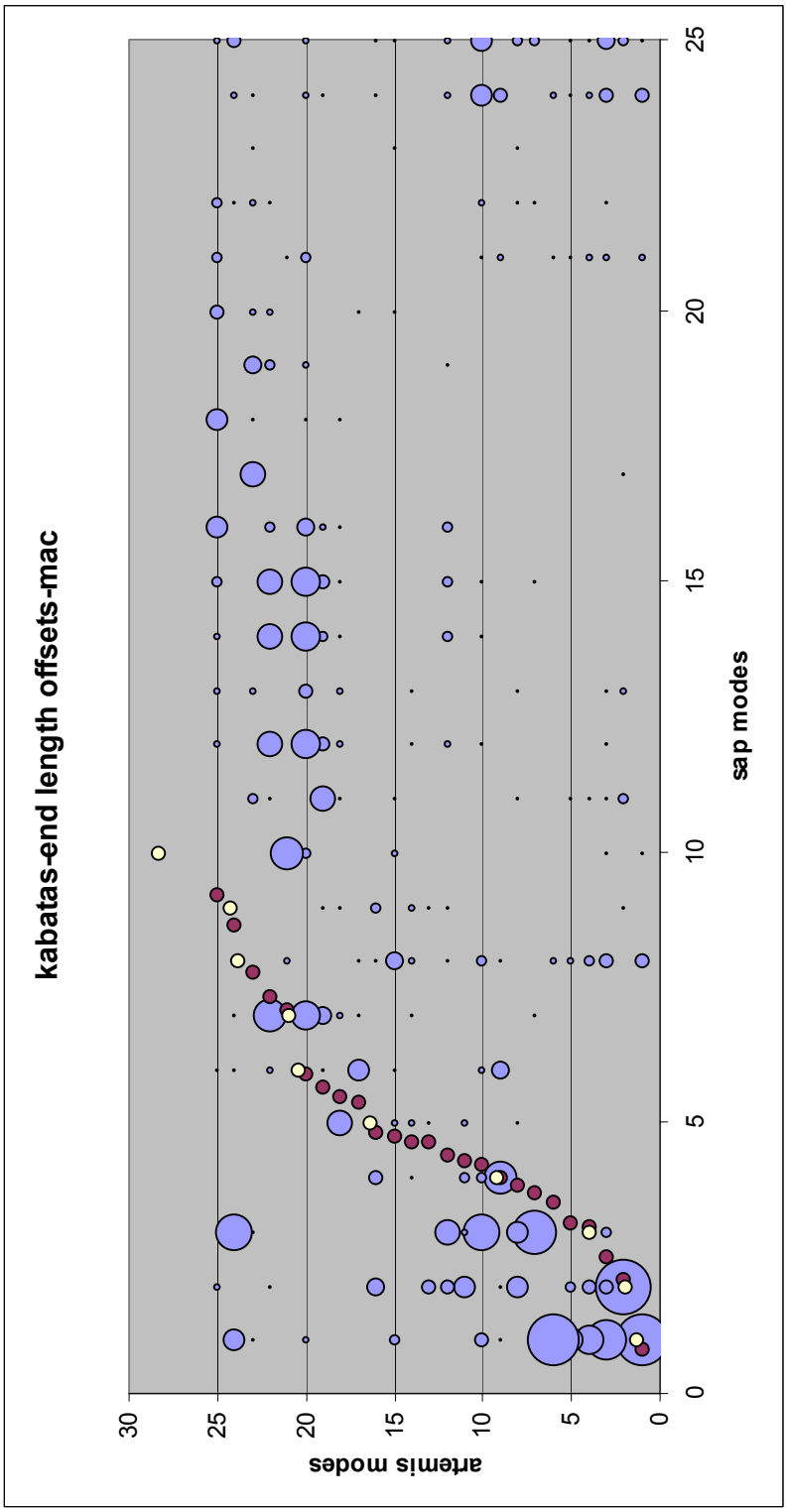

Figure 3.5 MAC comparison and frequency correlation between second analytical and experimental model

Table 3.2. Mode values of the second analytical model and experimental model

artemis			sap		mac	description
mode number	frequency	damping(%)	mode number	frequency		
1	3,124	2,138	1	3,6956	0,895	x-longitudinal
2	5,288	1,289	2	5,0891	0,947	y-longitudinal
9	15,22	4,412	4	15,255	0,581	translational-x
22	35,44	3,866	7	32,642	0,565	torsion-translation-y

Frequency and damping values of the experimental and analytical modes are given in Table 3.2. First matched mode is a longitudinal mode in x direction and the second is a longitudinal mode in y direction. Third matched mode is a bending mode and the fourth matched mode is a bending-torsion mode.

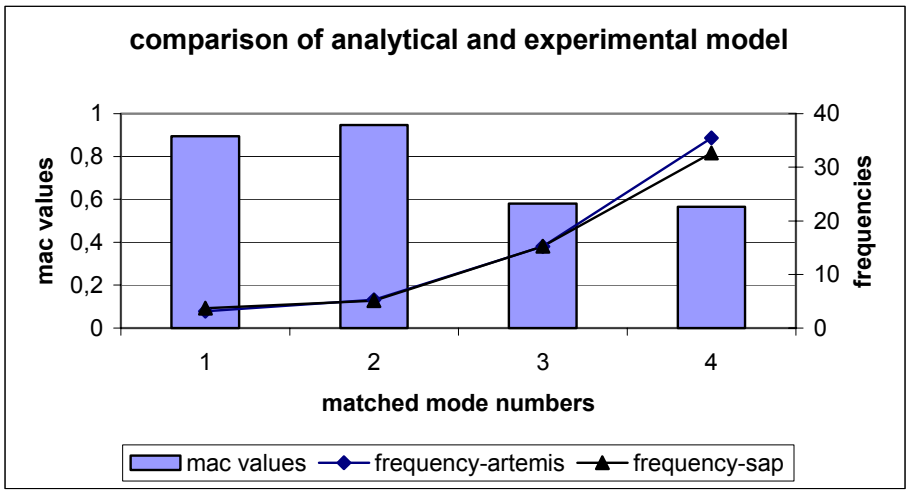

Figure 3.6 Frequency comparison of the matched modes of the second analytical model and experimental model according to their MAC values.

The results obtained from the first and second models are almost the same with negligible differences in MAC values and frequencies. Therefore, the FE model may be modeled using end length offsets or rigid members.

3.4. Calibration of the FEM

Several mathematical models were tried within the scope of the calibration study. In the first step, application of the strengthening project was tested. When the tested building was visited for the installation study, an additional information about the construction was learned: There was a cabin over the roof level which had nearly covering the elevator's motor. Furthermore an aluminum cover roof was seen in some part of the roof plan. Therefore, irregular mass distribution was tried for the roof story in the model and that irregular mass distribution was verified by the improved correlation results of the MAC matrices. First, irregular mass distribution was applied to the roof floor in the mathematical model by creating three mass source joints. By using irregular mass distribution on the roof story, better-matched modes were captured. Second, roof story was modeled using shell elements to create mass distribution. That condition created unnecessary vertical modes on the model. In spite of that situation, rest of the modes were well-matched. Since there were no structural source for additional lumped masses found in the key plans and visual inspection of the building, alternative modifications to the FE model were investigated such as reducing stiffness. In the next step, stiffness of the shear walls at the roof story were reduced. Slab, column and beam weights were manually calculated and entered to the model by using mass center joints. Shear wall mass quantities were automatically calculated by the software. Shear walls were defined as seen in the key plans of the building. Therefore, no shear walls were defined on the front face of the roof story. But at the roof story, elasticity modulus of the back side shear walls were reduced to reduce the stiffness to simulate possible connection fault between the shear wall and roof slab within the scope of the calibration study. Selected elasticity modulus for these shear walls was 20000MPa. The joints of these shear walls on the roof floor were not included to the diaphragm in the SAP2000 software and relatively better-matched modes were obtained. These sets of iterations showed that something about the shear walls of the roof story was wrong. As an additional alternative, shear walls at the roof story were modeled only at the rear corner where elevator was located and the modeled shear walls were not included to the diaphragm of the roof floor in SAP2000. By making this assumption, best-matched modes were captured. Thus, it was determined that all the shear walls of

the roof story which were seen in the structural plan were either not constructed in the application or not properly attached to the roof slab.

Tested building was constructed adjacent to another building from its left side from the front view . Therefore, additional springs were assigned at the joints of that side for all stories. Values of the spring constants were increased from the roof story towards the ground story. Different spring constant values were tried in that study. Comparison results (MAC values) showed that spring constants do not have any significant effect on the model.

Brick walls were defined as infill elements at the back and left side of the structure for analytical study (front and left sides have windows). To simulate the effect of the adjacent building, the elastic modulus values of the infill walls were increased. After several runs, it has been seen that defining two times larger elastic modulus value (2000Mpa) for the left side infill walls, gave the best MAC correlation. The elastic modulus values for the rear side infill walls kept constant and equal to 1000Mpa. (This elasticity modulus value of the hollow bricks was taken from the materials property part of the Turkish code about the strengthening of the moderately damaged structures.) When the rear infill walls completely removed, back side infills had no significant effect on the model. However adjacent building's effect due to strong and dominant shear wall existance at the rear side, were represented by the left side infills and they had significant effects on the model. Therefore, the rear side infill walls were removed (windows exist), only the left side infills were used in the model, and their elasticity value were chosen as 1000Mpa.

3.4.1. First Calibrated Model

The model in which shear walls were modeled by using end-length-offsets were calibrated as the first model. Locations of the shear walls at the roof story, elastic modulus value of the infill walls are the major calibration parameters for that

model. The final analytical model calibrated using the dynamic results had the following properties:

- Shear walls at the roof story were modeled only at the rear corner where elevator was located.
- Shear wall joints at the roof story were not included as a part of the roof floor diaphragm in SAP2000 software; in turn, making the shear wall slab connection weaker.
- Shear walls were modeled as large columns and end-length-offsets were defined on the beams to connect them to the shear walls. Rigid zone factor of the end-length-offsets were taken as one.
- Brick walls were created at the left side by using infill diagonal members (E:1000MPa, A:1161 cm^2) to model adjacent building expansion joint effects.

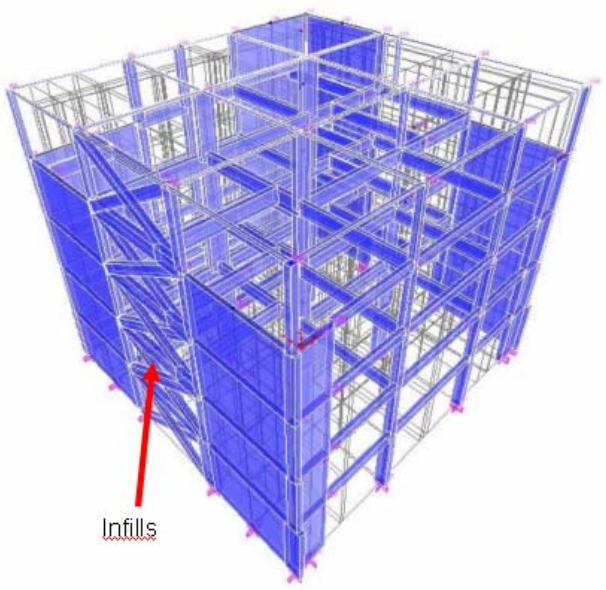

Figure 3.7 General view of the final calibrated model from SAP2000 software

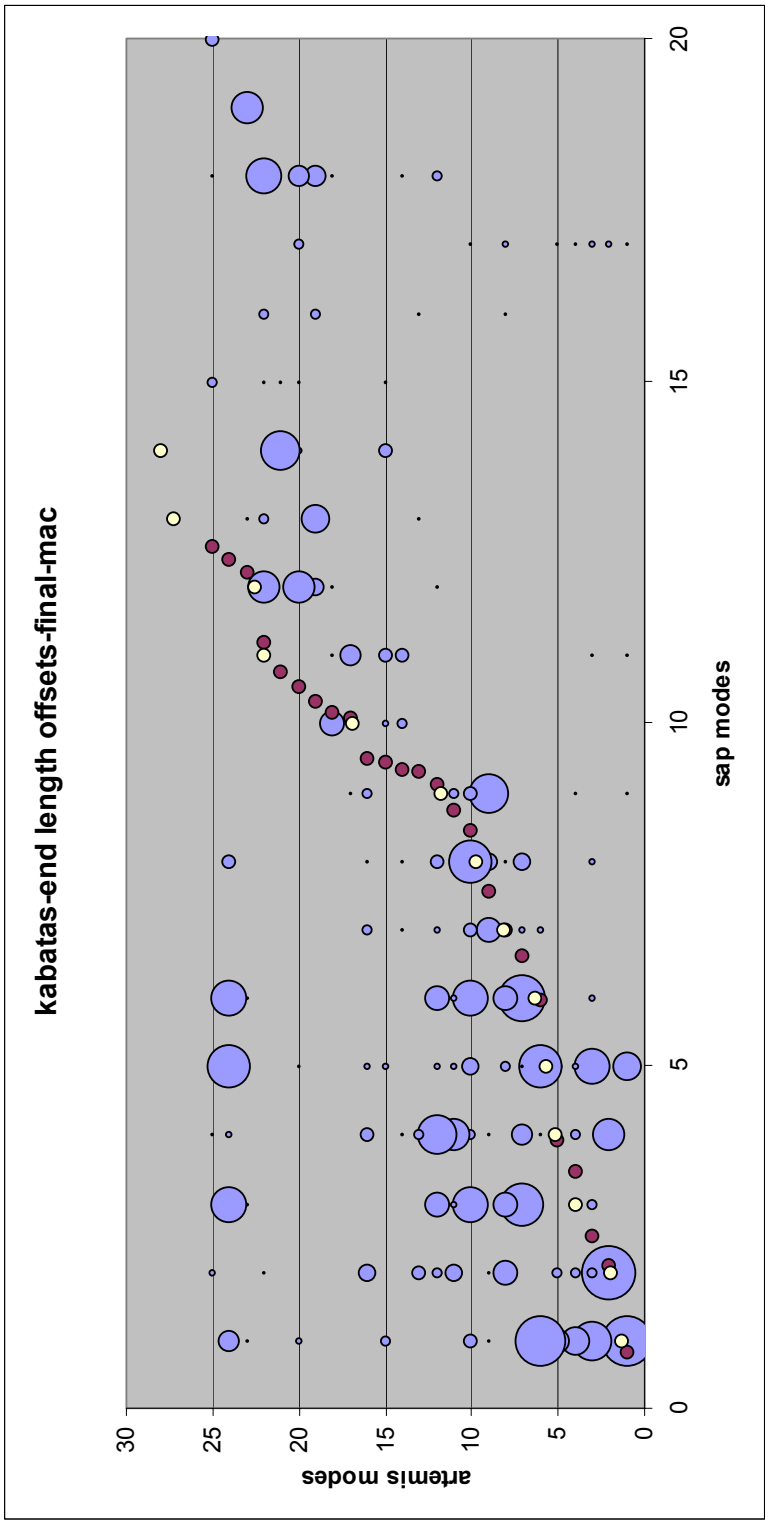

Figure 3.8 MAC comparison and frequency correlation between the first calibrated analytical model and experimental model

Figure 3.8 represents the MAC comparison and frequency resolution between the first calibrated analytical model and experimental model.

Calibrated model gave closer frequencies to the experimental model for the first eight modes (Table 3.3). These modes were matched with the experimental model. Longitudinal modes in x and y directions, torsional mode, translational modes in x direction, translational mode in y direction and two translational-torsional mixed modes were matched. General views of the some matched modes from Artemis and SAP2000 are seen in Figure 3.9 through Figure 3.13.

Table 3.3. Mode values of the first calibrated analytical model and experimental model

artemis			**sap**		**mac**	**description**
Mode number	frequency	damping(%)	mode number	frequency		
1	3,124	2,138	1	3,7454	0,898	x-longitudinal
2	5,288	1,289	2	5,1021	0,938	y-longitudinal
6	11,49	4,658	5	10,328	0,737	translational-x
7	12,94	6,787	6	11,526	0,81	torsion
9	15,22	4,412	7	14,182	0,467	2nd translational-x
10	16,73	6,986	8	16,189	0,771	translational-torsion
18	26,14	2,972	10	24,502	0,482	translational-y
22	35,44	3,866	12	37,375	0,585	translational-torsion-x-y

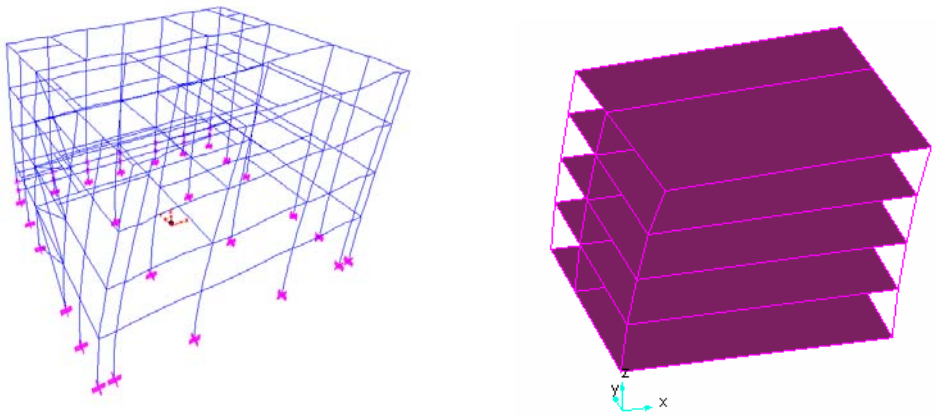

Figure 3.9 General view of the 1st matched modes

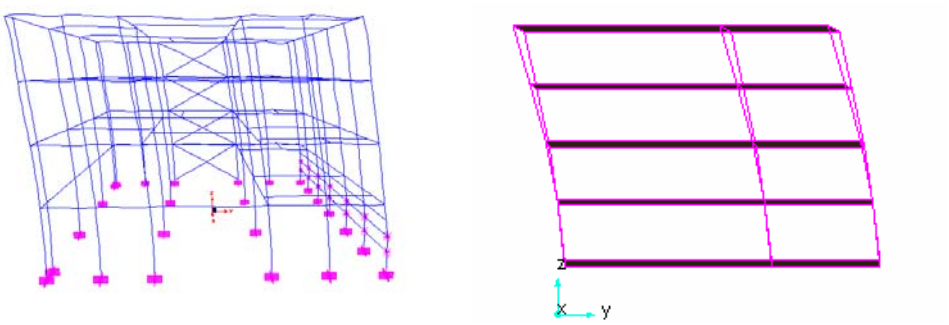

Figure 3.10 General view of the 2nd matched modes

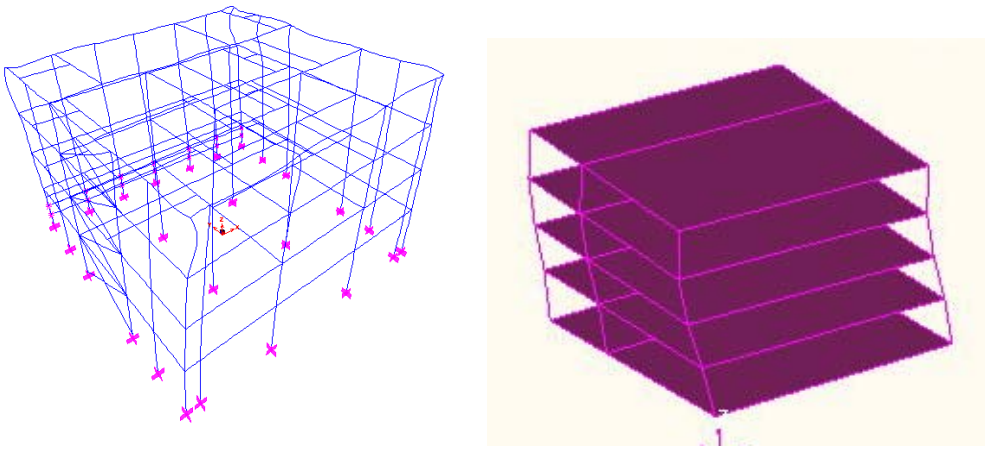

Figure 3.11 General view of the 4th matched modes

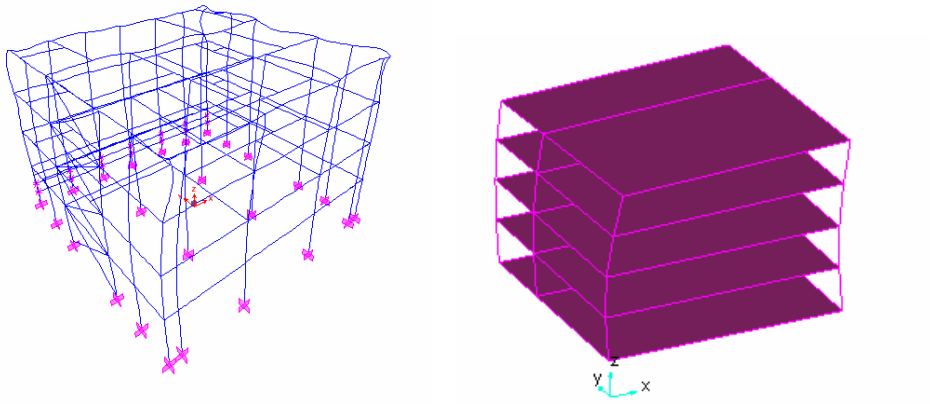

Figure 3.12 General view of the 6th matched modes

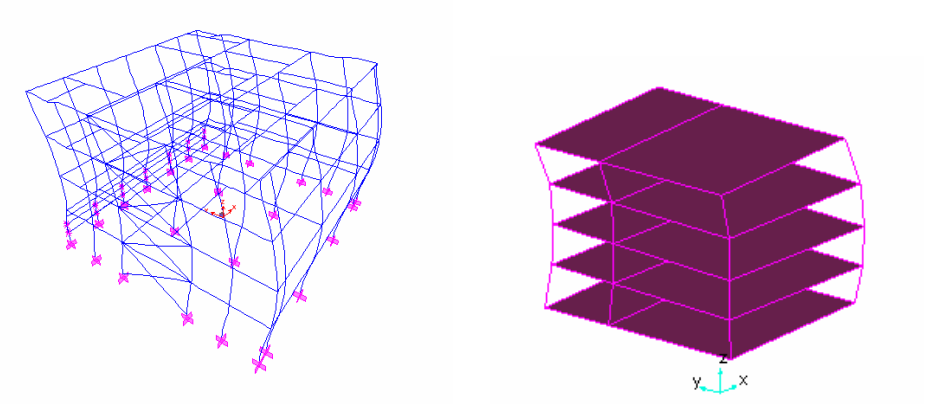

Figure 3.13 General view of the 7th matched modes

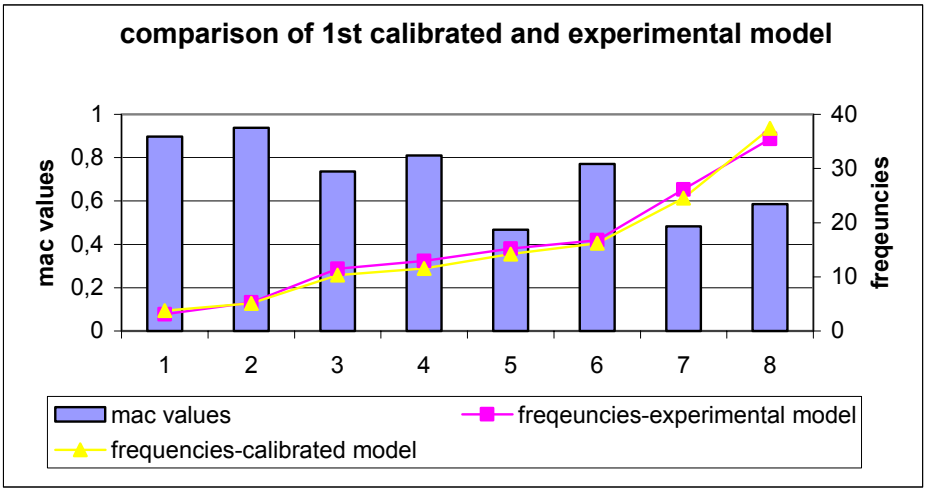

Figure 3.14 Frequency comparison of the matched modes of the first calibrated analytical model and experimental model according to the MAC values

Figure 3.14 represents the frequency comparison of the matched modes of the first calibrated analytical and experimental model according to the MAC values. Frequency values of the matched modes are closer to each other.

3.4.2. Second Calibrated Model

In the second calibrated model, shear wall columns were divided into four segments and connected to the corner columns by using four rigid beams for each

story. Shear wall joints were only connected to the floor diaphragms at the floor levels. It is assumed that by dividing the shear wall lines into four pieces and connecting them to the corner columns and to the perpendicular shear walls with four rigid links at every story, column-like shear wall elements would better represent the actual shear wall behavior.

The major properties and assumptions of the second calibrated model are the same as the first calibrated model, except for dividing frames of the shear walls in to smaller segments. The general view of the second model is given in Figure 3.15.

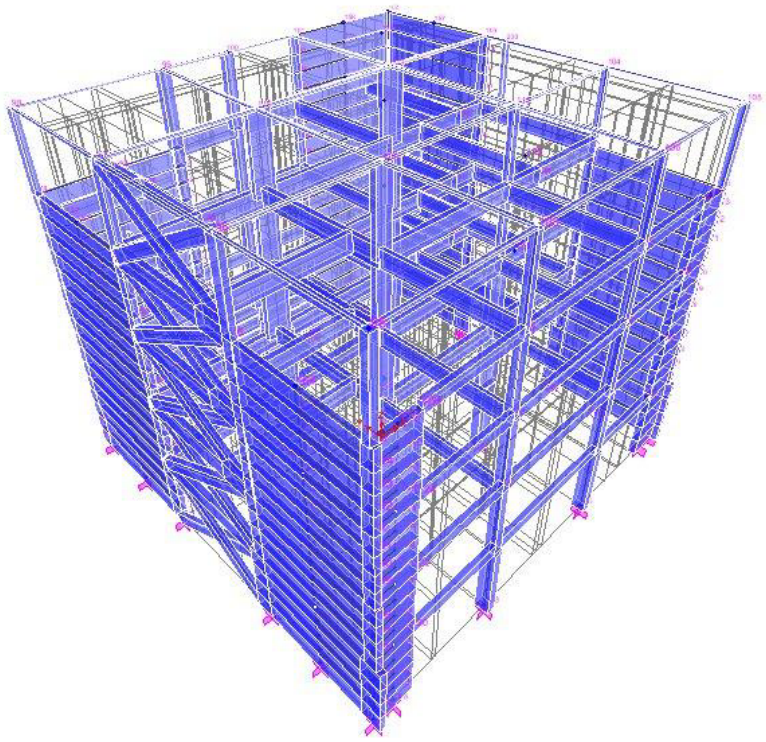

Figure 3.15 General view of the second calibrated model from SAP2000 software

Figure 3.16 represents the MAC comparison and frequency correlation between the second calibrated analytical model and experimental model. Five modes were matched according to their MAC values and frequency correlation.

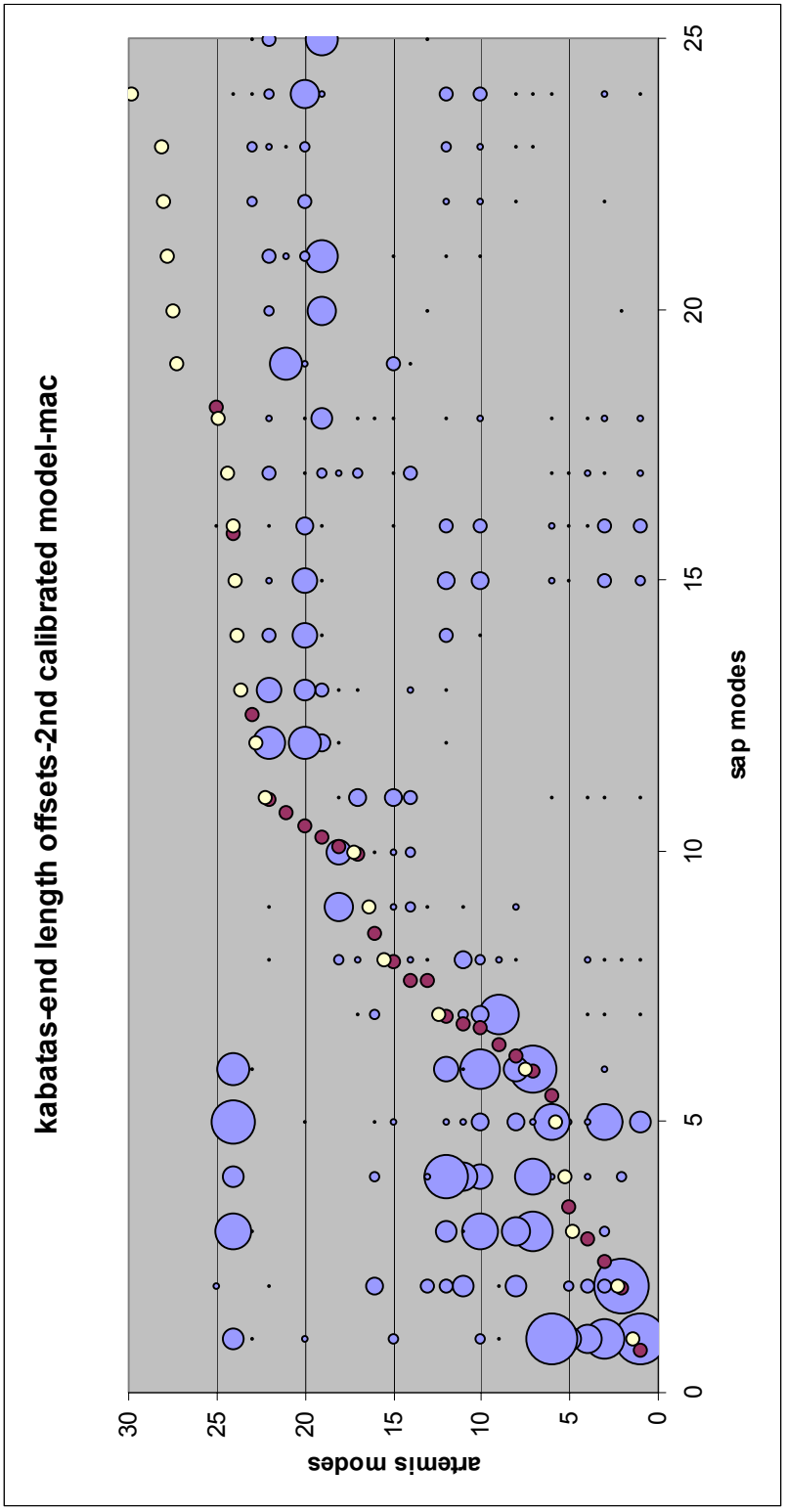

Figure 3.16 MAC comparison and frequency correlation between the second calibrated analytical model and experimental model

Table 3.4. Mode values of the second calibrated analytical model and experimental model

artemis			sap		mac	description
mode number	frequency	damping(%)	mode number	frequency		
1	3,124	2,138	1	3,9458	0,899	x-longitudinal
2	5,288	1,289	2	5,3768	0,943	y-longitudinal
6	11,49	4,658	5	10,772	0,62	translational-x
7	12,94	6,787	6	13,183	0,805	torsion
18	26,14	2,972	10	24,963	0,472	translational-y
22	35,44	3,866	12	37,987	0,581	translational-torsion-x-y

In the second calibrated model, same modes were matched with the experimental model like the first calibrated model. However, second model gave the modal frequency values relatively larger than the first calibrated model, most probably due to the fact that second calibrated model became relatively stiffer compared to the first model. Dividing the shear walls into four segments and connecting perpendicular shear walls with three horizontal rigid beams in addition to the floor level connection made the model a little stiffer resulting in slightly higher frequencies. Furthermore, 2nd translational mode in x-direction and one of the translational-torsional mode were not captured in the second calibrated model.

Mode values of the second calibrated analytical model and experimental model is given in Table3.5. First and second matched modes are longitudinal modes in x and y directions respectively. Third matched mode is a torsional mode and the fourth mode is a translational mode in y-direction.

Frequency comparison of the matched modes of the second calibrated analytical model and experimental model is seen in Figure 3.17.

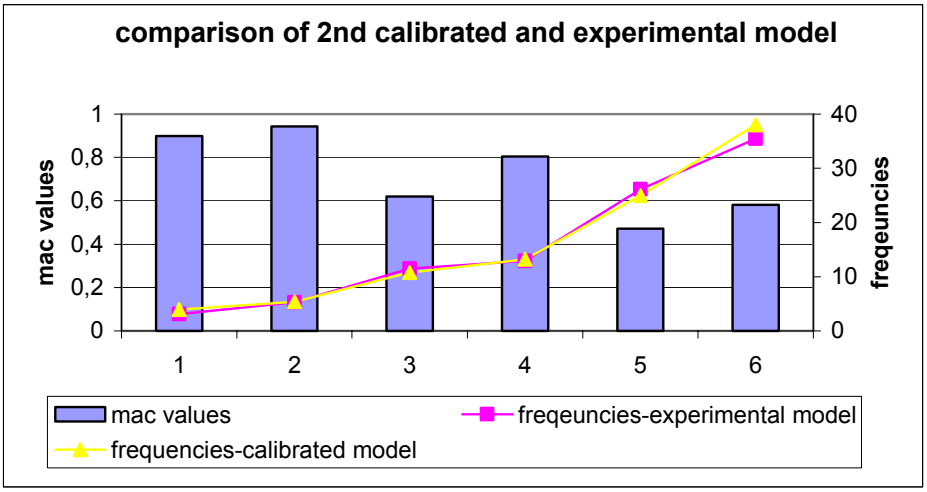

Figure 3.17 Frequency comparison of the matched modes of the second calibrated analytical model and experimental model

Several trials were made over these two models and the best results obtained from the both models are presented above. First calibrated analytical model captured more matched modes with closer frequency values to the experimental study. Therefore, first calibrated model was selected as the final calibrated model.

During the comparison and calibration studies between the measurement and analytical results, one of the problems was that the analytical model has four stories plus roof, while the instrumentation only covers four stories and ground floor. The response of the roof floor is indirectly incorporated to the dynamic measurements since mode shapes and modal frequencies are global parameters and also affected by structural properties of the roof floor.

Furthermore, pushover analyses conducted on the nominal and calibrated analytical models (see Appendix B).

CHAPTER 4

CONCLUSION

4.1. Summary

Ambient vibration measurements were performed on a four storey RC building within the scope of this study. 12 analog accelerometer, 1 tri-axial accelerometer, and a 15 channel data acquisition system were installed to the building. The transducers were used to continuously take readings at 100Hz and triggered readings at 200Hz. All the setups, outputs and configurations of the monitoring project were controlled by using Scream Software. Remote connection was established by using a telephone lane and a modem between METU computers and data logger's computer in Istanbul. Matlab routines and conversion programs were used to prepare recorded compressed data for the Artemis software input format. Artemis was used for the analysis of the recorded ambient vibration data. Simplistic model of the building was created inside the Artemis software to define locations of the transducers and obtain realistic mode shapes. All the readings were investigated in three different frequency ranges separately (0-10 Hz, 10-25 Hz, and 25-50 Hz) and the results were combined. Three different algorithms were used under Artemis software to obtain mode shapes, frequencies, and damping ratios. Results of the algorithms were compared among each other. The algorithm results which gave more accurate modes in the comparisons were accepted as the final frequencies and mode shapes. Four different data sets that were recorded at different times of a year processed using the same method and obtained results were compared against each other. The readings which gave the most confident results were accepted as the final result for the dynamic properties of the structure.

Finite element model of the tested building was created; the mode shapes and frequencies obtained from the analytical model were compared with their counterparts which were obtained from the experimental data processing.

Calibration studies conducted on different FE models, which revealed important information about the differences between the plans and the actual structure.

4.2. Conclusions

Majority of the objectives defined previously were achieved including ability to instrument and monitor a RC building, trigger and store data which may be remotely collected. Post processing of measured ambient dynamic data was successfully used to obtain mode shapes, frequencies, and periods.

Based on comparison of different post-processing algorithms, the dependability of the ambient acceleration data is found to be related with the frequency range. The modes obtained for the 0-10Hz. frequency range gave reliable and repeating modal information independent from the processing algorithm. The dynamic properties for that frequency range did not change when data recorded from different dates are used. For the higher frequency ranges, such as 10-25 Hz or 25-50 Hz ranges, modes were not clear and different results were obtained from different test data and using different algorithms. The instability of the modes above 10 Hz range may be affected by a number of factors which may be summarized as a) the ambient vibrations cannot properly excite high frequency modes beyond 10 Hz range, b) high frequency modes are highly damped and not responding to small ambient vibrations, c) higher frequency modes are highly sensitive to environmental changes such as support condition changes, traffic volume, human activity in the building or temperature changes between seasons, d) Artemis software was not capable of properly processing the higher frequency modes.

Calibration studies conducted on two different FE models were successful as 8 stable experimental modes and frequencies were also obtained using the analytical models. Comparison of nominal and calibrated analytical models revealed important differences between the plans of the strengthening plans and actual work conducted on the building. The shear walls at the rear corner at the roof level were missing in

the actual building and calibration results showed that the shear walls at the roof level were not properly connected to the roof slab.

Study results indicate that instrumented monitoring of buildings is useful in determining building characteristics at low vibrations and displacement levels. Although ambient vibrations were used instead of forced vibration, mode shapes, frequencies, and damping ratios were successfully obtained. Such a monitoring system may be required for buildings that underwent strengthening-retrofit work or buildings that are critical in nature. The same instrumentation system may be used to capture structural condition and performance of a building before, during, and after an earthquake. Comparison of mode shapes and frequencies may indicate if there are any permanent structural damage. A structural dynamic monitoring system would be recommended for important structures.

APPENDIX A

Input file of the Kabatas building used in Artemis software

Header

kabatas Building model input test #1

T

1.000E-02

Nodes

31	0.00000E+00	0.00000E+00	0.00000E+00
32	16.7000E+00	0.00000E+00	0.00000E+00
33	0.00000E+00	10.5000E+00	0.00000E+00
34	16.7000E+00	10.5000E+00	0.00000E+00
35	0.00000E+00	16.0000E+00	0.00000E+00
36	16.7000E+00	16.0000E+00	0.00000E+00
1	0.00000E+00	0.00000E+00	3.10000E+00
2	16.7000E+00	0.00000E+00	3.10000E+00
3	0.00000E+00	10.5000E+00	3.10000E+00
4	16.7000E+00	10.5000E+00	3.10000E+00
5	0.00000E+00	16.0000E+00	3.10000E+00
6	16.7000E+00	16.0000E+00	3.10000E+00
7	0.00000E+00	0.00000E+00	6.00000E+00
8	16.7000E+00	0.00000E+00	6.00000E+00
9	0.00000E+00	10.5000E+00	6.00000E+00
10	16.7000E+00	10.5000E+00	6.00000E+00
11	0.00000E+00	16.0000E+00	6.00000E+00
12	16.7000E+00	16.0000E+00	6.00000E+00

13	0.00000E+00	0.00000E+00	8.90000E+00
14	16.7000E+00	0.00000E+00	8.90000E+00
15	0.00000E+00	10.5000E+00	8.90000E+00
16	16.7000E+00	10.5000E+00	8.90000E+00
17	0.00000E+00	16.0000E+00	8.90000E+00
18	16.7000E+00	16.0000E+00	8.90000E+00
19	0.00000E+00	0.00000E+00	11.8000E+00
20	16.7000E+00	0.00000E+00	11.8000E+00
21	0.00000E+00	10.5000E+00	11.8000E+00
22	16.7000E+00	10.5000E+00	11.8000E+00
23	0.00000E+00	16.0000E+00	11.8000E+00
24	16.7000E+00	16.0000E+00	11.8000E+00

Lines

31	32
32	34
34	36
36	35
35	33
33	31
33	34
31	1
32	2
33	3
34	4
35	5
36	6
1	2
2	4
4	6
6	5
5	3
3	1

3 4
7 8
8 10
10 12
12 11
11 9
9 7
9 10
13 14
14 16
16 18
18 17
17 15
15 13
15 16
19 20
20 22
22 24
24 23
23 21
21 19
21 22
1 7
7 13
13 19
2 8
8 14
14 20
4 10
10 16
16 22
6 12
12 18

18 24
5 11
11 17
17 23
3 9
9 15
15 21

Surfaces

31 32 34
31 34 33
33 34 36
33 36 35
1 2 4
1 4 3
3 4 6
3 6 5
7 8 10
7 10 9
9 10 12
9 12 11
13 14 16
13 16 15
15 16 18
15 18 17
19 20 22
19 22 21
21 22 24
21 24 23

This is the definition group for the DOF information.

Description of the setups block

Record 1:

Field 1: (string) Data set label

Record 2:

Field 1: (string) File name where data is stored columnwise in ASCII

Record 3 through end

Field 1: (non-zero positive integer) Global transducer number

Field 2: (floating point) X-directional coordinate of the transducer

Field 3: (floating point) Y-directional coordinate of the transducer

Field 4: (floating point) Z-directional coordinate of the transducer

Field 5: (floating point) Reference value to apply on dB plots of PSD

Field 6: (string) Unit of the data - No blank spaces allowed

Field 7: (string) Measurement quantity.

Field 8: (string) ID string of the transducer.

Note:

Records 1 to 3 are repeated for each data set.

Fields 5 through 8 are optionally. However, leaving out a field means leaving out the rest of the fields as well. The default value of field 5 is 1.0.

Setups

Measurement 1

C:\ARTEMİS-WORKS\a.txt

4 0 -1 0 0.000001 m/s² Acceleration Free Transducer 1

3 1 0 0 0.000001 m/s² Acceleration Free Transducer 2

3 0 -1 0 0.000001 m/s² Acceleration Free Transducer 3

10 0 -1 0 0.000001 m/s² Acceleration Free Transducer 4

9 1 0 0 0.000001 m/s² Acceleration Free Transducer 5

9 0 -1 0 0.000001 m/s² Acceleration Free Transducer 6

16 0 -1 0 0.000001 m/s² Acceleration Ref. Transducer 7

15 1 0 0 0.000001 m/s² Acceleration Ref. Transducer 8

15 0 -1 0 0.000001 m/s² Acceleration Ref. Transducer 9

22 0 -1 0 0.000001 m/s² Acceleration Free Transducer 10

21 1 0 0 0.000001 m/s² Acceleration Free Transducer 11

21 0 -1 0 0.000001 m/s² Acceleration Free Transducer 12

---

equations

node(13,2)=node(15,2)

node(17,2)=node(15,2)

node(14,2)=node(16,2)

node(18,2)=node(16,2)

node(16,1)=node(15,1)

node(13,1)=node(15,1)+10.50*(node(16,2)-node(15,2))/16.70

node(14,1)=node(13,1)

node(17,1)=node(15,1)-5.50*(node(16,2)-node(15,2))/16.70

node(18,1)=node(17,1)

node(23,2)=node(21,2)

node(19,2)=node(21,2)

node(24,2)=node(22,2)

node(20,2)=node(22,2)

node(22,1)=node(21,1)

node(19,1)=node(21,1)+10.50*(node(22,2)-node(21,2))/16.70

node(20,1)=node(19,1)

node(23,1)=node(21,1)-5.50*(node(22,2)-node(21,2))/16.70

node(24,1)=node(23,1)

node(11,2)=node(9,2)

node(7,2)=node(9,2)

node(8,2)=node(10,2)

node(12,2)=node(10,2)

node(10,1)=node(9,1)

node(7,1)=node(9,1)+10.50*(node(10,2)-node(9,2))/16.70

node(8,1)=node(7,1)

node(11,1)=node(9,1)-5.50*(node(10,2)-node(9,2))/16.70

node(12,1)=node(11,1)

node(5,2)=node(3,2)

node(1,2)=node(3,2)

node(2,2)=node(4,2)

node(6,2)=node(4,2)

node(4,1)=node(3,1)

node(5,1)=node(3,1)-5.50*(node(4,2)-node(3,2))/16.70

node(6,1)=node(5,1)

node(1,1)=node(3,1)+10.50*(node(4,2)-node(3,2))/16.70

node(2,1)=node(1,1)

APPENDIX B

Pushover Analysis

Pushover analysis were conducted by using frame type three dimensional models. SAP2000 computer software was used for the push-over analyses. Plastic hinges of the beams and columns were defined and the model was pushed incrementally by the lateral loads. During these analysis, the mass center of the roof story was chosen as the control node for each model. Lateral loads were applied to the model with an increasing uniform distribution from roof story to the ground story. During the pushover analysis, the magnitude of the control node's displacement was increased and the sequence of cracks, yielding, plastic hinge formulations and failure of various structural components were calculated by the analysis software.

When the structure reached a limit state or collapse condition, software stopped pushing the analytical model of the structure and total applied shear force and associated lateral displacement at each increment was plotted automatically, which is called as the pushover (capacity) curve.

As mentioned in the previous sections, reinforcement details of the columns and beams were not available. Therefore, minimum required reinforcements were defined for columns and beams. Minimum required column reinforcements are taken as 1% of the column area. However, minimum required reinforcements of the beams were calculated according to the limitations of the TS500. Since hinges occurred on some of the beams under dead load of the structure in the pushover analysis part, reinforcements of the beams were determined as three times greater than the minimum required reinforcement values in the analytical model.

Furthermore, reinforcement area of the shear walls were taken same as the strengthening plan.

Since the first dominant mode of the strengthened structure and the calibrated model were in the x-direction, analytical model was pushed in x and negative-x-directions. The period of vibration in the x-direction is longer than the period of vibration in the y-direction. Hence, the stiffness in the x-direction is lower than the stiffness in the y-direction. The first mode of the first model (the model before the strengthening project) was in y-direction but for comparison purposes the model was pushed in x and negative x-directions also.

In that study, pushover curves of the analytical modes were taken from the SAP2000 software. The force-displacement curves provided information about how the structure behave after exceeding its elastic limit. Furthermore, the structural members (on which hinges were developed) were investigated according to their hinge properties which were generated during the pushover analysis.

Demands of the analytical models were manually calculated by using Capacity Spectrum Method. Turkish Earthquake Response spectrum was chosen as the response spectrum in the analysis. The elastic spectrum was reduced by applying %5 damping which was then translated into the inelastic response spectrum by using spectral reduction value in constant acceleration range of the spectrum (SR_A) and spectral reduction value in constant velocity range of the spectrum (SR_V) as defined in ATC-40. Pushover curves which were taken from SAP2000 were also translated to the spectral acceleration (Sa) versus spectral displacement (Sd) format (ADRS format) manually. The pushover (capacity) curves which are in ADRS format are called capacity spectrums. Capacity curve is transformed to ADRS format using the equations from 1.1 to 1.5 as shown below.

$$PF_1 = \left[\frac{\sum_{i=1}^{N} \left(w_i \phi_{i1} \right) / g}{\sum_{i=1}^{N} \left(w_i \phi_{i1}^{\ 2} \right) / g} \right] \tag{1.1}$$

$$\alpha_1 = \frac{\left[\sum_{i=1}^{N}(w_i\phi_{i1})/g\right]^2}{\left[\sum_{i=1}^{N} w_i/g\right]\left[\sum_{i=1}^{N}\left(w_i{\phi_{i1}}^2\right)/g\right]} \quad (1.2)$$

$$Sa = \frac{V/W}{\alpha_1} \quad (1.3)$$

$$Sd = \frac{\Delta_{roof}}{PF_1\phi_{roof,1}} \quad (1.4)$$

The period values used in the demand curve are converted to Sd values using the following equation.

$$Sd = \frac{Sa}{4\pi^2}\cdot T^2 \quad (1.5)$$

Bilinear representation of the capacity spectrum and the reduced response spectrum (inelastic spectrum) were plotted on the same graph, which is used to determine the performances of the analytical models.

Pushover Analysis of the Unstrengthened Model

The model which has no shear walls representing the condition of the building before strengthening studies was investigated in this part. The analytical model (Figure 1) was pushed 6,5098 cm by the software and its base shear force was calculated to be 1495,651 kN (Figure 2). Immediate Occupancy and Life Safety conditions were passed for most of the columns. Furthermore, one of the columns which is located at the right side of the third story yielded during the analysis.

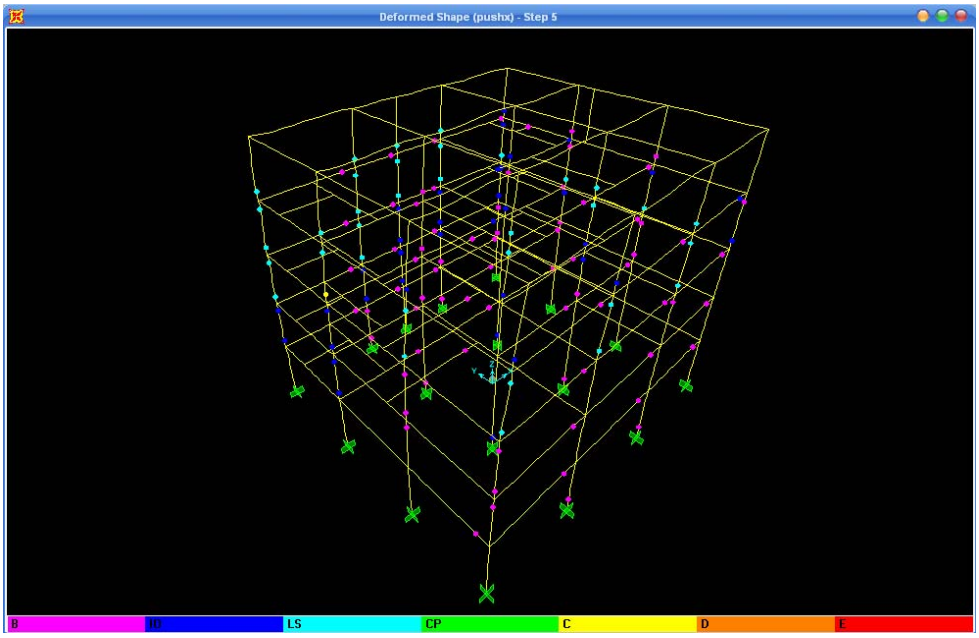

Figure 1. View of the occurred hinges on the analytical model

In the structural plan of the structure no beams were shown on the roof floor. When modeling the structure, small beams with 10cmx10cm dimensions were created on the roof floor of the model. In the pushover analysis of all models, hinges were not defined on these small beams.

While creating the inelastic spectra of the model, effective viscous damping (βeff) was calculated as 18.99 % manually. From the bilinear representation of the capacity curve, ay, dy, api, dpi values were calculated as 0,162, 1.025, 0.2835 and 4.390 respectively.

$$\beta eff = (63.7\kappa(ay.dpi - dy.api)/api.dpi) + 5 \qquad (1.6)$$

As seen from the capacity spectrum diagram (Figure 3), there is no intersection between the inelastic spectra and the bilinear representation of the capacity spectrum of the model. That means, under the earthquake condition, structure will show a poor performance.

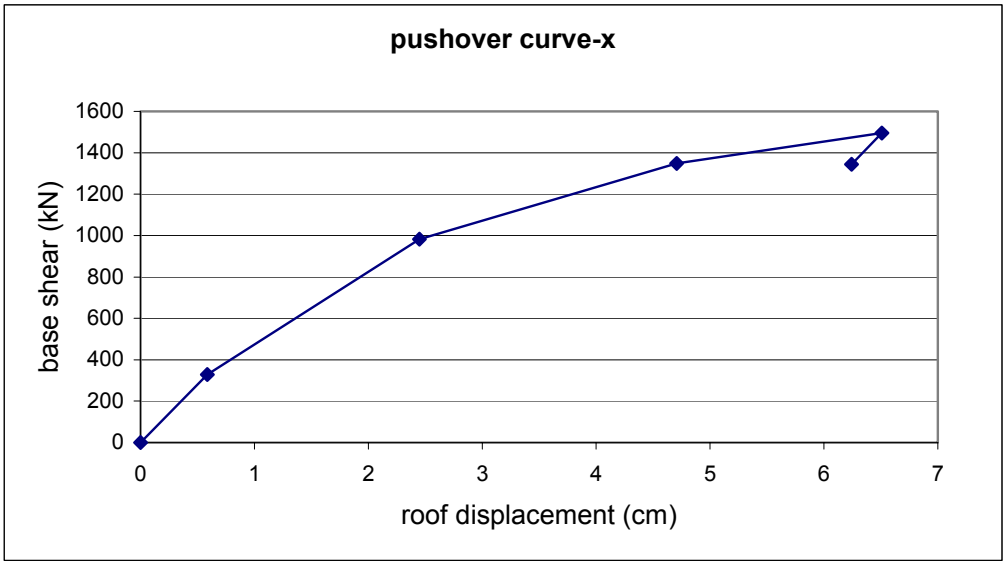

Figure 2. Pushover curve of the unstrengthened model

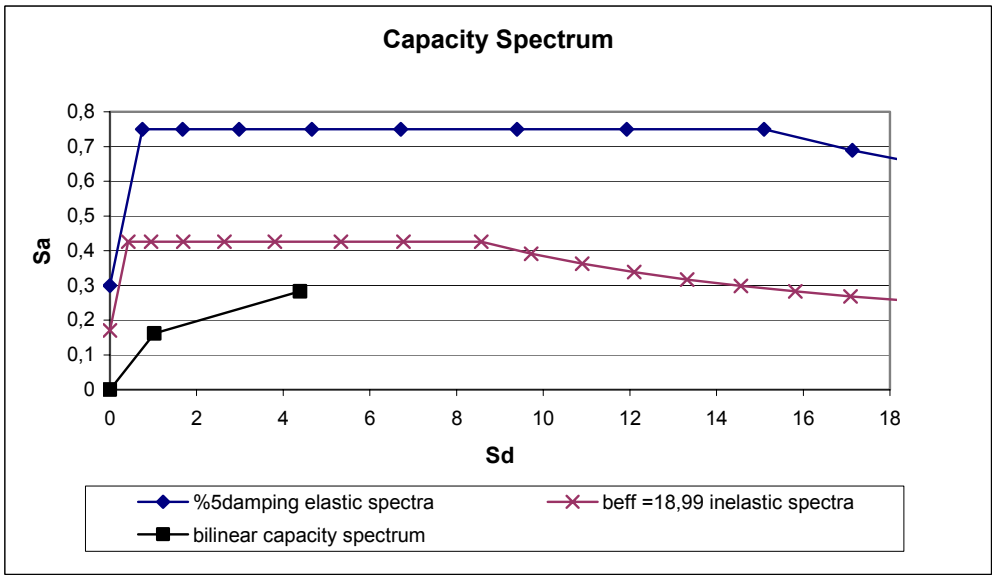

Figure 3. Capacity spectrum of the unstrengthened model

The capacity curve of the model reached 4.39 cm spectral displacement with 0.2835 cm spectral acceleration value.

Pushover Analysis of the Strengthened Model

The analytical model of the strengthened structure was pushed to the 8,94cm by 6376,6 kN shear force (Figure 4). Most of the columns reached to the yield force during the pushover analysis. Three of them yielded and lost their force carrying capacity. Two of the yielded columns were located on the roof story and the other was on the first floor.

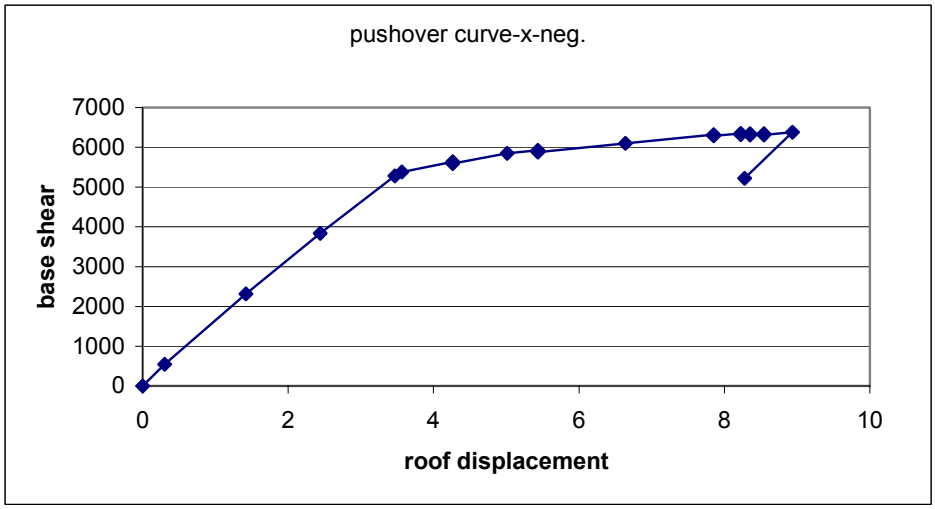

Figure 4. Pushover curve of the strengthened model

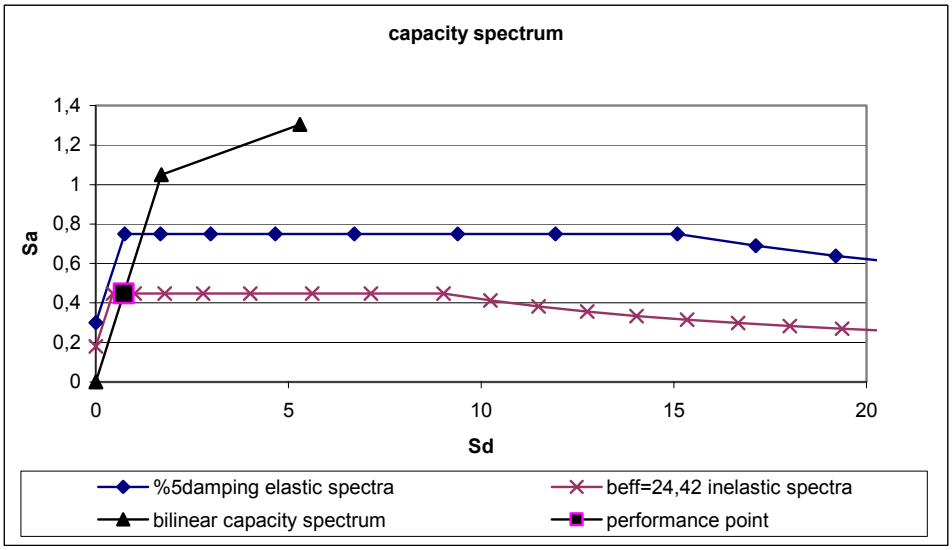

Figure 5. Capacity spectrum of the strengthened model

Effective viscous damping (βeff) of the model was calculated as % 24,42 manually. From the bilinear representation of the capacity curve, ay, dy, api, dpi values were calculated as 1.05, 1.699, 1.304 and 5.298 respectively.

From the intersection between the inelastic curve and the capacity spectrum, performance point was determined as 0,72599 cm spectral displacement. The spectral displacement was converted to the displacement by using Equation 4 and it was calculated as 1,225 cm which is the expected displacement of the building under an earthquake condition. Therefore, the model was pushed to that displacement and hinge properties were investigated in the light of that pushover analysis.

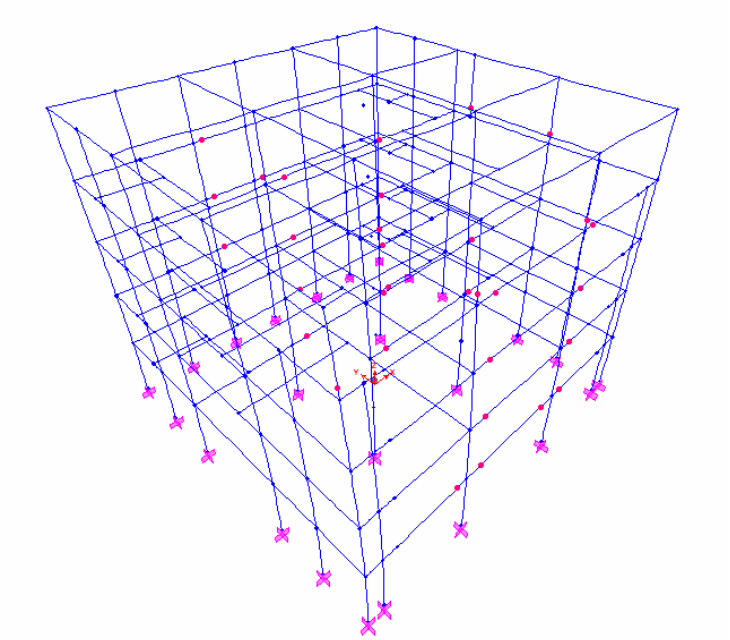

Figure 6. Hinges of the model

Since the performance point of the model stayed in the linear range of the capacity curve, none of the elements on the model reached to the yielding point in the pushover analysis as seen from Figure 6. According to the analysis results and calculations, that building is expected to show a good performance under earthquake conditions.

Pushover Analysis of the Final Calibrated Model

During the calibration studies, some discrepancies were determined between the strengthening plan and the application of the structure. Most important difference was about the locations of the shear walls on the roof story. It was realized that some of the shear walls were missing and the existing ones were not properly connected to the roof ceiling.

According to the general rules of the pushover analysis, roof level displacement is used for plotting the pushover curve. Therefore, the pushover analysis results were found to be quite different for the strengthened and calibrated models.

The analytical model of the calibrated model was pushed to the 2.16cm by 1352,5 kN shear force (Figure 7) and the hinges were mostly occurred on the roof story. Final collapse and loss of gravity load capacity was obtained on three columns which were located on the front facade of the roof story (Figure 8). Furthermore, strength degradation was occurred on some of the roof story columns. Roof story showed a weak behavior when compared with the whole building. Since the columns on the roof story were yielded and collapsed, capacity curve was stopped on smaller displacement values than the expected level of displacement (Figure 9).

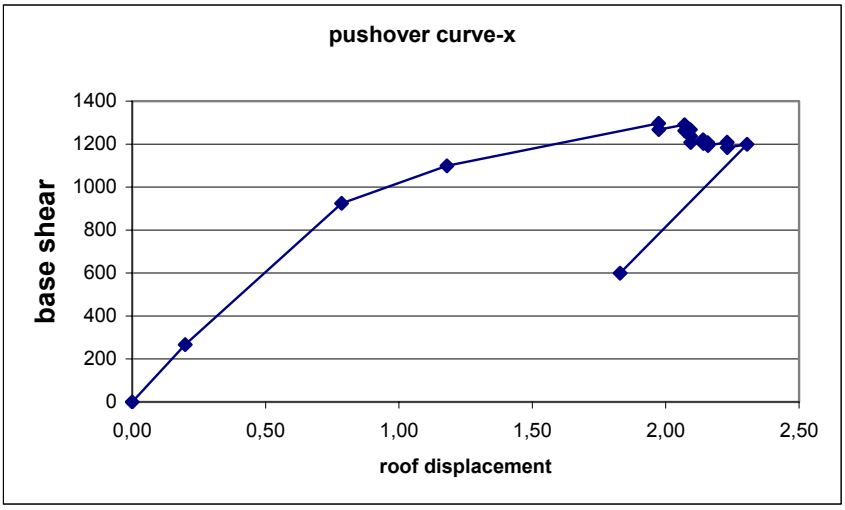

Figure 7. Pushover curve of the calibrated model

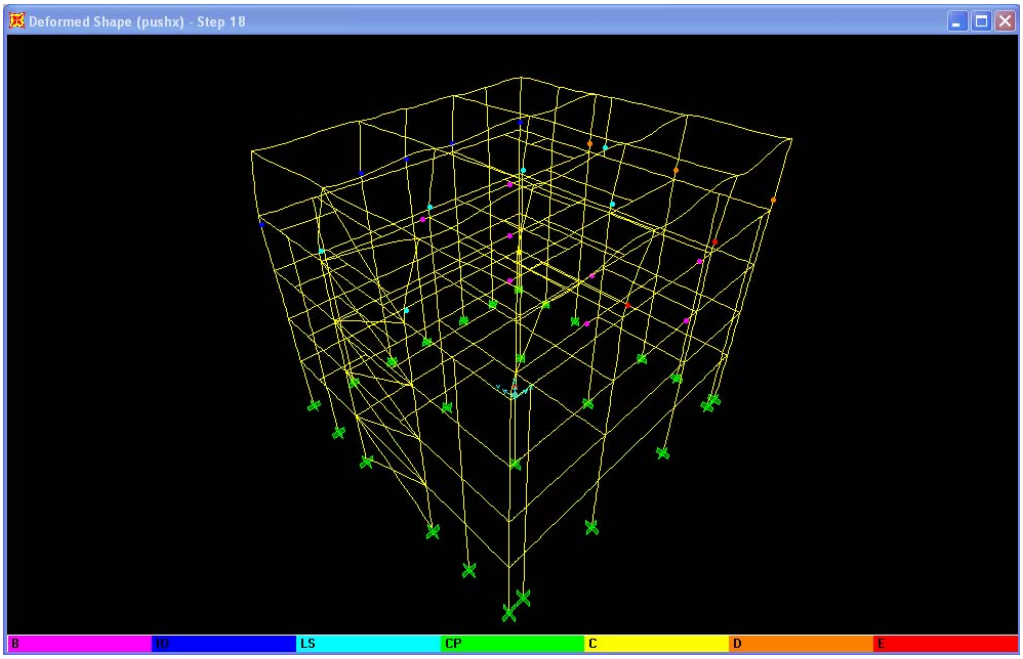

Figure 8. View of the hinges occurred in the calibrated model

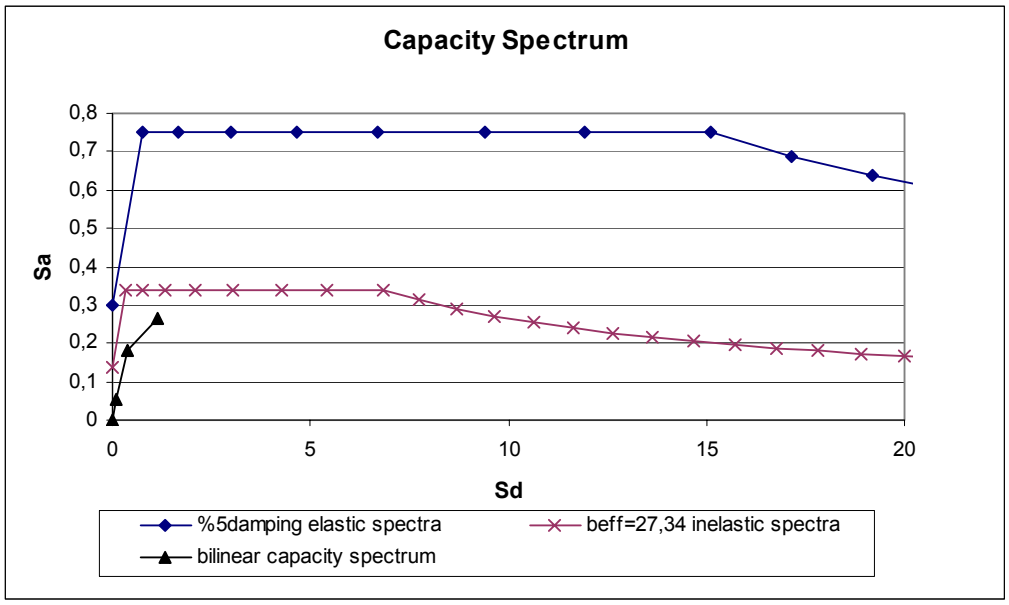

Figure 9. Capacity spectrum of the calibrated model

While creating the inelastic spectra of the model, $\beta_{eff.}$ was manually calculated as 27,34%. However, there is no intersection between the inelastic spectra with 27,34% effective viscous damping and the capacity curve of the model, which means that under earthquake loads, the structure will show a poor performance.

Pushover analyses conducted on the nominal and calibrated analytical models also showed significant differences. The FE model which was constructed using the available plans showed good performance while the calibrated FE model pushover results were inferior and indicated collapse at the roof level.

REFERENCES

1. Peeters, B., De Roeck, G., Hermans, L., Wauters, T., Krämer, C., De Semet, C.A.M, "Comparison of System Identification Methods Using Operational Data of a Bridge Test." Proceedings of ISMA 23, the International Conference on Noise and Vibration Engineering, pp. 923-930, K.U. Leuven, Belgium, September 1998

2. Dyke, S.J., Johnson, E.A., "Monitoring of a Beenchmark Structure for Damage Identification" Proceedings of the Engineering Mech. Speciality Conf., Austin, Texas, May 21-24, 2004

3. Ren, W., Zong, Z., "Output-Only Modal Parameter Identification of Civil Engineering Structures" Structural Engineering and Mechanics, Vol. 17, No. 3-4 (2004) 000-000

4. Farrar, C.R., Sohn, H., Doebling, S.W., "Structural Health Monitoring at Los Alamos National Laboratory" The 13th International Congress and Exhibition on Condition Monitoring and Diagnostic Engineering Management (COMADEM 2000), Houston, TX, USA, December 3-8, 2000

5. Ivanović, S.S., Trifunac, M.D., Todorovska, M.I., "Ambient Vibration Tests of Structures – A Review" Bull. Indian Soc. Earthquake Tech., Dec.2000, Special Issue on Experimental Methods

6. Kaya, H. "Experimental Modal Analysis of a Steel Grid Frame." M.S. Thesis, Middle East Technical University, 2004.

7. Chopra, A.K., " Dynamics of Structure", Prentice Hall, 1995

8. Avaitable, P., “Could You Explain Modal Analysis For Me.” Society of Experimental Techniques, February 1998

9. Avaitable, P., “Could You Explain The Difference Between Time Domain, Frequency Domain and Modal Space .” Society of Experimental Techniques, April 1998

10. Avaitable, P., “How Many Point Are Enough When Running a Modal Test.” Society of Experimental Techniques, June 2000

11. Avaitable, P., “Someone Told Me Structural Dynamic Modification Will Never Work.” Society of Experimental Techniques, February 2000

12. Avaitable, P., “Why Is Mass Loading and Data Consistency so Important.” Society of Experimental Techniques, October 2000

13. Ventura, C.E., Horyna, T., “Measured and Calculated Modal Characteristics of The Heritage Court Tower in Vancouver, B.C.” International Modal Analysis Conference –XX: A Conference on Structural Dynamics, Proceedings of the Conference held in 2000, pp. 1070-1074

14. Reynolds, P., Pavic, A., İbrahim, Z., “A Remote Monitoring Sytem for Stadia Dynamics” Proceedings of the 22nd International Modal Analysis Conference, Orlando, Florida, USA, February 2003

15. Kharrazi, M.H.K, “Experimental Benchmark Problem in Structural Health Monitoring” Results of Ambient Vibration Studies, Direct Studies Report, University of British Columbia, 48p. 2000

16. Structural Vibration Solutions ApS, “Artemis Extractor, Release 3.0, User’s Manual”, Denmark, 2001

17. Ewins, D.J., "Modal Validation: Correlation for Updating", Sadhana, Vol.25, Part 3, June 2000, pp. 221-234

18. Tamura, Y., Zhang, L., Yoshida, A., Cho, K., Nakata S., and Naito, S., "Ambient Vibration Testing & Modal Identification of an Office Building with CFT columns", 20th International Modal Analysis Conference, pp141-146, 2002

19. Doebling, S.W., Farrar C.R., and Prime M.B., "A Summary Review of Vibration- Based Damage Identification Methods", Engineering Analysis Group, Los Alamos National Laboratory, Los Alamos, NM

20. Ewins, D.J., " Modal Testing: Theory and Practice", Research Studies Press LTD., 1995

21. Silva, C.W., " Vibration Fundamentals and Practice", CRC Press, 2000